Rear-Slope Revetment Stability Approached by the Wave Overtopping Simulator

Experiments Regarding the Stability of Single-Layer Cube Revetment on Breakwater Crests and Rear Slopes

by

A.F.W Rietmeijer

June 22, 2017

Rear-Slope Revetment Stability Approached by the Wave Overtopping Simulator

Experiments Regarding the Stability of Single-Layer Cube Revetment on Breakwater Crests and Rear Slopes

by

A.F.W Rietmeijer

to obtain the degree of Master of Science
at the Delft University of Technology,
to be defended publicly on Monday July 3, 2017 at 15:00 PM.

Student number: 1540912

Graduation Committee:
Prof. Dr. Ir. W.S.J. Uijttewaal
Delft University of Technology
Dr. Ir. B. Hofland
Delft University of Technology
Ing. C. Kuiper
Delft University of Technology
Ir. B. van den Berg
Witteveen+Bos
Dr. Ir. M.R.A. van Gent
Deltares

An electronic version of this thesis is available at http://repository.tudelft.nl/. The dataset is available at http://researchdata.4tu.nl.

Abstract

Contrary to a breakwater outer slope, rear-slope revetment does not have to withstand breaking waves. However, generally, an equal dimensioned revetment is used on both the inner- and outer slope. Although with low-crested breakwaters severe overtopping occurs, the application of similarly sized armour on both sides still results in an over-dimensioned inner-slope revetment. An (economical) optimisation is possible in this regard.

The tests executed by Hellinga (2016) in this topic, showed large scatter in the found stability results of single-layer cube revetment at the rear slope. This scatter was party introduced by the large number of influencing factors in the test scope (Hellinga, 2016). By developing an overtopping simulator, the scope of the model-tests is delimited to solely the breakwater crest and rear slope. Moreover, larger scale tests are feasible in the same flume, reducing scaling errors.

The main objective of this thesis is a) determine if the approach of a (semi-)small scale overtopping experiment using an overtopping simulator is increasing the reliability of the test results, and (b) to increase the understanding of failure mechanisms of single-layer cube revetment on the crest and rear side of low-crested breakwaters.

To design and construct a simulator that is able to generate realistic waves, the relevant mechanisms of overtopping waves were determined and boundary conditions were composed. The behaviour of the simulator was tested in combination with a ‘mock’ breakwater. Seven types of realistic breakwater models were installed to investigate both the hydraulic behaviour of the overtopping volume and the stability behaviour of the revetment. The determination of the layout of a configuration is every time well substantiated by the results from the former configuration.

The water level inside the Wave Overtopping Simulators (WOS) reservoir showed a skewed drop during the release of an overtopping volume. Consequently, the water level measured at one single point was not accurate to determine the volume (change) inside the reservoir, and hence the discharge and velocity.

Different test configurations failed, where others remained stable during exposure to simulated waves in the test range. Compared to stability numbers of the theoretical front side, the cubes are relatively stable. The transition of the crest and rear slope showed to be a weak point, and outwash of the rock material filling the gap is a significant possibility.

Improvements on the WOS are possible to enhance the ability to simulate the characteristics of a realistic overtopping wave volume and to give a more detailed evaluation of the magnitudes of these overtopping characteristics. The normal forces between the cubes at the slope are more important for the stability than the own weight of the cubes. The lack of interaction between the cubes at the crest results in a significantly lower resistance to hydraulic loads compared to the cubes at the rear slope. The layout of a sharp inner crest-line transition, if well designed, showed a stable alternative for a rounded transition.

Keywords: Overtopping; Wave Overtopping Simulator; WOS; Breakwater; Rear-slope; Single layer; Cube; Stability; Revetment; Crest; Transition.

Preface

As the grande finale of my Master Hydraulic Engineering at the Delft University of Technology, I conducted research in the topic of overtopping simulators and rear-slope revetment, which took place from July 2016 until May 2017.

For this thesis, I got support from a number of people. At first, I want to thank my graduation committee. Wim Uijttewaal (Professor at the Delft University of Technology), Marcel van Gent (Head of department Coastal Structures & Waves at Deltares), Bas Hofland (Assistant Professor of Coastal Structures at the Delft University of Technology), Coen Kuiper (Part-time lecturer at the Delft University of Technology) and Bert van den Berg (Project Engineer at Witteveen+Bos). Moreover, I want to thank the guys from the Fluid Mechanics Laboratory at the Delft University of Technology for their input during the design process of the Wave Overtopping Simulator. Special thanks to Tom and Lennart, from DEMO, for the detailed design of the WOS. Furthermore, I want to thank my family and roommates for their support during the writing of this thesis. At last, I want to thank all the people of the group Coast and Rivers of Witteveen+Bos for their interest and assistance during my thesis writing.

Anton Rietmeijer

29 May 2017

List of Figures

1.1 Standard rubble mound breakwater failure modes (CIRIA, 2007) 4

2.1 Scheme of used method (with corresponding sections) based on van der Meer (1995) 7
2.2 Overtopping processes on a breakwater (Verhagen et al., 2004) 8
2.3 Methodology for the study of hydraulic loads, with at the top the hydraulic parameters and at the bottom the structural parameters. The corresponding paragraphs are indicated as well 9
2.4 Wave run-up 9
2.5 Wave tongue on top of the crest 11
2.6 Idealised overtopping flow parameters in time (Hughes, 2011) 14
2.7 Velocities in a wave tongue (Coticone, 2015) 15
2.8 Attached and detached tongue at the rear slope 16
2.9 Relation between stability and freeboard (Hellinga, 2016) 21
2.10 Forces on a protruding single-layer cubic block (Kuiper et al., 2006) 22
2.11 Wave load (Coeveld and Klein Breteler, 2003) 23
2.12 Ill and well clamped areas (Coeveld and Klein Breteler, 2003) (/textbfnog een vertaling bij) 23
2.13 Failure mechanisms of placed revetment (Coeveld and Klein Breteler, 2003) 24
2.14 Example of excess work (volume) above the threshold discharge in overtopping wave. (Hughes and Thornton, 2016) 27
2.15 Failure examples of scale tests performed by Taveira-Pinto et al. (2015) . . 28

3.1 Schematization of an overtopping wave: indicating the amount of scatter in the hydraulic parameters in the project scope is less with the usage of an overtopping simulator 30
3.2 Conceptual principals of van Dijk (2001) 33
3.3 Sketch of the used experimental set-up of van Dijk (2001) 33
3.4 Sketch of the Dutch Overtopping Simulator (van der Meer, 2006) 34
3.5 Calculated distribution of overtopping volumes and proposal for simulation. Mean discharge q = 30 l/s per m (van der Meer, 2006) 34
3.6 Set-up of prototype indicating parameters changed during calibration (van der Meer, 2006) 35
3.7 Figure of outer and inner box of the US Wave Overtopping Simulator . . 35
3.8 US simulator in action 35
3.9 Idealised simulated overtopping flow parameters in time (as discussed in Section 2.1.2) (Hughes, 2011) 36
3.10 Valve opening mechanisms 39
3.11 Valve opening mechanisms 39

3.12 Concept design of simulator with support legs outside the flume 40
3.13 Concept design of available ITEM-frame with mounted linear actuator mounted on green flume walls (without reservoir and valve) 41
3.14 Top-view detail of concept design of the valve inside and outside of the reservoir 42
3.15 The Wave Overtopping Simulator (The WOS) 43
3.16 Side-views of stainless steel frame 44
3.17 Top-view of wooden reservoir with (at the bottom) the outlet guidance . . 44
3.18 Detail of device connecting actuator shaft to the valve 44
3.19 The valve 45
3.20 Measured valve movement ($v_{max} > 8$ m/s) 46
3.21 Top view detail of door post 47
3.22 Water level inside the reservoir without opening of the valve 49
3.23 Orifice with different valve opening heights 49
3.25 Typical course of the water level during a wave simulation cycle 50
3.26 Water level inside the reservoir (h_{res}) in time with varying opening heights d_{valve} ($w_{res}(t = 0) = 0.60$ m) 51
3.27 Water level in reservoir during emptying 51
3.28 Discharge in time ($w_{res} = 0.40$ m) 53
3.29 Velocity in time ($w_{res} = 0.40$ m) 54
3.30 Valve opening distances (d_{valve}) in time. $h = \mu\, d_{valve}$ for the period where $h_{res} > d_{valve}$ 55
3.31 Theoretical parameter courses based on physical relation between the h_{res}, $u(t)$ and $q(t)$ 56
3.32 Interdependencies of parameters for calculating simulated overtopping characteristics (in blue), with the used boundary conditions indicated in the right corners 57
3.33 Overtopping volumes in a fictive storm ordered in magnitude, using Eq. 3.3 ($N_{ow} = 100$, a=0.35 and b=0.8) 58
3.34 Simulated overtopping volumes 60

4.1 Schematisation of the test set-up 64
4.2 Measured parameters (not on scale) 66
4.3 Wave tongue propagating on crest with green line as detected waterline . 68
4.4 Front view of Configuration 0a 69
4.5 Front view of Configuration 0b 69
4.6 Wooden mock breakwater 70
4.7 Wave tongue on top of wooden breakwater 70
4.8 Configuration 1 72
4.9 Configuration 2 73
4.10 Configuration 3 74
4.11 Configuration 4 75
4.12 Configuration 5 76
4.13 Configuration 5 77
4.14 Configuration 6 78
4.15 Configuration 7 79
4.16 Wave tongue propagating on crest with green line as detected waterline . 80
4.17 Averaged front velocities on the crest 81
4.18 Side view of overtopping volumes using Wave 7 82

4.19 Damage numbers $\frac{H_s}{\Delta \cdot D}$ and θ . . . 83
4.20 Most unfavourable front velocity vs. front velocity measured of damaging wave . . . 84
4.21 Cubes placed on top of a crest . . . 84
4.22 Transition Configuration 1 . . . 86
4.23 Transition Configuration 5 . . . 86
4.24 Schematisation of inner crest line transition possibilities . . . 87

B.1 Wooden disign . . . 104
B.2 ITEM-frame with steel reservoir . . . 105
B.3 Stainless steel frame and reservoir . . . 106

D.1 Block diagram of PID controller (Wescott, 2016) . . . 117

F.1 Discharge in time with $h_{res}(0)$=0.60 m for different flume axial widths . . 125
F.2 Discharge in time with $h_{res}(0)$=0.40 m for different flume axial widths . . 126
F.3 Discharge in time with $h_{res}(0)$=0.20 m for different flume axial widths . . 127

G.1 Theoretical waves in a storm. With $H_s = 0.24\ m,\ s = 0.4,\ R_c = 0.35\ m,\ t = 3$ hours, $\tan\alpha = 0.5$. . . . 129

List of Tables

2.1 Coefficients for Equations 2.1 and 2.2 10
2.2 Coefficients for wave run-up predictions, using H_{m0} and $T_{m-1,0}$ (van Gent, 2002b) 11
2.3 Studies on describing overtopping parameters 13
2.4 Coefficients for the rear side of the crest (van Gent, 2002a) 16

3.1 Starting point 38
3.2 Pre-tests 48
3.3 Tested waves 59

4.1 Tested configurations 71
4.2 Result overview 71

D.1 Effects of increasing a parameter independently (Ang et al., 2005) 117
D.2 Final values at used in the WOS 118

F.1 Simulated waves 124

H.1 Values of coefficients 131

List of Symbols

Symbol	**Unit**	**Description**
α	-	front slope angle
α_i	-	angle of plunge impact
β	-	rear slope angle
Δ	-	relative density
Δ_{s_x}	m	impact location of jet in x direction
Δ_{s_y}	m	impact location of jet in y direction
γ_β	-	influence factor for oblique wave attack
γ_b	-	berm reduction factor in wave run-up
γ_c	-	friction of the crest
γ_{f-C}	-	influence factor for roughness elements on the crest
γ_f	-	foreshore coefficient in wave run-up
γ_f	-	influence factor for roughness elements on the outer slope
γ_i	-	influence factor of the angle of the incoming waves
Λ	m	leakage length
μ	-	orrifice distraction coefficient
ϕ	m	piezometric head
ρ_c	kg/m^3	density of concrete
ρ_r	kg/m^3	density of rock
ρ_w	kg/m^3	density of water
σ	varies	standard deviation
θ_i	°	incoming wave angle
ξ	-	breaker parameter
ξ_{0m}	-	breaker parameter based on the deep water wave length
$\xi_{m-1,0}$	-	breaker parameter based on
C_D	-	drag coefficient
C_L	-	lift coefficient
d	m	local water depth
D_n	m	cube size
$d_{n,50}$	m	median nominal diameter
g	m/s^2	acceleration of gravity

Symbol	**Unit**	**Description**
$h(x)$	m	water layer thickness at x
H_{m0}	m	spectral significant wave height (=H_s)
h_{max}	m	maximum wave layer thickness in storm
h_{peak}	m	peak layer thickness in single overtopping event
h_{res}	m	water level in simulator
L	m	local wave length
L_0	m	deep water wave length
m	kg	mass
n	-	packing density
n	-	wave number
N_d	-	damage number
N_w	-	number of waves
N_{ow}	-	number of overtopping waves
P	-	probability
q	m^2/s	overtopping discharge
q_{max}	m^2/s	maximum wave discharge in storm
q_{mean}	m^2/s	mean overtopping discharge during a storm
q_{peak}	m^2/s	peak discharge in single overtopping event
R_c	m	crest height relative to water level
R_u	m	wave run-up height
s	-	wave steepness
t	s	time
T	s	wave period
T_m	s	mean wave period
$T_{m-1,0}$	s	Spectral wave period based on the first neg. moment of the energy spectrum
T_{ovt}	s	overtopping duration
T_p	s	peak wave period
T_s	s	significant wave period
u	m/s	velocity in x-direction
u'	m/s	turbulent velocity fluctuation in x-direction
$u(i)$	m/s	velocity at impact of the jet
u_{max}	m/s	maximum wave velocity in storm
u_{peak}	m/s	peak velocity in single overtopping event
$V(x)$	m^3	volume of an overtopping wave passing x
V_{inf}	m^3	infiltrated volume in the crest
W	N	unit weight
W_c	m	crest width
x	m	coordinate along the crest

Contents

Abstract iii

Preface v

List of Figures ix

List of Tables xi

List of Symbols xiii

1 Introduction 3

1.1 Current State of Knowledge on Rear-Side Single-Layer Cube Revetment: Room for Improvement 3

1.2 Research Framework 4

1.2.1 Research objective 4

1.2.2 Research questions 5

1.2.3 Methodology 5

1.3 Outline of the Report 6

2 Theoretical Background on Overtopping Waves and Armour Stability 7

2.1 Hydraulic Loads of Overtopping Waves 8

2.1.1 Wave run-up 9

2.1.2 Wave propagation on top of the crest 11

2.1.3 Waves at the rear slope 16

2.1.4 Wave overtopping probability 18

2.2 Armour Stability 19

2.2.1 Concrete units 20

2.2.2 Placed revetment 22

2.2.3 Rock armour breakwater 23

2.2.4 Dykes 25

2.3 Damage Description 27

2.3.1 Damage characterisation 27

2.3.2 Damage criteria 28

3 Wave Overtopping Simulator Design 29

3.1 Introduction to Overtopping Simulators (OS) 29

3.1.1 General advantage and disadvantages of the usage of an OS 29

3.1.2 Reference simulators 32

3.2 Design Aspects of the WOS 36

3.2.1 Preferences and requirements for the WOS 36

3.2.2 Starting point of the design of the WOS 37
3.2.3 Design elements 38
3.2.4 Summary 42
3.3 The Wave Overtopping Simulator (WOS) 43
3.3.1 Support structure 43
3.3.2 Reservoir 44
3.3.3 Valve and linear actuator 45
3.3.4 Door post 45
3.3.5 Outlet guidance 46
3.3.6 Turbulence introduction 46
3.3.7 Protection board 46
3.3.8 Depth-meter in reservoir 46
3.4 Callibration of the Wave Overtopping Simulator 48
3.4.1 Properties of the Wave Overtopping Simulator 48
3.4.2 Individual simulated wave volumes 51
3.5 Storm Simulation Approach 57
3.5.1 Determination of overtopping parameter magnitudes 57
3.5.2 Distributions of parameter values in storm simulation 58
3.5.3 Boundary conditions and parameter ranges 58
3.5.4 Application of the WOS 59
3.6 Discussion on (the applicability of) the Wave Overtopping Simulator 61
3.6.1 Properties of the Wave Overtopping Simulator 61
3.6.2 Storm simulation 62

4 Breakwater Experiments 63
4.1 Test Outline 63
4.2 Experimental Set-Up 64
4.2.1 Breakwater model 64
4.2.2 Instruments and measurements 66
4.3 Test Approach 69
4.4 Tested Configurations and Results 69
4.4.1 Impermeable breakwater model 69
4.4.2 Permeable breakwater models 70
4.5 Breakwater Experiments Analysis and Discussion 80
4.5.1 Hydraulic (load) aspects 80
4.5.2 Stability aspects 82

5 Conclusions and Recommendations 89
5.1 Conclusions 89
5.2 Recommendations 93
5.2.1 Wave Overtopping Simulator 93
5.2.2 Hydraulic research 93
5.2.3 Single-layer rear-slope cube revetment 94

Bibliography 94

A Parameter Scaling **99**
A.1 Similarity . . . 99
A.1.1 Geometric Similarity . . . 99
A.1.2 Kinematic Similarity . . . 99
A.1.3 Dynamic Similarity . . . 99
A.2 Scaling Conditions . . . 101

B Reservoir (Support) Principles **103**
B.1 Wooden structure . . . 104
B.2 Existing frame . . . 105
B.3 Completely steel . . . 106

C Technical Drawings of the WOS **107**

D Tuning of the PID controller **117**

E Data Processing **119**
E.1 Float Data Analysis . . . 119
E.2 Video Analysis . . . 120

F Simulated Waves **123**

G Storm Simulation Example **129**

H WOS Behaviour **131**

I Lessons Learned: Tips for Testing in the Fluid Mechanics Laboratory **133**

Chapter 1

Introduction

In order to create a calm environment in front of a shore or inside a harbour, a breakwater can be constructed to dampen the incoming waves. In this way, sand transport is dampened or ships can moor comfortably at a quay. There are several types of breakwaters, e.g. a rubble mound breakwater consists of a rubble core. To protect this core, an armour layer has to be installed on the outer line. This layer may consist of rock or concrete elements.

This thesis focusses on the stability of single-layer cubic concrete blocks on the crest and rear slope of a low-crested breakwater. Contrary to the outer slope, rear-slope revetment does not have to withstand breaking waves. Nevertheless, generally, an equal dimensioned revetment is used on both the inner- and outer slope. Although severe overtopping occurs at low-crested breakwaters, the usage of similarly sized armour on both sides still results in an over-dimensioned inner-slope revetment. An (economical) optimisation is possible in this regard.

1.1 Current State of Knowledge on Rear-Side Single-Layer Cube Revetment: Room for Improvement

The armour layer of rubble mound breakwaters can be constructed out of different armour types. Large rubble rocks or concrete units are commonly used as top-layer. Several types of concrete units are available. Some derive their stability from their own weight, others are stable by interlocking with nabouring units. The placement of these interlocking units is a very precise job and careful placement is crucial for their stability. The cubic units can be placed randomly or in a specific pattern, in one or multiple layers. This study focusses on single-layer concrete cube revetment.

The choice for concrete cubes over complex interlocking units is preferred in situations where the fabrication and placement of the concrete units is executed by personnel which is not well-trained. The pre-casting of the cubic units is a simpler process compared to the fabrication of interlocking units. Since the formwork can be removed earlier, the production rate of cubes is higher compared to interlocking units (Van Gent and Luis, 2013).

Several failure mechanisms threaten a rubble mound breakwater. Hydraulic damage at the outer slope is feasible, as well as internal erosion and erosion of the subsoil. Erosion of the toe and slip-circles are possibilities as well. As Figure 1.1 demonstrates, this research focusses on mechanisms 5 and 6: damage at the crest and the rear side of a breakwater.

Hellinga (2016) executed overtopping tests in the Fluid Mechanics Laboratory at the

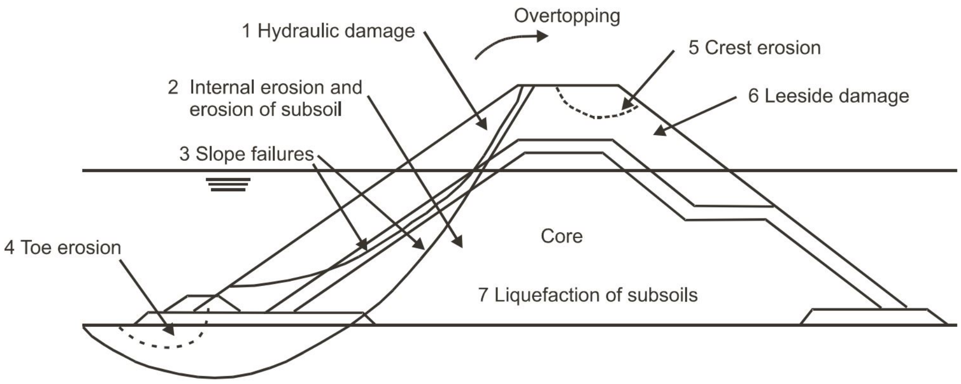

Figure 1.1: Standard rubble mound breakwater failure modes (CIRIA, 2007)

Delft University of Technology. The study was conducted in a wave flume using a wave generator. The research showed that damage at the rear slope occurred later than expected based on prior calculations. The approach for these calculations was based on the stability formulas for randomly placed rock developed by van Gent and Pozueta (2004) and subsequently scaled by the difference of stability between randomly placed and regular placed cubes (using the known stability numbers of the front slope). The damage appeared to be limited to the first row below the water level, indicating smaller cubes can be installed at the other rows. The conclusions found in the study by Hellinga (2016) were not consistent and a number of anomalies between predicting overtopping formulas and found values were detected. Presumably, this was caused by the large number of aspects affecting an overtopping wave. An elaboration of the findings of Hellinga (2016) is shown in Section 2.2.

Hence, there is currently a lack of know-how regarding the failure mechanisms of single-layer armour units on the rear side of rubble-mound breakwaters. This results in large uncertainties concerning the stability of the breakwater rear side.

1.2 Research Framework

In the course of the current study, additional experiments were conducted, applying the stated conclusion and recommendations in the thesis of Hellinga (2016). Still, the approach was different compared to the method used in the research of Hellinga (2016), as this research was executed using an overtopping simulator, limiting the influencing factors in the scope.

1.2.1 Research objective

The main objective of this thesis is (a) determine if the approach of a (semi-)small scale overtopping experiment using an overtopping simulator is increasing the reliability of the test results, and (b) to increase the understanding of failure mechanisms of single-layer cube revetment on the crest and rear side of low-crested breakwaters.

1.2.2 Research questions

The main research question of this thesis is: *Is the Wave Overtopping Simulator an appropriate tool to investigate the failure mechanisms of single-layer armour units which are loaded with overtopping waves; and what are the single-layer cube rear-slope stability mechanisms of low-crested breakwaters?* This main research question is split up in several sub-questions. Sub-questions concerning the design of the overtopping simulator are:

1. Which hydraulic parameters are relevant for the normative individual overtopping waves?
2. How should the overtopping simulator function, in order to generate waves with these hydraulic parameters?
3. Is it possible to simulate wave overtopping volumes with accurate water layer thicknesses, turbulence intensities and wave front velocities using a small scale wave overtopping simulator?

Sub-questions concerning the single-layer stability are:

5. How does an overtopping wave propagate on a low-crested breakwater crest, transition, and inner slope?
6. How does an overtopping wave influence the single-layer cube revetment?
7. Which mechanisms are responsible for the stability and damage of the revetment, and what is the governing mechanism?

1.2.3 Methodology

To answer the above-stated research questions, various experiments were executed. Physical small-scale model tests were performed in the sediment flume in the Fluid Mechanics Laboratory at the Delft University of Technology. Using the Wave Overtopping Simulator, overtopping waves were generated.

De Vries (1982) stated that modelling is making a detour from a prototype problem to a prototype solution. Using an overtopping simulator reduces this detour. The scope of the model-tests is delimited by solely the breakwater crest and rear slope. When using a wave flume, the generated wave has to travel along the flume before it reaches the toe of the breakwater-model. This allows the waves to deform. When reaching the toe, the wave breaks and runs up the front slope. Hence, the front slope is highly significant for the overtopping wave volume and its characteristics. With all these different factors scatter introduces (Hellinga, 2016). With an overtopping simulator the exact volume, front velocity and layer thickness are known for each single overtopping wave at the outer crest line. Moreover, the minimum water depth is restricted in a wave flume for the generated waves to be able to propagate. This is not an issue with the overtopping simulator. Consequently, using the exact same flume, larger waves can be tested. Thus reducing the scaling deviations.

To design and construct a simulator that is able to generate realistic waves, the relevant mechanisms of overtopping waves must be known. Formulas describing the hydraulic parameters of overtopping waves must be investigated thoroughly. Over the years, more and more data on overtopping waves has been produced through the CLASH-programme (Crest Level Assessment of Coastal Structures by Full Scale Monitoring, Neural Network

Prediction and Hazard Analysis on Permissible Wave Overtopping), making the data-based empirical formulas increasingly reliable. This CLASH-programme, funded by the EU, investigated wave overtopping for different structures both small and full scale. The results of the CLASH programme were used to develop a prototype wave overtopping simulator which is able to simulate overtopping waves, which may occur at design conditions at real scale (Van der Meer et al., 2006).

The requirements and preferences of the overtopping simulator were clarified and the design of the simulator was made. Initial testing was done for the calibration of the overtopping simulator and the test programme. Every test cycle had two purposes, both investigating the revetment stability and acquiring data of the overtopping simulators generated water volume. The behaviour of the simulator with its generated waves and the findings of the stability tests are analysed.

The scope of this research extends solely to load and stability mechanisms of single-layer cube revetment at the crest and rear slope. Therefore, a number of elements must fall outside this scope. First, this research does not incorporate any crest elements on top of the crest. second, the strength of the individual cubes is not encompassed by this research. Bandwidths and ratios of the investigated parameters were similar as in this thesis of Hellinga (2016) for comparison of the results. The fact that the influence of possible wave transmission is not tested in this approach of using an overtopping simulator and that the input for the simulator is truly dependent on former research on overtopping waves has to be kept in mind.

1.3 Outline of the Report

The report starts with the literature study focussing on hydraulic boundary conditions for the design of the Wave Overtopping Simulator. This is done on a spatial basis, starting at the front side of the breakwater with the wave run-up, then the hydraulic parameters at the crest and ending with the inner slope assuming a detached jet. After the hydraulic parameters, the structural parameters of the armour layer are discussed.

The main part is split up in two chapters, where Chapter 3 focusses on the WOS and Chapter 4 on the stability experiments. Considering the calibration of the WOS is exectuded using the test setup, some sections in Chapter 3 refer to Chapter 4.

As mentioned, in Chapter 3 the Wave Overtopping Simulator (WOS) is elaborated upon. Starting with a general introduction of overtopping simulators, and subsequently treating the design of the WOS. The behaviour the simulator and its simulated waves are treated and a concept is given for the approach of a representative storm simulation. At the end of the chapter, the simulator is further discussed.

Chapter 4 discusses the stability experiments. First, the test outline and set-up are treated, where after the test approach and tested configurations are presented. In the last section the found results are analysed and discussed.

In Chapter 5 the conclusions are given for both the WOS and the stability study on single-layer cube revetment on the crest and rear-side of low-crested breakwaters. Chapter 5 ends with recommendations for further study and adaptations for the WOS.

Chapter 2

Theoretical Background on Overtopping Waves and Armour Stability

This chapter resumes the studies relevant for answering the research questions, starting with the description of the hydraulic loads of an overtopping wave on a spatial basis. Subsequently, the stability of different kinds of revetments are treated, including corresponding stability formulas. The last section contains the damage characterization and tolerances of resulting damage.

The general approach to study the stability of a breakwater is shown in Figure 2.1. Starting with the environmental boundary conditions and structural parameters, the hydraulic parameters can be determined. Those, in their turn, generate the hydraulic load which together with the structural strength of the breakwater determine the eventual damage.

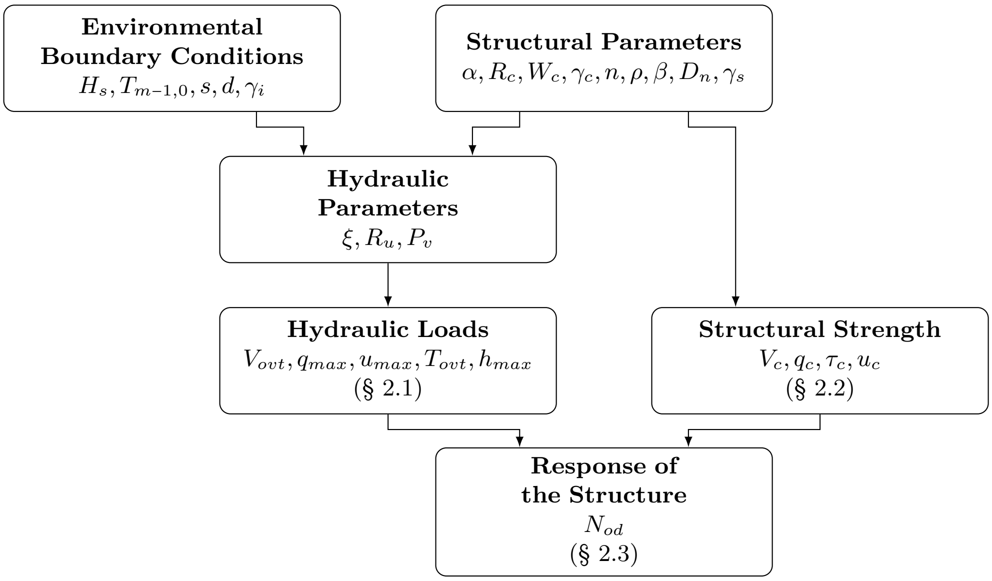
Environmental Boundary Conditions
$H_s, T_{m-1,0}, s, d, \gamma_i$
Structural Parameters
$\alpha, R_c, W_c, \gamma_c, n, \rho, \beta, D_n, \gamma_s$
Hydraulic Parameters
ξ, R_u, P_v
Hydraulic Loads
$V_{ovt}, q_{max}, u_{max}, T_{ovt}, h_{max}$
(§ 2.1)
Structural Strength
V_c, q_c, τ_c, u_c
(§ 2.2)
Response of the Structure
N_{od}
(§ 2.3)

Figure 2.1: Scheme of used method (with corresponding sections) based on van der Meer (1995)

2.1 Hydraulic Loads of Overtopping Waves

Numerous studies are performed regarding hydraulic loads of overtopping waves on breakwaters and dykes. A significant number of studies is focused on dykes, hence dykes are discussed in this report as well, even though two big differences can be appointed between dykes and breakwaters: in general, one can consider dykes as impermeable and the dykes' slope as smooth. In contrary to dykes, rubble mound breakwater slopes with concrete cube revetment are considered permeable and rough.

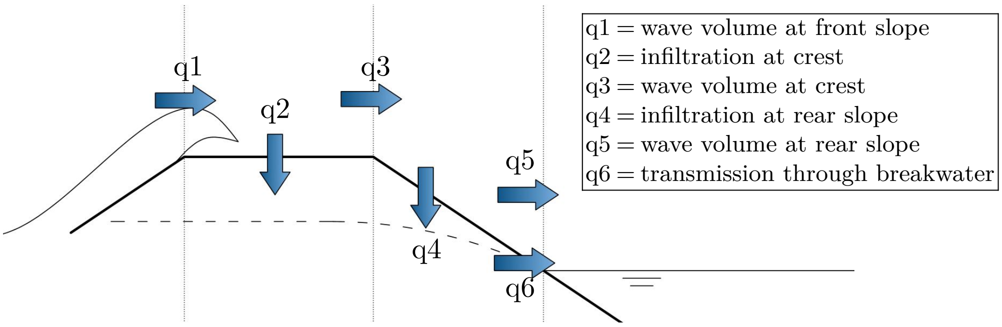
q1
q3
q2
q5
q4
q6
q1 = wave volume at front slope
q2 = infiltration at crest
q3 = wave volume at crest
q4 = infiltration at rear slope
q5 = wave volume at rear slope
q6 = transmission through breakwater

Figure 2.2: Overtopping processes on a breakwater (Verhagen et al., 2004)

Figure 2.2 shows the six different overtopping processes on a breakwater. The overtopping volume rushes upwards on the outer slope (q1) and will infiltrate in the crest (q2). The volume which reached the outer slope (q3) will plunge into the inner slope and will partly infiltrate (q4) and partly rush along the rear slope (q5). The flow due to transmission through the breakwater is indicated with q6 (Verhagen et al., 2004).

As mentioned above, a large number of studies focussed on dykes. The overtopping processes relevant to dykes are indicated in Figure 2.2 as q1, q3 and q5. In this section the emphasis lies on these processes, considering very little is known about the infiltration. The influence of transmission through the breakwater on the stability of the rear slope is assumed to be negligible. The load executed by a wave tongue of an overtopping wave is discussed in this section on a spatial basis. Starting with the wave run-up, then the wave tongue on the crest and ending with the flow at the rear slope (Figure 2.3).

The last part of this section discusses the probability of overtopping, including the probabilities for certain overtopping volumes. This is especially relevant for determination of the largest wave in a storm. With the hydraulic load parameters known, the effect of a wave on the single-layer stability at the inner slope is investigated in the next section.

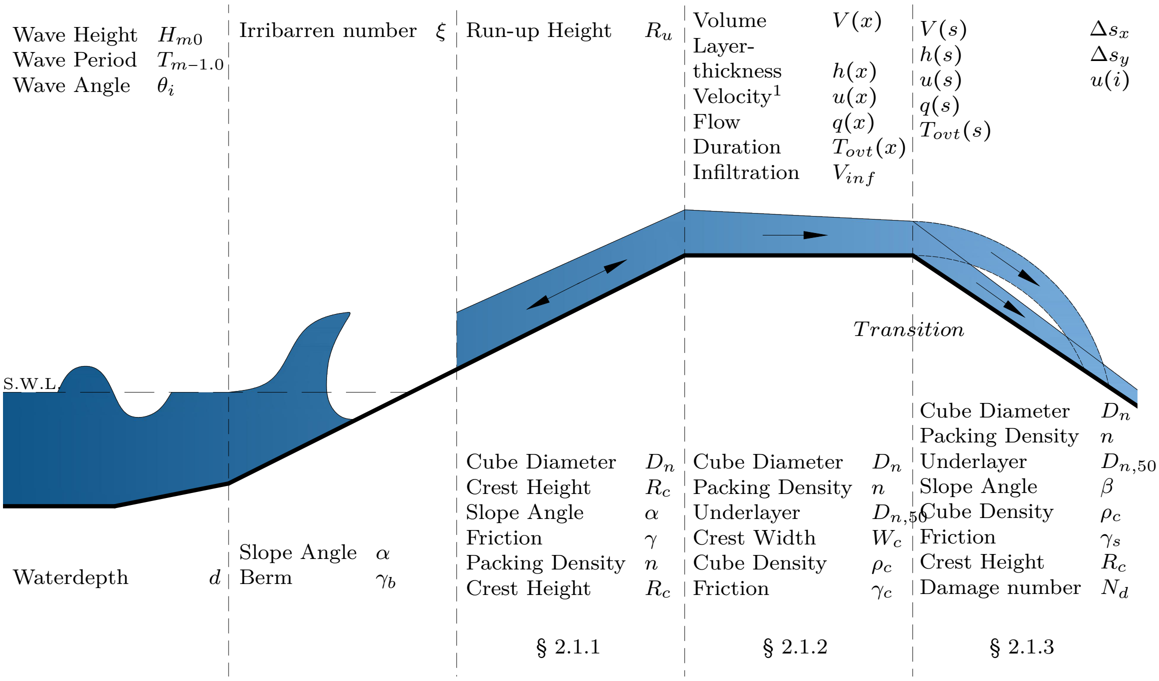
Wave Height H_{m0}
Wave Period $T_{m-1.0}$
Wave Angle θ_i
Irribarren number ξ
Run-up Height R_u
Volume $V(x)$
Layer-thickness $h(x)$
Velocity[1] $u(x)$
Flow $q(x)$
Duration $T_{ovt}(x)$
Infiltration V_{inf}
$V(s)$
$h(s)$
$u(s)$
$q(s)$
$T_{ovt}(s)$
Δs_x
Δs_y
$u(i)$
S.W.L.
Transition
Waterdepth d
Slope Angle α
Berm γ_b
Cube Diameter D_n
Crest Height R_c
Slope Angle α
Friction γ
Packing Density n
Crest Height R_c
Cube Diameter D_n
Packing Density n
Underlayer $D_{n,50}$
Crest Width W_c
Cube Density ρ_c
Friction γ_c
Cube Diameter D_n
Packing Density n
Underlayer $D_{n,50}$
Slope Angle β
Cube Density ρ_c
Friction γ_s
Crest Height R_c
Damage number N_d
§ 2.1.1
§ 2.1.2
§ 2.1.3

---

[1] This research focusses on the front velocity of the overtopping wave

Figure 2.3: Methodology for the study of hydraulic loads, with at the top the hydraulic parameters and at the bottom the structural parameters. The corresponding paragraphs are indicated as well

2.1.1 Wave run-up

The overtopping water volume at the rear side of the breakwater starts at the front slope as wave run-up. This run-up is driven by the wave energy and is defined as the distance from the still water level up to the (fictive) maximum run-up at the slope. For calculation purposes, the fictional run-up height is used (Figure 2.4). The run-up is i.e. dependent on the wave height, wave period, the slope angle, slope friction, angle of incidence and the presence of a berm. These factors are all included in the formulas for the run-up height (Equations (2.1) to (2.4)).

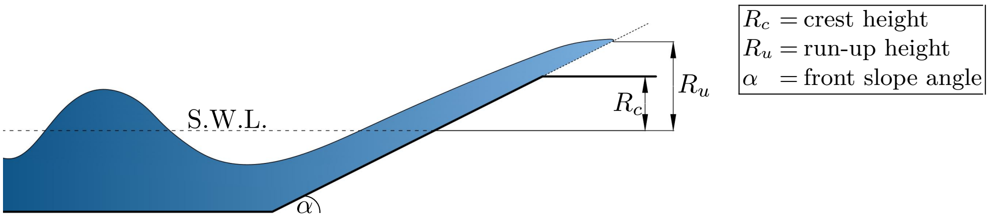
R_c = crest height
R_u = run-up height
α = front slope angle
S.W.L.
R_u
R_c
α

Figure 2.4: Wave run-up

Because the stability of the revetment is correlated to the extreme loads, a level of which n percent of the waves exceeds that certain height is used to describe the run-up height. When for example $n = 2$, one can speak of the 2% wave run-up height, $R_{u,2\%}$. Longer waves generate higher run-up, therefore $T_{m-1,0}$ should be applied in the run-up formulas (van Gent, 1999, 2001). The generally used formula for the wave run-up height on slopes is (van der Meer, 2002):

$$\frac{R_{u,n\%}}{H_{m0}} = A \cdot \gamma_b \cdot \gamma_f \cdot \gamma_\beta \cdot \xi_{m-1,0} \tag{2.1}$$

with a maximum of

$$\frac{R_{u,n\%}}{H_{m0}} = \gamma_b \cdot \gamma_{f,surging} \cdot \gamma_\beta \left(B - \frac{C}{\sqrt{\xi_{m-1,0}}} \right) \tag{2.2}$$

where:

$R_{u,n\%}$ = maximum run-up height exceeded by n % of the incident waves [m]
H_{m0} = significant wave height [m]
γ_b = berm reduction factor [-]
γ_f = roughness reduction factor [-]
γ_β = angle of attack reduction factor [-]
ξ = surf similarity parameter [-]

Table 2.1: Coefficients for Equations 2.1 and 2.2

	A	B	C
Deterministic	1.75	4.3	1.6
Probabilistic	1.65	4.0	1.5

These formulas are valid from $0.5 < \gamma_b \, \xi_{m-1,0} \leq 8$ or 10. The variation coefficient in relation to the average line is $\mu/\sigma = 0.07$. Starting from $\xi_{m-1,0} = 1.8$ the roughness factor increases linearly up to 1 for $\xi_{m-1,0} = 10$, which can be described by:

$$\begin{aligned} \gamma_{f surging} &= \gamma_f + (\xi_{m-1,0} - 1.8) \cdot \frac{1-\gamma_f}{8.2} \\ \gamma_{f surging} &= 1 \quad \text{for} \quad \xi_{m-1,0} > 10 \end{aligned} \tag{2.3}$$

For a permeable core, a maximum is reached for $R_{u,2\%}/H_{m0} = 2.11$ (1.97 for deterministic approach) (van der Meer, 2002). In the subsection below the influence of permeability is questioned.

Next to the formula of van der Meer (2002), Schuttrumpf and van Gent (2003) proposed a different formula to calculate the run-up height:

$$\begin{aligned} \frac{R_{u,n\%}}{\gamma H_{m0}} &= c_0 \cdot \xi_{m-1,0} \quad \text{for} \quad \xi_{m-1,0} \leq p \\ \frac{R_{u,n\%}}{\gamma H_{m0}} &= c_1 - \frac{c_2}{\xi_{m-1,0}} \quad \text{for} \quad \xi_{m-1,0} \geq p \end{aligned} \tag{2.4}$$

where $c_2 = 0.25 \, \frac{c_1^2}{c_0}$ and $p = 0.5 \, \frac{c_1}{c_0}$. In Table 2.2 the empirical coefficients are shown for different values of n. Hughes (2008) stated that both formulas give estimates that fall within the scatter of the 2% run-up data. Therefore, both formulas give reasonable values to base the overtopping flow parameters on. In this thesis, it is opted to use the above-stated approach of calculating the run-up using the formulas of van der Meer (2002) as stated in the Eurotop Manual (2016).

Table 2.2: Coefficients for wave run-up predictions, using H_{m0} and $T_{m-1,0}$ (van Gent, 2002b)

n	c_0	c_1
1	1.45	5.1
2	1.35	4.7
10	1.10	4.0

Influence of roughness and permeability on the run-up height

Molines and Medina (2015) studied roughness factor γ_f to determine the influence of the armour unit geometry, the number of layers in the armour and the structural characteristics. These parameters have an influence on the amount of dissipation of the wave energy and hence on the run-up height. It was stated that the single-layer placement of cubes generates a higher roughness factor and therefore higher overtopping discharges than a double-layer system. They used the data from the CLASH-Project (Pearson et al., 2004) to find the roughness factors with their rMSE. For single-layer cubes, $\gamma_f = 0.53$ with a rMSE of 16.9% was found. This is a larger value of γ_f as Bruce et al. (2009) determined for a single-layer system ($\gamma_f = 0.49$). This difference can be explained by model and scale effects. In this thesis, the conservative value of $\gamma_f = 0.53$ will be used. Note that this value is solely applicable for the outer slope considering the source of the data.

Concerning the wave run-up height, the core permeability does not play a significant role in the case of rock armour rubble mound breakwaters (van Broekhoven, 2011). It was stated that the reduction of the run-up height was entirely caused by the dissipation of energy in the pores of the armour layer. This conclusion is not valid for the prolongation of the volume on top of the breakwater.

Run-up probability distribution

It is assumed that the wave run-up distribution is equal to the wave height distribution at the toe of the breakwater. This distribution is fairly dependent on the bathymetry of the foreshore, nevertheless generally speaking a Rayleigh distribution for the run-up heights can be assumed (van der Meer and Janssen, 1994).

2.1.2 Wave propagation on top of the crest

Once this run-up height is larger than the crest height the volume passes the outer crest line. The term 'overtopping' refers to this process. The overtopping characteristics are partly described by the wave run-up height. On top of the crest, the wave tongue will propagate from the outer edge line to the edge of the lee side slope (Figure 2.5). During this propagation, layer thicknesses and velocities of the wave tongue will alter due to friction and infiltration. The spatial distribution is discussed in this subsection.

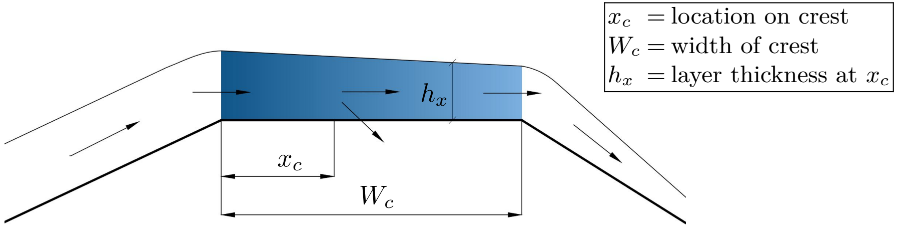

Figure 2.5: Wave tongue on top of the crest

Seaward crest line

It is evident that the overtopping wave tongue on the crest starts at the seaward side. On top of the crest, at the outer crest line, the parameters can be described as follows (Schüttrumpf, 2001) (van Gent, 2002b):

$$\frac{h_{n\%}(x_c = 0)}{H_{m0}} = c'_{h,n\%} \cdot \left(\frac{R_{u,n\%} - R_c}{\gamma_f H_{m0}}\right) \tag{2.5}$$

$$\frac{u_{n\%}(x_c = 0)}{\sqrt{gH_{m0}}} = c'_{u,n\%} \cdot \left(\frac{R_{u,n\%} - R_c}{\gamma_f H_{m0}}\right)^{0.5} \tag{2.6}$$

$$\frac{q_{n\%}(x_c = 0)}{\sqrt{gH^3_{m0}}} = c'_{q,n\%} \cdot \left(\frac{R_{u,n\%} - R_c}{\gamma_f H_{m0}}\right)^{1.5} \tag{2.7}$$

Where:

$h_{n\%}$ = peak layer thickness exceeded by n % of the incident waves (m)
$u_{n\%}$ = peak velocity exceeded by n % of the incident waves [m/s]
$q_{n\%}$ = peak flow exceeded by n % of the incident waves [m^2/s]
R_c = crest height [m]
x_c = distance from seaward edge of the crest [m]
$c'_{h,n\%}$ = empirical coefficient [-]
$c'_{u,n\%}$ = empirical coefficient [-]
$c'_{q,n\%}$ = empirical coefficient [-]

Trung (2014) re-analysed the data from the tests of van Gent (2002b) and found the following formulas:

$$\frac{h_{n\%}(x_c = 0)}{H_{m0}} = c'_{h,n\%} \frac{V_{n\%} \cdot sin\alpha}{R_{u,n\%} - R_c} \tag{2.8}$$

$$\frac{u_{n\%}(x_c = 0)}{\sqrt{gH_{m0}}} = c'_{u,n\%} \cdot cos\alpha \sqrt{\frac{gV_{n\%}}{\sin\alpha H_s}} \tag{2.9}$$

with $V_{n\%}$ as the overtopping volume exceeded by n% of the *overtopping* waves and α the outer slope angle. Different values for $c'_{h,n\%}$, $c'_{u,n\%}$ and $c'_{q,n\%}$ can be found in the literature for $n = 2$. An overview is given in table 2.3.

Table 2.3: Studies on describing overtopping parameters

	Schuttrumpf (2001)	**van Gent[1](2002)**	**Bosman et. al. (2008)**	**van der Meer et. al. (2010)**	**Trung (2014)**
Dataset	Schuttrumpf (2001)	van Gent (2002)	Schuttrumpf (2001) + van Gent (2002)	Schuttrumpf (2001) + van Gent (2002) + Flowdike, Lorke et. al. (2009)	van Gent (2002)
Slope	1:6	1:4	1:4-1:6	1:3-1:6	1:4
γ_f	1	1 and 0.5	1	1	1 and 0.5
$\frac{h_{n\%}(x_c=0)}{H_{m0}}$	$c'_{h,n\%}\cdot\left(\frac{R_{u,n\%}-R_c}{\gamma_f H_{m0}}\right)$				$c'_{h,n\%}\cdot\frac{V_{n\%}\cdot sin\alpha}{R_{u,n\%}-R_c}$
$\frac{u_{n\%}(x_c=0)}{\sqrt{gH_{m0}}}$	$c'_{u,n\%}\cdot\left(\frac{R_{u,n\%}-R_c}{\gamma_f H_{m0}}\right)^{0.5}$				$c'_{u,n\%}\cdot cos\alpha\sqrt{\frac{gV_{n\%}}{\sin\alpha H_s}}$
$c'_{h,2\%}$	0.33	0.15	$9\cdot10^{-3}/\sin^2\alpha$	0.13	1.1
$c'_{u,2\%}$	1.37	1.3	$0.30/\sin\alpha$	$0.35\cot\alpha$	0.88

[1] Run-up formula used of van Gent (2001)

With $q_{n\%} = u_{n\%}\cdot h_{n\%}$, the flow coefficient of Bosman et al. (2008) is $c'_{q,2\%} = c'_{u,2\%}\cdot c'_{h,2\%} = \frac{2.7\cdot10^{-3}}{sin^3(\alpha)}$.

Hughes (2015) suggests the following empirical formulas for the description of the discharge and velocity linked to a single volume:

$$q_{peak} = 7.405\cdot\frac{V\sqrt{\tan\alpha}}{T_{m-1,0}} \tag{2.10}$$

$$u_{@qpeak} = 25.99\cdot\frac{\sqrt{V\tan\alpha}}{T_{m-1,0}} \tag{2.11}$$

These equations are based on the Flowdike 1 and Flowdike 2 (Lorke et. al., 2009) results. A distinction was made between the peak velocity found, and the velocity found at the moment of peak discharge.

Hughes et al. (2012) studied the progress in time of the individual parameters at $x_c = 0$. The development of the parameters can be schematized as a linear or exponential decrease, as it starts at a maximum value of the parameter. The course of the overtopping parameters in time can be described as (Hughes, 2011) :

$$h(t) = h_{max}\left(1-\frac{t}{T_{ovt}}\right)^n \quad \text{for} \quad 0\le t\le T_{ovt} \tag{2.12}$$

$$u(t) = u_{max}\left(1-\frac{t}{T_{ovt}}\right)^m \quad \text{for} \quad 0\le u\le T_{ovt} \tag{2.13}$$

$$q(t) = q_{max}\left(1-\frac{t}{T_{ovt}}\right)^{n+m} \quad \text{for} \quad 0\le q\le T_{ovt} \tag{2.14}$$

Using m=n=1 the schematized course is shown in Figure 2.6 per single wave.

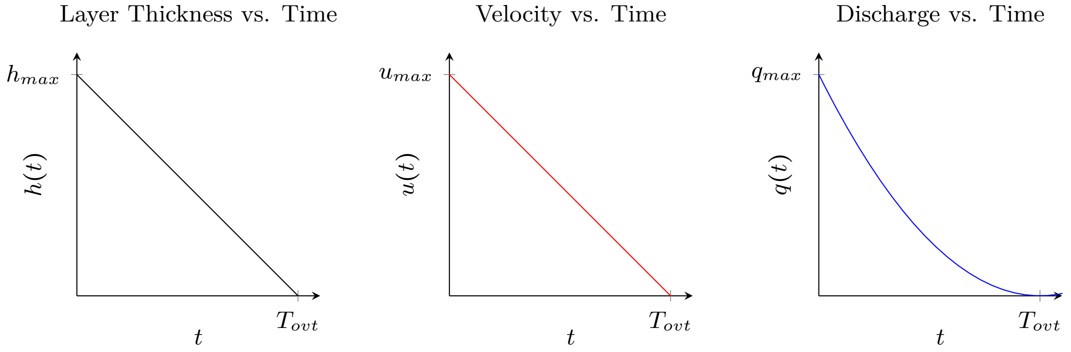

Figure 2.6: Idealised overtopping flow parameters in time (Hughes, 2011)

The total duration of the overtopping wave at the outer crest line could be described by Equation 2.15 (Bosman et al., 2008).

$$\frac{T_{ovt,n\%}(x_c = 0)}{T_{m-1.0}} = c'_{T,n\%} \cdot \left(\frac{R_{u,n\%} - R_c}{\gamma_f H_{m0}} \right)^{0.5} \tag{2.15}$$

On top of the breakwater crest

On top of the crest, the water volume infiltrates, spreads and flattens out. Schüttrumpf (2001) developed formulas with exponential factors to describe the spatial changes of the layer thickness and velocities along the crest for dykes, therefore infiltration and roughness are not included (although a friction factor is incorporated in the formulas).

$$\frac{h_{n\%}(x_c)}{h_{n\%}(x_c = 0)} = c_{trans,h} \cdot \exp\left(-c''_{h,n\%} \cdot \frac{x_c}{\gamma_c L_0} \right) \tag{2.16}$$

$$\frac{u_{n\%}(x_c)}{u_{n\%}(x_c = 0)} = \exp\left(-c''_{u,n\%} \cdot \frac{x_c}{\gamma_c h_{n\%}(x_c)} \right) \tag{2.17}$$

where:

$c_{trans,h}$ = influence due to transition from outer slope to crest [-]
γ_c = friction factor on the crest (=1 for a smooth surface) [-]
L_0 = deep water wave length [m]

with for both regular and irregular waves and $n = 2$: $c_{trans,h} = 0.81, c''_h = 6$ and $c''_u = 0.042$. These equations are valid for $0.03 < x_c/L_0 < 0.3$ (Bosman, 2007). Trung (2014) suggested $c''_{h,2\%} = 2.24$, $c_{trans,h} = 1$ and $c''_{u,2\%} = 1.82$. Van der Meer et al. (2016) suggests the decay of the flow velocity along the crest for smooth impermeable structures as given below:

$$\frac{u_{2\%}(x_c)}{u_{2\%}(x_c = 0)} = \exp\left(-\frac{1.4 x_c}{L_{m-1,0}} \right) \tag{2.18}$$

For an impermeable and smooth crest the overtopping duration on a certain location on the crest can be described by (Bosman et al., 2008):

$$\frac{T_{ovt,n\%}(x_c)}{T_{ovt,n\%}(x_c = 0)} = \left(1.67 + 0.24 \log\left(\frac{x_c}{L_0} \right) \right) \tag{2.19}$$

Velocities and air entrapment in the wave tongue. In overtopping waves rushing over the crest, numerous different velocities can be defined (Figure 2.7). A distinction can be made between the front velocity of the overtopping wave and the inner velocities, such as the bottom velocity, mean velocity and characteristic velocity (Verhagen et al., 2003).

The overtopping wave tongue has a high percentage of entrained air (Hughes, 2011). This air plays a role for the impulse generated by an impinging jet at the rear side, discussed in the next subsection.

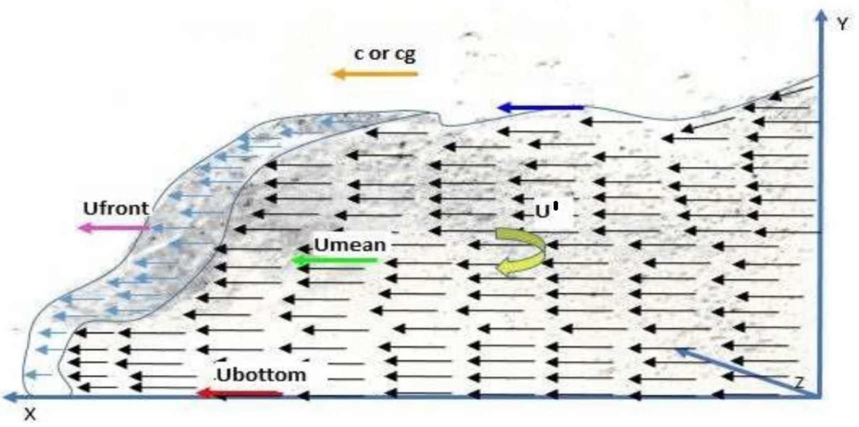

Figure 2.7: Velocities in a wave tongue (Coticone, 2015)

Friction and Infiltration. Although there is a factor included in the formulas for the friction on top of the crest, little is known about the value of that factor. Trung (2014) suggested different values for the influence of the friction on the water layer thickness and velocity of the wave tongue. On the crest, values of the friction factors were found of respectively 0.9 and 0.7 for grass slopes. Especially with permeable structures, this value can be of great significance due to infiltration of the water. The infiltrated volume does not reach the lee slope and can therefore not contribute to the external hydraulic loads on the lee-side armour layer.

Verhagen et al. (2004) focussed on the wave overtopping volume infiltration at the crest at rubble mound breakwaters, in relation to the crest width. The conclusion was that a considerable part of the overtopping volume infiltrates in the breakwater and does not damage the rear slope. The magnitude of this infiltrated volume is hard to determine and differs per armour type and filter layer.

Rear crest line

The crest has an influence on the water layer thickness and velocity on the edge of the crest and the rear slope. In the research of van Gent (2002a) solely the crest lee side edge was investigated, hence the formulas are valid at $x_c = W_c$:

$$\frac{h_{n\%}(x_c = W_c)}{H_{m0}} = c'_{h,n\%} \cdot \left(\frac{R_{u,n\%} - R_c}{\gamma_f H_{m0}} \right) \tag{2.20}$$

$$\frac{u_{n\%}(x_c = W_c)}{\sqrt{gH_{m0}}} = c'_{u,n\%}(\gamma_{f-c})^{0.5} \cdot \left(\frac{R_{u,n\%} - R_c}{\gamma_f H_{m0}} \right)^{0.5} / \left(1 + c''_u \frac{W_c}{H_{m0}} \right) \tag{2.21}$$

$$\frac{q_{n\%}(x_c = W_c)}{\sqrt{gH_{m0}^2}} = c'_{q,n\%}(\gamma_{f-c})^{0.5} \cdot \left(\frac{R_{u,n\%} - R_c}{\gamma_f H_{m0}}\right)^{1.5} / \left(1 + c''_q \frac{W_c}{H_{m0}}\right) \tag{2.22}$$

In Table 2.4 the empirical coefficients are shown. The formulas assume a crest width larger than the wave height ($W_c > H_{m0-toe}$).

Table 2.4: Coefficients for the rear side of the crest (van Gent, 2002a)

Parameters	c'	c"	σ
$h_{2\%}$	0.1	-	0.0095
$u_{2\%}$	1.7	0.1	0.1075
$q_{2\%}$	0.17	0.1	0.0117

2.1.3 Waves at the rear slope

At the rear slope, two main flow mechanisms can be distinguished: the flow can either detach from the crest and generate an impinging jet or it can follow the outer dimensions of the breakwater and stay attached to the slope as displayed in Figure 2.8. Both mechanisms differ substantially in the forces they exert on the revetment.

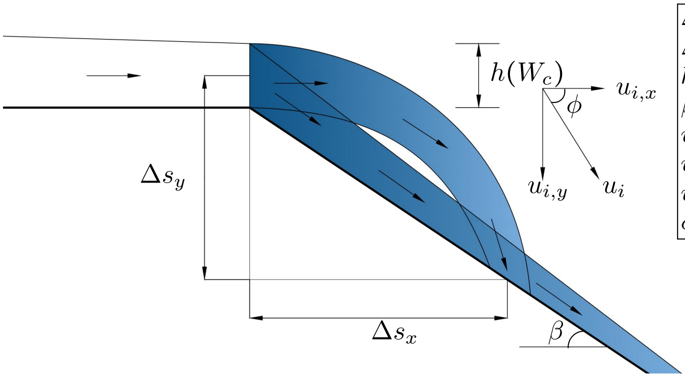

Δs_x = horizontal distance from crest line
Δs_y = vertical distance from crest line
$h(W_c)$ = layer thickness at $x = W_c$
β = rear slope angle
u_i = velocity of impinging jet
$u_{i,x}$ = horizontal velocity of impinging jet
$u_{i,y}$ = vertical velocity of impinging jet
ϕ = angle of incidence

Figure 2.8: Attached and detached tongue at the rear slope

Perpendicular flow

The values of the hydraulic parameters at the rear crest line are boundary conditions for the layer thickness and velocities of the wave tongue on the rear slope. The basis for the description of the wave tongue at the rear slope is the one-dimensional stationary shallow water equation (2.23).

$$u\frac{du}{ds_B} + g\left(cos\phi\frac{dh}{ds_B} - sin\phi\right) + \frac{1}{2}f_L\frac{u^2}{h} = 0 \tag{2.23}$$

where:

u = Depth-averaged velocity along the slope [m/s]
h = Water-layer thickness perpendicular to the slope [m]
ϕ = Slope angle [°]
f_L = Characteristic friction along the inner slope [-]

With the assumption that $| \frac{dh}{ds} | \ll tan(\phi)$ and $h = q/u$. The discharge is taken constant and specified at the crest as $q = h_0 \cdot u_0$. Substituting $\alpha = \sqrt[3]{g \sin\phi}$ and $\beta = \sqrt[3]{\frac{1}{2}\frac{f_L}{h_0 u_0}}$ the equation can be written as (van Gent, 2002b):

$$u\frac{du}{ds_B} - \alpha^3 + \beta^3 u^3 \approx 0 \tag{2.24}$$

Suggesting a slow variation ($\mid u\frac{du}{ds_B} \mid \ll \beta^3 u^3$) implies $u = \alpha/\beta + u'$ with $\mid u' \mid \ll \alpha/\beta$. With linearisation the solution for the wave-layer thickness and velocity along the slope can be found (van Gent, 2002b).

$$u_{n\%}(s_B) = \frac{\alpha}{\beta} + \mu \exp\left(-3\alpha\beta^2 s_B\right) \tag{2.25}$$

$\mu = u_0 - \frac{\alpha}{\beta}$ and s_B is the coordinate along the rear slope. f_L is the influence factor of the friction on the inner slope. For a smooth surface $f_L = 0.005$. For $s_B \to \infty$:

$$\lim_{s_B \to \infty} u_{n\%}(s_B) = \sqrt[3]{\frac{2 \cdot g \cdot h_0 \cdot u_0 \cdot sin\beta}{f_L}} \tag{2.26}$$

With the continuity equation:

$$h_{n\%}(s_B) = \frac{h_{n\%}(s_B = 0) \cdot u_{n\%}(s_B = 0)}{u_{n\%}(s_B)} \tag{2.27}$$

The standard deviations of the differences between measured and calculated (non-dimensional) parameters $h_{2\%}$, $u_{2\%}$ and $q_{2\%}$ at the inner slope are respectively $\sigma = 0.008$, $\sigma = 0.139$ and $\sigma = 0.018$ (van Gent, 2002b).

These formulas are derived using the continuity equation, hence the water volume is kept constant. This is valid for impermeable slopes. Presumably, this assumption of a constant volume is not valid on permeable structures. Therefore these formulas are highly theoretic and perhaps not applicable at a permeable rubble mound breakwater. The same holds for the formula of Trung (2014). He suggested the following equation:

$$\frac{h_{n\%}(s_b)}{h_{n\%}(x_c = B)} = \exp\left(c'''_{h,n\%}\frac{y_c}{\tan\beta L_{m-1,0}}\right) \tag{2.28}$$

$$\frac{u_{n\%}(s_b)}{u_{n\%}(x_c = B)} = \left(1 + c'''_{u,n\%}\frac{y_c}{\tan\beta L_{m-1,0}}\right) \tag{2.29}$$

Using $c'''_{h,2\%} = -5.4$ and $c'''_{u,2\%} = 2.82$.

Jet impact

Kudale and Kobayashi (1996) describe a situation with a detachment of the wave tongue at the edge of the crest and an impinging water jet at the inner slope. With the assumption that the jet is a quasi-steady jet falling freely due to gravitational acceleration, the jet can be described as the detached jet as shown in Figure 2.8. With:

$$u_{i,x} = u(W_c) \tag{2.30}$$

$$\Delta s_x = g^{-1}\left(u^2 \tan\beta + \left(u^4 \tan^2\beta + ghu^2\right)^{1/2}\right) \tag{2.31}$$

$$\Delta s_y = \Delta x \tan\beta + \frac{h}{2} \tag{2.32}$$

$$u_{i,y} = \frac{g\Delta x}{u} \tag{2.33}$$

$$u_i = \left(u_{i,x}^2 + u_{i,y}^2\right)^{1/2} \tag{2.34}$$

The study of Verhagen et al. (2003) likewise concluded that the volume can separate from the slope and create a plunging jet. Ponsioen (2016) investigated the loads on a dike innerslope and concluded that a jet was visible. The so called Wave Impact Approach was elaborated for grass covered dikes.

2.1.4 Wave overtopping probability

Even though a breakwater is low-crested, not all incoming waves have a run-up height that is larger than the crest height. Victor et al. (2012) found a relation between the probability that a wave is an overtopping wave and the (steep) slope angle, wave height and wave run-up:

$$P_{ow} = \exp\left(-\left((1.4 - 0.3\cot\alpha)\frac{R_c}{H_{m0}}\right)^2\right) \tag{2.35}$$

The friction on the outer slope is not incorporated in this formula. In this study the formula of van der Meer and Janssen (1994) will be used which results in lower overtopping probabilities:

$$P_{ow} = \exp\left[-\left(\frac{1}{\chi}\frac{R_c}{H_{m0}}\right)^2\right] \tag{2.36}$$

Where,

$$\chi = \frac{R_{u,2\%}}{H_{m0}}\frac{1}{\sqrt{-\ln(0.02)}} \approx 0.51\frac{R_{u,2\%}}{H_{m0}} \tag{2.37}$$

Hence the number of overtopping waves in a certain test with N_w incoming waves is $N_{ow} = N_w \cdot P_{ow}$.

Average overtopping flow

The average flow of overtopping waves is an important design parameter (van der Meer and Bruce, 2014) and can be described for low-crested slopes as follows (Victor, 2012):

$$\frac{q}{\sqrt{g \cdot H_{m0}^3}} = \frac{0.023}{\sqrt{\tan\alpha}} \cdot \gamma_b \cdot \xi_{m-1,0} \cdot \exp\left[-\left(2.7\frac{R_c}{\xi_{m-1,0} \cdot H_{m0} \cdot \gamma_b \cdot \gamma_f \cdot \gamma_\beta \cdot \gamma_v}\right)^{1.3}\right] \tag{2.38}$$

With a maximum of:

$$\frac{q}{\sqrt{g \cdot H_{m0}^3}} = a \cdot \exp\left[-\left(b\frac{R_c}{H_{m0} \cdot \gamma_f \cdot \gamma_\beta}\right)^c\right] \tag{2.39}$$

and:

$$a = 0.09 - 0.01(2 - \cot\alpha)^{2.1} \quad \text{for} \quad \cot\alpha \leq 2 \text{ and} \quad a = 0.09 \text{ for } \cot\alpha > 2 \tag{2.40}$$

$$b = 1.5 - 0.42(2 - \cot\alpha)^{1.5} \quad \text{maximum of b=2.35 and } b = 1.5 \text{ for } \cot\alpha > 2 \tag{2.41}$$

together with c=1.3. For Equation 2.38: $\sigma(0.023) = 0.003$ and $\sigma(2.7) = 0.20$, the factors a and b have a standard deviation of respectively $\sigma(0.09) = 0.013$ and $\sigma(1.5) = 0.15$.

Probability distribution

The probability distribution of different overtopping volumes can be described by a two-parameter Weibull distribution (Hughes et al., 2012):

$$P_V = P(\underline{V} \geq V) = \exp\left(-\left(\frac{V}{a}\right)^b\right) \tag{2.42}$$

with (non-dimensional) (Zanuttigh, 2013):

$$b = 0.73 + 55\left(\frac{q}{gH_sT_{m-1,0}}\right)^{0.8} \tag{2.43}$$

and (dimensional) (Victor et al., 2012):

$$a = 1.13 \cdot \tanh(1.32 \cdot b)\frac{q \cdot T_m}{P_{ow}} \tag{2.44}$$

Van der Meer et al. (2016) suggested:

$$a = \left(\frac{1}{\Gamma\left(1 + \frac{1}{b}\right)}\right)\frac{q \cdot T_m}{P_{ow}} \tag{2.45}$$

The scale factor a and the shape factor b play an important role in this formula. With a small value of b, relatively less small wave volumes are expected and extreme large wave volumes are plausible. The maximum wave volume is presented by (van der Meer, 1995):

$$V_{max} = a \cdot (\ln(N_{ow}))^{1/b} \tag{2.46}$$

2.2 Armour Stability

Large numbers of different types of revetment are applied on breakwaters. The stability of these revetment types at the front slope is investigated extensively, in contrast to the rear side where limited studies are performed. The stability mechanisms of all those revetment types are very dependent on the type of armour units used. Most of the clay dykes in The Netherlands are covered with grass on the crest and land side. The inner slopes of breakwaters are usually covered with the same material as installed on the front side.

This section starts with the examination of the main topic of this research: rear slope concrete armour. Subsequently, studies on the stability of front slope concrete armour are evaluated. Next, the rear slope stability of rock armour breakwaters is discussed, elaborating the hydraulic forces on a single rock and the proposed stability formulas. Lastly, dykes are elaborated, where possibly the proposed load formulas using the excess of velocity/stress/work could likewise be applicable to rear slope concrete revetment.

2.2.1 Concrete units

Different concrete units can be used as armour layer for rubble mound breakwaters. A division can be made between their stability mechanisms. Some units rely on interlocking for their stability, some use mutual friction and others use their own weight for their overall stability. The number of layers of the revetment units is of great importance as well. This is normally one or two layers thick. For single-layer interlocking units such as Xblocs, no design formulas for the rear side are available (Delta Marine Consultants, 2014).

Concrete cubic armour layer at the rear slope

In the study of Hellinga (2016), the rear slope stability parameters were altered to find their influence on the stability of the rear slope armour layer. The main conclusions are listed below:

Freeboard: It is likely that although a large freeboard reduced the overtopping volume, more damage is found due to the larger exposure of the rear slope revetment to impinging jets. (Figure 2.9)

Rear slope angle: Differences between the tested 1:2 and 2:3 slopes were not found, suggesting the slope angle (in this range) is of minor influence on the stability.

Packing density: The packing density is of large importance. No optimal values are concluded in this thesis.

Cube dimension: During tests, the stability of the rear slope cubes appeared to be much higher than predicted with the formulas used for rock armour layers. Hence, no failure was seen during the initial tests.

Cube placement: The influence of the underlayer turned out the be very significant. Large irregularities in the underlayer cause protruding cubes, these units were more likely to fail when exposed to overtopping waves.

Minimum rows below SWL: For a maximum of 4 cubes below the mean water level damage can be found, suggesting the extension of the cube revetment parallel to the slope for a minimum of 4 cubes below the water level is required.

The study did not succeed in relating the extreme front velocities in combination with overtopping volumes to certain damage levels. The collected data relating sea state and overtopping volume did not provide a clear relationship or pattern. The stability numbers found were in the rather large range of 3.8 (low packing densities) up to 6.6 (steep waves), although with very little confidence. This could be caused by some complications of the set-up (ie. relative large front cube size and too small volume buckets at the rear crest). Several recommendations were given. To acquire a valid design formula, small subsequent steps between different parameter values should be used. This aids to find the exact start of damage. The transmission was not taken into account during these experiments. It is not clear whether this is relevant for the stability relations. To understand the complex mechanism of overtopping volumes more research in this topic is recommended. The rear edge transition between the crest and the rear slope appeared to be an important design aspect. Erosion of the transition could cause local failure.

As mentioned before, little is known about the stability of breakwater rear slopes with a single-layer concrete unit armour layer. Hellinga (2016) investigated the stability of breakwater rear slopes with a single-layer concrete armour layer. This study is elaborated in Chapter 4.

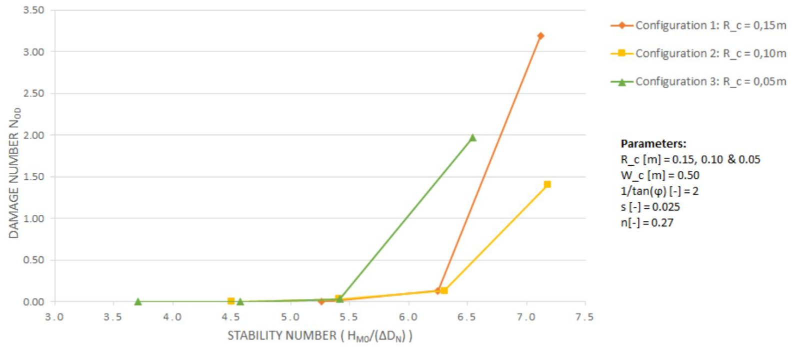

Figure 2.9: Relation between stability and freeboard (Hellinga, 2016)

Concrete cubic armour layer at the front slope

Van Gent et al. (2001) and Van Gent and Luis (2013) listed important parameters influencing the stability of single-layer cubic revetment:

Packing density This research focusses on single-layer concrete cubes placed in a stretching bond. The most favourable packing density for a single-layer cubic armour layer is $n = 0.28$ (van Buchem, 2009), which is in line with the conclusion from Van Gent et al. (2002) stating the placing density should be between 0.25 and 0.30. This packing density is lower compared to the packing density of placed block revetment, hence water can flow more easily through the armour layer compared to placed block revetment (shorter leakage length).

Placement pattern A stretching bond increases the wave height at which initial damage occurs compared with an irregular pattern.

Filter layer A size ratio of $D/D_{n50,f} = 1.8$ is preferred. A larger $D_{n50,f}$ will lead to more irregularities, where a smaller filter layer could wash out.

Crest level Wave action will cause the cubes to settle. At the transition with the crest and the slope, a (weak) gap will arise. With a higher crest level, this gap will be less exposed to incoming waves.

Toe The toe is essential for the support of the armour layer. Especially with single-layer cubes, the forces of the weight is for a large part transferred to the toe.

This section treated the stability parameters, where the damage of the single-layer armour layer is discussed in section 2.3.

Stability of placed block revetment

Looking at the stability of placed block revetment on a dike, significant pressure differences above and below the blocks during an impacting wave can be found. These pressure differences reduce quickly using lower placement densities, as used with single-layer cube revetment. A load comparison can be made in the case of a protruding unit. Figure 2.10 shows the loads on a protruding block on a rear slope, indicating the significant pressure differences induced by the elevation. Klein Breteler et al. (2014b) suggested the following stability equation for placed block revetment at the wave run-up zone at the front slope:

$$\Delta D > \frac{2(R_{u,2\%} - R_c)(d_b - 0.11D)}{B(\cos\alpha - 0.5\sin\alpha)} \tag{2.47}$$

With B the width of the block and d_b as the maximum unevenness; the vertical difference between two adjoined blocks. This formula indicates that if the elevation of a stone is smaller than $0.11D$ it has no effect on the stability.

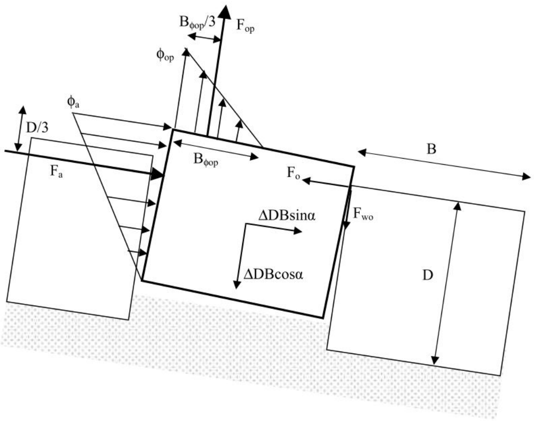

Figure 2.10: Forces on a protruding single-layer cubic block (Kuiper et al., 2006)

Assuming the failure of placed revetment occurs in the section with ill-placed blocks, only a small group of blocks can be considered. Hence, studies on the stability of the placed revetment should focus on the ill-placed areas. The duration of the loads is important for materials with large creep behaviour such as asphalt. This creep is negligible at placed blocks without any sludge or clay in the joints (Coeveld and Klein Breteler, 2003).

2.2.2 Placed revetment

A placed block revetment can be considered as a relatively smooth and impermeable slope (Klein Breteler et al., 2014b). The similarities between this type of armour and single-layer cube revetment are the shape and the fact that it is placed in a single-layer. Because the units are placed close together, large pressure differences can occur in contrary to cubic blocks revetment with much shorter leakage lengths. Due to this relatively smooth surface, flow forces have little influence on the dimensioning of the top layer. Figure 2.11 shows the wave load on place revetment. Large differences are seen in upwards and downwards forces due the pressure differences over the top layer (Figure 2.11), which influences the stability (Klein Breteler et al., 2014a).

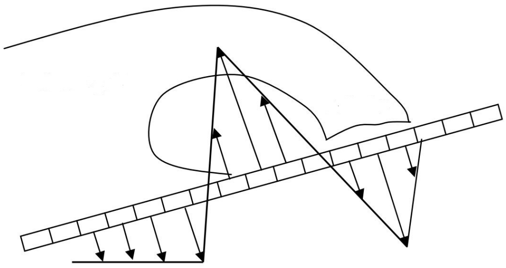

Figure 2.11: Wave load (Coeveld and Klein Breteler, 2003)

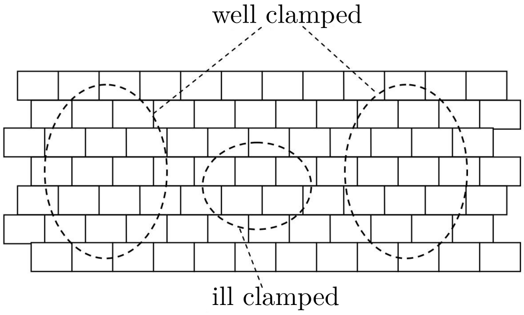

Figure 2.12: Ill and well clamped areas (Coeveld and Klein Breteler, 2003) (/textbfnog een vertaling bij)

The amount of clamping of a certain dyke section also differs per area, some parts are well clamped and other parts are poorly clamped (Figure 2.12). This influences the top-layer stability.

Top-layer failure mechanisms

The pressure differences can cause three main failure mechanisms (Coeveld and Klein Breteler, 2003):

Z-profile Due to the high shear forces in the top layer generated by the pressure differences, mutual shifting of blocks can take place. This causes the creation of a Z-profile as seen in Figure 2.13a.

Buckling-mechanism Likely to happen in the well-clamped area instead of failure due to Z-profile. Buckling (Figure 2.13b) creates extra normal forces hence interaction increases between the stones (Peters, 2003). Therefore, it is not likely a long row of blocks shifts upwards like a piston.

Piston-mechanism Presumable failure mechanism with ill clamped blocks (Figure 2.13c)

2.2.3 Rock armour breakwater

A rock armour breakwater has more similarities with a cubic armoured breakwater as a clay dyke with respect to roughness and permeability. On the other hand, rocks behave differently than single-layer cubes because of the lack of coherence between the units. Nonetheless, a comparison can be made.

Due to the short leakage lengths, porous flow is of minor importance compared to external flow forces on the stability of rock top-layer on the front side (Schiereck, 2012). The most likely location of damage of the revetment on the rear side is around the water level (Verhagen et al., 2003); The stability of the revetment blocks decreases due to the buoyancy of the water. Further below the waterline the dampening effect of the water against the impinging jet is predominant. Therefore, the damage decreases rapidly with the water depth (Verhagen et al., 2003).

Flow forces on a single rock-unit at the rear slope

The forces on a single rock on the lee side of an overtopped breakwater are distinguished as follows (Kudale and Kobayashi, 1996):

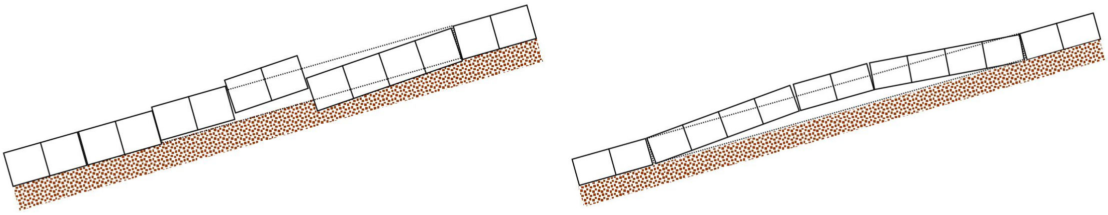

(a) Z-Profile *(b) Buckling-mechanism*

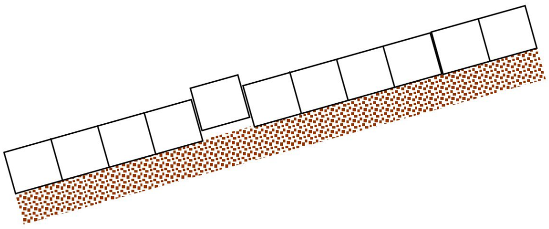

(c) Piston-mechanism

Figure 2.13: Failure mechanisms of placed revetment (Coeveld and Klein Breteler, 2003)

Drag Force:
$$F_D = \frac{1}{2}\rho C_D C_2 (d)^2 u_i^2 \tag{2.48}$$

Lift Force:
$$F_L = \frac{1}{2}\rho C_L C_2 (d)^2 u_i^2 \tag{2.49}$$

Inertia Force:
$$F_I = \rho C_M C_3 (d)^3 \frac{du_i}{dt} \tag{2.50}$$

Where,

$\rho =$ fluid density which is assumed constant

C_D, C_L and $C_M =$ drag, lift, and inertia coefficients

C_2 and $C_3 =$ area and volume coefficients of the armour unit

$d =$ characteristic length of the armour unit

$\frac{du_i}{dt} =$ acceleration of the impinging water

Using the water velocity and depth of the overtopping flow a hydraulic stability model for armour units of the lee side slope was developed, shown in the next subsection.

Stability formulas for rock revetment at the rear slope

The following stability formula is introduced using the stability number $N_s = H_S/\Delta D_{n,50}$ and normalised impinging jet velocity $u_i^* = u_i/\sqrt{gH_s}$ (Kudale and Kobayashi, 1996):

$$N_s \quad \leq \quad N_R = \frac{2C_3^{2/3}\sin(\theta-\beta)}{C_2 u_i^* 2[C_L \sin\theta + C_D \cos(\theta+\phi-\beta)]}\left[\frac{C_M}{\Delta}+1\right] \tag{2.51}$$

Where,

$\phi =$ angle of jet incidence

$\theta =$ angle of repose of armour units

The velocity of overtopping waves is used in the description of the stability of the individual rock armour. The slope angle and incident wave angle were added to the formula of Nederpel (2002), relating the velocity of the overtopping volume and the stability of the rock armour units (Verhagen et al., 2003):

$$\Theta_{u_{char\|},R_c,\beta,i} = \frac{(u_{char}\cos(\phi-\beta))^2}{\Delta g D_{n50}} \frac{R_c}{D_{n50}} \sin(\beta)\sqrt{N_w} \tag{2.52}$$

The characteristic velocity (u_{char}) is the time averaged velocity on the crest during the plunge of the wave. A study by van Gent and Pozueta (2004) suggested the following formula based on hydraulic model tests using a given damage level S:

$$D_{n50} = 0.008\left(\frac{S}{\sqrt{N_w}}\right)^{-1/6}\left(\frac{u_{1\%}T_{m-1,0}}{\Delta^{0.5}}\right)(\cot\beta)^{-2.5/6}(1+10\cdot\exp(-R_c/H_{m0}))^{1/6} \tag{2.53}$$

Andersen (2006) extended research at the rear slope. The found damage was linked to the flow. A dimensionless mobility parameter θ was introduced:

$$\theta = \frac{q}{\sqrt{g\cdot\Delta\cdot D_{N,50}^3}} \tag{2.54}$$

For a 1:1.25 slope limits for θ are identified from no damage to severe damage at the rear side in 4 intervals.

2.2.4 Dykes

Erosion at the land-side from wave overtopping is the leading failure mechanism of dyke breaches (Van der Meer et al., 2006). Consequently, a large number of overtopping research is executed on smooth, impermeable dykes. Those dykes are prominently constructed out of clay, with the crest and rear-side covered with a grass layer. A grass-layer with its roots in the clay has an entirely different stability mechanism than an armour layer of cubic concrete blocks. An analogy of the stability mechanisms between single-layer cubes and a grass cover is, therefore, challenging to make. Relevant for this thesis is that some studies used the threshold of motion to describe the load on a grass layer, which will be treated in this section.

Dean et al. (2010) developed a methodology using a certain threshold for the velocity, the shear stress or the flow work to describe the erosion at the land side of earthen levees, accounting for time-variant characteristics of incoming waves. The following equations were proposed, containing the cumulative addition from velocities higher than the threshold only. The formulas show respectively the dependency of erosion of velocity, velocity squared or velocity cubed:

Excess velocity:

$$E_u = \sum_{n=1}^{n} K_u\,(u_n - u_c)\,\Delta t \tag{2.55}$$

Excess shear stress:

$$E_\tau = \sum_{n=1}^{n} K_\tau (\tau_n - \tau_c) \Delta t = \sum_{n=1}^{n} K_\tau \alpha_\tau \left(u_n^2 - u_c^2\right) \Delta t \tag{2.56}$$

Excess of work:

$$E_W = \sum_{n=1}^{n} K_W (W_n - W_c) \Delta t = \sum_{n=1}^{n} K_W \beta_W \left(u_n^3 - u_c^3\right) \Delta t \tag{2.57}$$

Where,

E = erosion
N = number of overtopping waves
K = coefficient
u_c = velocity above a threshold [m/s]
τ_c = shear stress above a threshold [N/m^2]
W_c = work above a threshold [N m/s]

Hughes (2011) derived α_τ and β_W. Assuming fully turbulent open-channel flow, the shear stress can be described by:

$$\tau_0 = \frac{1}{8} \rho f_D u^2 \tag{2.58}$$

With f_D the Weisbach-Darcy friction factor and ρ the mass density of water. From Equation 2.56 it can be seen that:

$$\alpha_\tau = \frac{1}{8} \rho f_D \tag{2.59}$$

Stream power P_s is described by the shear stress times the flow velocity:

$$P_s = \frac{dW}{dt} = \tau \cdot u = \frac{1}{8} \rho f_D u^2 \cdot u = \frac{1}{8} \rho f_D u^3 \tag{2.60}$$

$$\beta_w = \frac{1}{8} \rho f_D = \alpha_\tau \tag{2.61}$$

Dean et al. (2010) concluded that the excess of work best describes the erosion. Hughes (2011) states that it is likely that the excess of work is proportional to the excess turbulent energy levels in an overtopping wave and hence the sum of the time-varying discharge above a critical discharge threshold can represent the overtopping wave:

$$W_E = \int_{T_A}^{T_B} [q(t) - q_c] dt = V_E \quad \text{for} \quad q(t) \geq q_c \tag{2.62}$$

Where W_e is the excess flow work, which is equal to V_E

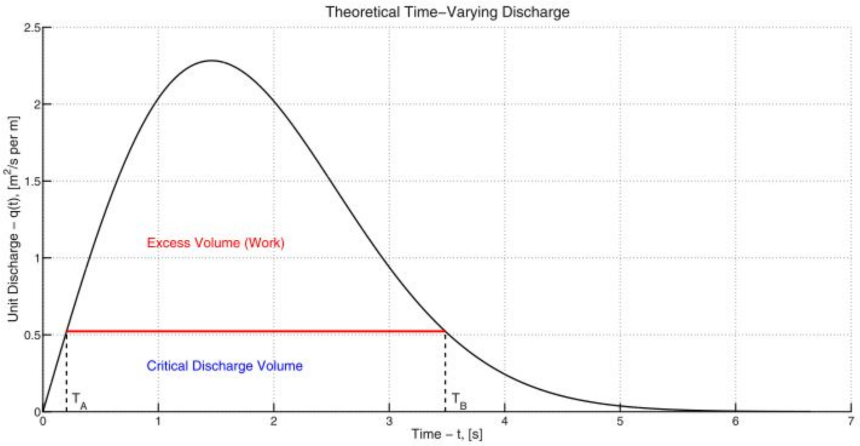

Figure 2.14: Example of excess work (volume) above the threshold discharge in overtopping wave. (Hughes and Thornton, 2016)

Contrary to previous conclusions, van der Meer et al. (2011) argued that the duration could be omitted because it has no significant influence.

2.3 Damage Description

This section discusses the different types of damage of a single-layer concrete armour layer, including their allowable magnitude before failure. Single-layer cubic revetments on a breakwater respond differently to wave impacts than rock revetment or a double top layer of concrete cubes. A single layer behaves more brittle than a double layer variant considering more reserve stability is created by the second layer of cubes. This is caused by the fact that the stability of the cubes is created by the next laying downward cube. This results in a 10 times smaller allowance of damage compared to randomly placed blocks (Van Gent and Luis, 2013).

2.3.1 Damage characterisation

Different types of damage of the armour layer can be distinguished. Hofland and van Gent (2016) specified different ways to characterise the damage next to extracted and displaced units: s

- rocking of units
- rotation of units
- armour unit slumping
- toe support to the armour layer
- upward movement of the armour layer
- movement of under-layer material
- flapping of the entire top layer during the test

Focussing on the displaced units, Taveira-Pinto et al. (2015) divided several damage states: no movement at all, a balance, a single unit moved between $0.5D$ and D, a larger displacement than D (i.e. removal from the layer) and multiple units sliding with the settlement of the armour layer.

The damage can be expressed by the Damage Numbers N_d, N_{od} and N_{or}. N_d considers the total number of units moved in respect to the total number of units in a reference area. Van der Meer (1995) introduced N_{od} expressed as:

$$N_{od} = \frac{\text{Number of displaced units}}{\text{Armour layer width}/D} \tag{2.63}$$

The term N_{od} does not contain the magnitude of displacement from its original position. With parameter N_{or} Taveira-Pinto et al. (2015) describe the number of totally removed blocks from the layer. With 'remove' the displacement magnitude is larger than D.

$$N_{or} = \frac{\text{Number of removed units}}{\text{Armour layer width}/D} \tag{2.64}$$

Settlement itself only influences the stability if the settlement is uneven, therefore N_{or} could be favourable to express the damage of the slope.

In Figure 2.15 is the advancement of the damage visible, ending with complete rupture.

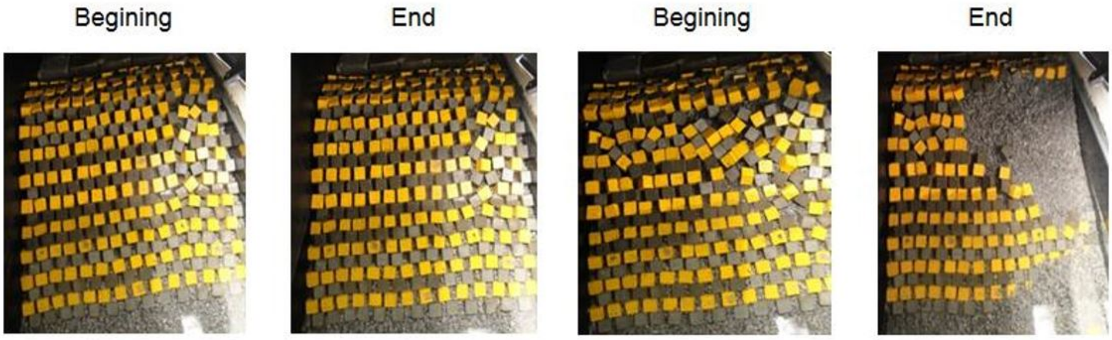

Figure 2.15: Failure examples of scale tests performed by Taveira-Pinto et al. (2015)

2.3.2 Damage criteria

The Rock Manual (CIRIA, 2007) states that failure of a revetment occurs at $N_{od} = 2$. As mentioned before, with single layer revetment the armour layer behaves brittle. Therefore, initial damage quickly leads to total collapsing and will expose the under-layer. Hence the start of the damage will be the leading value of $N_{od} = 0.2$ (CIRIA, 2007).

Chapter 3

Wave Overtopping Simulator Design

Studies in the topic of overtopping waves, especially in the stability of rear-slope revetment of levees or breakwaters, can be executed in several facilities. Prevailing methods are small-scale model tests in a flume (2D) or basin (3D). Rear-side stability studies using an overtopping simulator use a different approach (van Dijk, 2001).

The specific objective of an overtopping simulator is to simulate a representative overtopping wave on the crest and rear side of a levee or breakwater. By releasing a water volume on top of the crest, comparable loads are exerted on the structure as with the occurrence of an actual overtopping wave. In this way, the stability of certain components of the structure can be studied.

In this study, an entirely new small-scale overtopping simulator is developed: the Wave Overtopping Simulator (WOS). This chapter gives an introduction to overtopping simulators in general and elaborates the design and application of the WOS.

3.1 Introduction to Overtopping Simulators (OS)

There are several reasons to use an overtopping simulator in overtopping stability studies. The advantages and disadvantages are discussed below, where some arguments are applicable to this thesis and some are applicable in other situations. Next to that, reference studies where an overtopping simulator was used, are reviewed.

3.1.1 General advantage and disadvantages of the usage of an OS

There are several advantages of using an overtopping simulator in overtopping experiments over the usage of a normal wave flume. Those advantages differ per situation and are elaborated below:

(i) Exact knowledge of magnitudes of hydraulic parameters at one point on the crest (at the orifice of the overtopping simulator)
(ii) Larger test scale feasible in the same facility
(iii) Ability to perform full-scale tests without full-scale wave flume
(iv) Possibility to execute in-situ tests

Advantages (i) and (ii) of the list above apply to this thesis.

Exact knowledge of magnitudes of hydraulic parameters

When investigating overtopping waves, large scatter can be found in the values of the hydraulic parameters describing the overtopping wave; both on model-scale as prototype scale. Starting offshore towards the lee-side of the breakwater, with every spatial step more influencing factors are involved in the propagation of the (overtopping) wave. It is hard to quantify exactly the magnitudes of those influencing factors. Hence, with the propagation of the (overtopping) wave more and more scatter is introduced in the hydraulic parameters describing the characteristics of the wave.

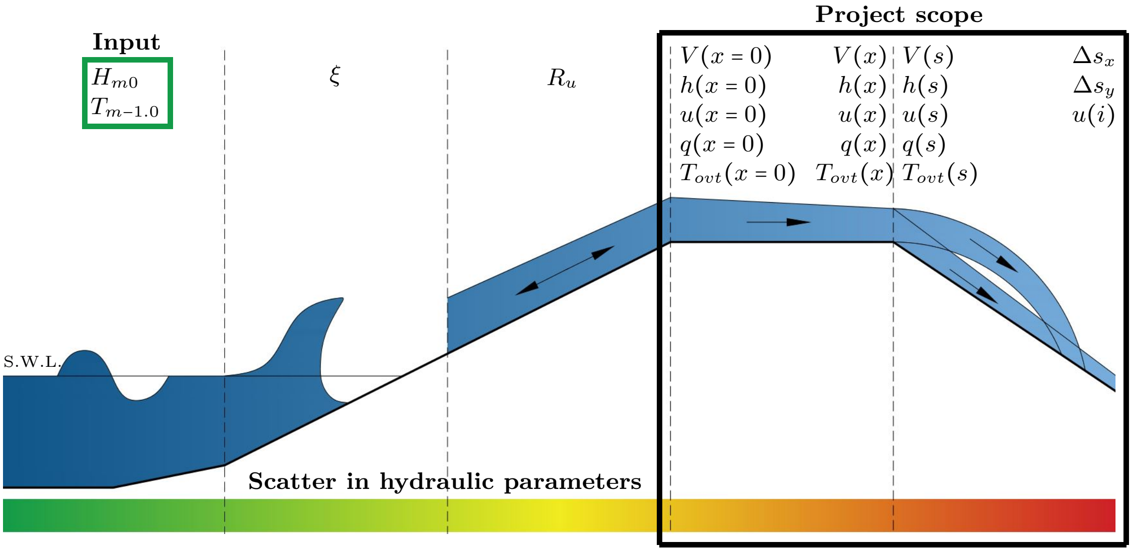
Project scope
Input
H_{m0}
$T_{m-1.0}$
ξ
R_u
$V(x=0)$
$h(x=0)$
$u(x=0)$
$q(x=0)$
$T_{ovt}(x=0)$
$V(x)$
$h(x)$
$u(x)$
$q(x)$
$T_{ovt}(x)$
$V(s)$
$h(s)$
$u(s)$
$q(s)$
$T_{ovt}(s)$
Δs_x
Δs_y
$u(i)$
S.W.L.
Scatter in hydraulic parameters

(a) Sea state as input

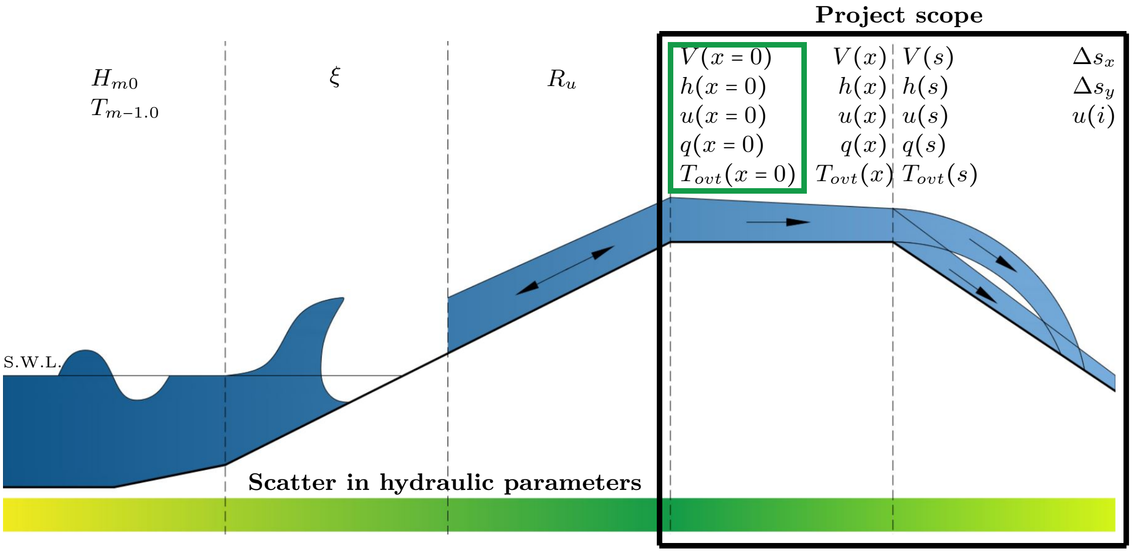
Project scope
H_{m0}
$T_{m-1.0}$
ξ
R_u
$V(x=0)$
$h(x=0)$
$u(x=0)$
$q(x=0)$
$T_{ovt}(x=0)$
$V(x)$
$h(x)$
$u(x)$
$q(x)$
$T_{ovt}(x)$
$V(s)$
$h(s)$
$u(s)$
$q(s)$
$T_{ovt}(s)$
Δs_x
Δs_y
$u(i)$
S.W.L.
Scatter in hydraulic parameters

(b) Wave characteristics at outer crest line as input

Figure 3.1: Schematization of an overtopping wave: indicating the amount of scatter in the hydraulic parameters in the project scope is less with the usage of an overtopping simulator

Figure 3.1a shows a schematization of the different stages of an overtopping wave. At the bottom, on a slightly arbitrary colour scale, the amount of variation in the hydraulic parameters describing the overtopping wave is shown. Green indicating little scatter and red indicating a large amount of scatter. When using a 'normal' wave generator in a flume, the input of the system is the sea state (indicated by the green box): the wave height, length and spectrum. The figure shows that in the scope area a larger amount of variations can be found solely due to the fact the overtopped wave is influenced by a variety of factors in front of the outer crest line.

In Figure 3.1b the same schematization is shown although the input of the system is, in this case, the wave characteristics on the outer crest line (indicated by the green box). The amount of deviation in the hydraulic parameters in the project scope is decreased by excluding (unclear) influencing factors in front of the outer crest line. This is illustrated with the colour bar.

Larger test scale feasible in the same facility

Without the requirement of an actual wave, it is possible to test larger scale waves in the same dimensioned flume. In a wave flume, the wave height is limited by the water depth. In addition, for the propagation of a wave, a minimal length of the wave flume of 3-5 wavelengths is needed to allow for adaptation of the waves to local bathymetry. Waves generated by an overtopping simulator do not need to propagate through the flume, hence lower water levels can be applied or larger waves can be generated. This increases the scale of the possible experiments, hence decreasing scaling errors in the experimental results.

Ability to perform full scale tests without full-scale flume

For testing grass dykes, it is complicated to execute scale tests as a result of the fact that grass is not scalable. Full-scale tests are therefore needed, which are expensive and require a large investment for a full-scale flume. When only interested in the wave tongue of an overtopping wave on the crest and rear side, an overtopping simulator can be an excellent alternative.

Possibility to execute in-situ tests

The strength of a grass dyke differs per location. This is partly influenced by the origin of the clay layer and the age of the dyke (Hai Trung, 2014). When executing in-situ tests, the original conditions are tested. Hence the acquired test data is more accurate.

Disadvantages

Next to the elaborated advantages, some elements are not included in tests with a simulated overtopping wave.

Turbulence. It is plausible that the turbulence in an actual overtopping wave is not similar to the turbulence in a simulated wave. Where actual waves run up the outer slope and arrive at the outer crest line with an abundance of whitewash, simulated waves are relatively laminar. The rolling movements and air entrapment in the wave tongue are hard to mimic. The magnitude and the influence of this difference are not known.

Transmission. Executing breakwater stability tests with an overtopping simulator does not include the effect of a transmitted wave through the core. However, the influence is questioned considering a large part of the wave energy gets dissipated inside the breakwater core. It goes without saying that with impermeable dykes this factor is not in question.

Link to sea state. The original goal of rear side stability tests is to link the sea state to a certain damage level. With the usage of an overtopping simulator, the steps from the sea state to the water volume parameters on top of the crest are theoretical.

3.1.2 Reference simulators

Nowadays, various different overtopping simulators are designed, build and used in stability studies on both dykes and breakwaters. Those simulators are shortly reviewed in the next subsections.

Plunge Machine (van Dijk, 2001)

The first experiments with an overtopping simulator in Fluid Mechanics Laboratory at the Delft University of Technology were executed by van Dijk (2001). This study focussed on the rear slope stability of rubble mound revetment. Hence, only the breakwaters rear slope was modelled. Another starting point was that a plunge with certain characteristics represented the hydraulic behaviour of the overtopping wave.

At the time, not many studies were executed on mutual relations and magnitudes of the plunge characteristics. The report of van Gent (2002a) was used to estimate the magnitude of the plunge parameters. Keeping in mind the sensitivity of the parameters to variations of the wave characteristics, the simulator reservoir was dimensioned with a certain oversize for the 2% wave using the formulas of van der Meer and Janssen (1994) and van Gent (2002a). As a starting point, the rock size of D_{n50} = 3 cm on the front slope was assumed.

For the generation of the plunging jet several conceptual designs of the simulator were discussed, where after one design was elaborated. The conceptual principals treated where: a chute (Figure 3.2a), a tipping hopper (Figure 3.2b), a large reservoir with a valve (Figure 3.2c) and a small reservoir with a gate (Figure 3.3). The latter was preferred because of the fact that the size of the reservoir and the size of the orifice were easily adaptable in this way. In Figure 3.3 the whole set-up used is shown.

The valve is operated by hand, but the maximum opening of the gate is limited by adjustable bolts on the inside, this ensured the right opening distance. The front velocity of the generated wave is measured on the crest by two wave height meters mounted on a rail above the set-up. In this research the influence of the crest was not included, therefore the crest of the breakwater is covered with smooth impermeable material.

The test series consisted of both single and cumulative tests on the rear slope. Where was started with the cumulative tests with the smallest wave and increasing the size of the wave until failure of the slope. The opening heights of the gate were varied with each configuration between 4 cm and 8 cm.

Dutch Overtopping Simulator (van der Meer, 2006)

Scale tests for grass dykes are hard to execute due to the simple fact that grass is not scalable. For this reason, a full-scale overtopping simulator was designed and constructed to install in-situ on top of an existing grass dyke (van der Meer (2006), van der Meer et al. (2008)).

The exact dimensions of the simulator were based on the largest wave in a storm normative to the Dutch Coast, together with the requirement that the device should be transportable. The normative storm had a wave height H_s = 2.0 m, peak period T_p = 5.7 s(wave steepness

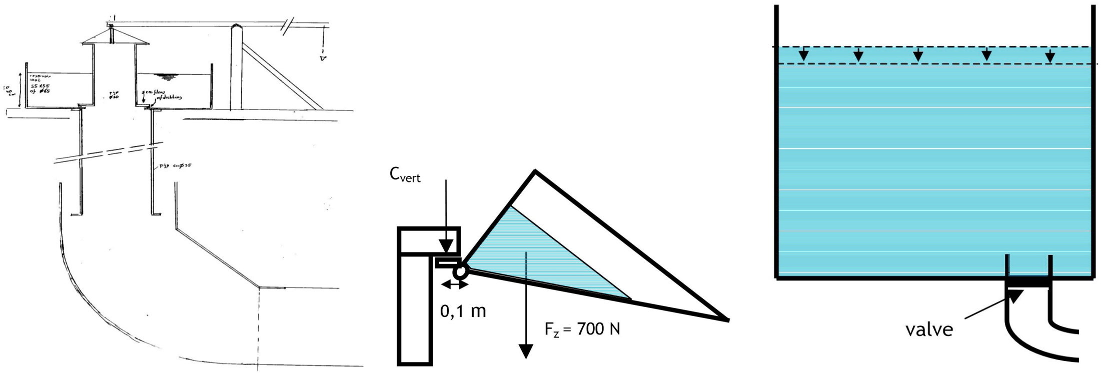

(a) Chute *(b) Tipping Valve* *(c) Valve*

Figure 3.2: Conceptual principals of van Dijk (2001)

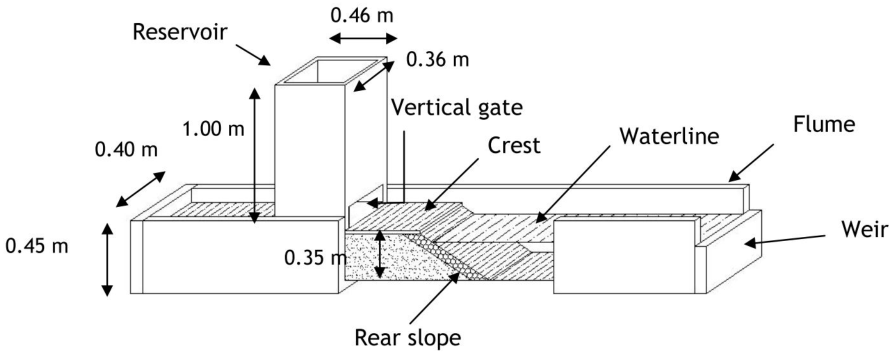

Figure 3.3: Sketch of the used experimental set-up of van Dijk (2001)

s_{op} = 0.04) and a mean period T_m = 4.7 s. A storm duration of 6 hours was assumed. The starting point of the dimensioning of the reservoir is the mean overtopping discharge calculated using the overtopping equations in TAW (2002). Assuming discharges of q = 0.1 L/s up to q = 30 L/s per meter width the maximum calculated storm is shown in Figure 3.5. The volumes are indicated with the black line. This figure also indicates with the blue line the simulated waves. These simulated volumes are discretized because it is assumed that exact mimicking every volume is not required. Moreover, it shows that the largest waves are not simulated using a simulator of 3.5 m^3/m. The effect of this cut of the largest waves could be significant considering one could argue that the largest wave generates the largest impact and hence the largest damage. The target layer thicknesses and velocities were based on the formulas of **?**.

To create the large velocities belonging to large volumes a slender structure was created. The ratio between the volume and the velocities is exponential, hence a relatively wide bottom was constructed. In this way, the smaller volumes had a relative smaller velocity to the larger volumes. The orifice was located at the bottom and closed by a butterfly valve. Underneath the structure, guidance was installed to transfer the water velocity from a vertical direction to a horizontal direction (Figure 3.4).

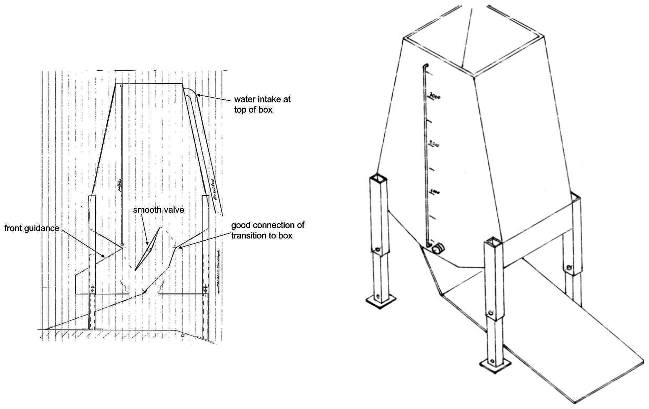
water intake at top of box
smooth valve
front guidance
good connection of transition to box

Figure 3.4: Sketch of the Dutch Overtopping Simulator (van der Meer, 2006)

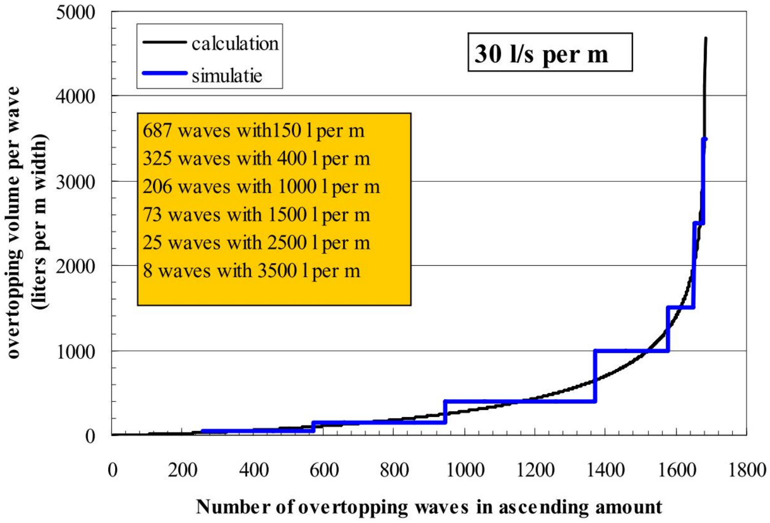

Figure 3.5: Calculated distribution of overtopping volumes and proposal for simulation. Mean discharge q = 30 l/s per m (van der Meer, 2006)

The calibration parameters are indicated in Figure 3.6. Variations were applied to (van der Meer, 2006): 'the height of the valve above the crest (h), the angle (α) which the transition slope makes with the crest, the length (l) of the transition slope and the width (w) to which the valve was opened.' The values of those parameters are of course only valid for this valve mechanism and set-up. Later on, in Vietnam and the US comparable simulators were built. The latter is discussed below.

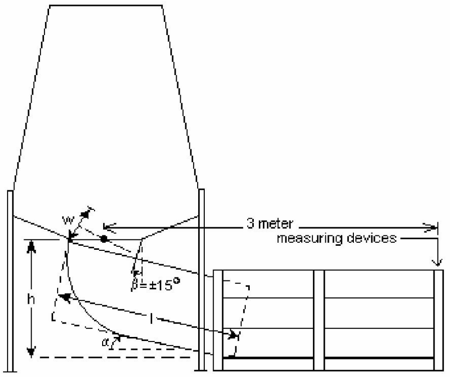
w
3 meter
measuring devices
β=±15°
h
l
α

Figure 3.6: Set-up of prototype indicating parameters changed during calibration (van der Meer, 2006)

US Overtopping Simulator (van der Meer et al., 2011)

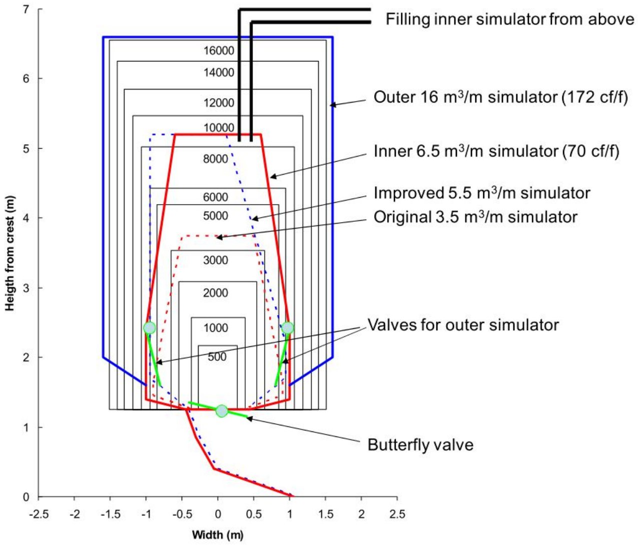
Filling inner simulator from above
Outer 16 m3/m simulator (172 cf/f)
Inner 6.5 m3/m simulator (70 cf/f)
Improved 5.5 m3/m simulator
Original 3.5 m3/m simulator
Valves for outer simulator
Butterfly valve
16000
14000
12000
10000
8000
6000
5000
3000
2000
1000
500
Heigth from crest (m)
Width (m)
0
1
2
3
4
5
6
7
-2.5
-2
-1.5
-1
-0.5
0
0.5
1
1.5
2
2.5

Figure 3.7: Figure of outer and inner box of the US Wave Overtopping Simulator

Figure 3.8: US simulator in action

After the hurricane Katrina, the Colorado State University installed their own wave overtopping simulator. The design is based on the design of van der Meer (2006). The main difference between the Dutch Overtopping Simulator and The US Overtopping Simulator is that the latter is fixed on a permanent position. Therefore, the grass is transported to the simulator instead of the other way around (van der Meer et al., 2011). The simulator is constructed with two different boxes. One smaller box of $6m^3$ inside an outer tank of 16 m^3 (Figure 3.7), in this way smaller volumes are better modelled considering smaller volumes can have relatively high velocity values.

In contrary to conventional storm duration of 3 or 6 hours, a normative storm of 1 hour was used for the design of the US Overtopping Simulator. With this manoeuvre a significant smaller 'maximum wave' in a storm is calculated, hence a significant smaller simulator can be designed to simulate the stated mean overtopping discharge of 200 L/s.

3.2 Design Aspects of the WOS

This section discusses the design process of the overtopping simulator. The Wave Overtopping Simulator is placed inside the 'Sediment Flume' of the Fluid Mechanics Laboratory of the TU Delft. In this way, a constant water level of the environment can be accomplished easily. This section starts with the requirements and preferences for the overtopping simulator, followed by the starting points of the design. Subsequently, some significant design elements are discussed.

3.2.1 Preferences and requirements for the WOS

This section describes the preferences and requirements for the design of the overtopping wave which results from the wave characteristics, physical- and practical boundary conditions.

Requirements

The requirements are divided in requirements concerning the wave characteristics, the physical boundary conditions and the usability boundary conditions.

Wave characteristics. The simulator should mimic the overtopping wave characteristics as accurate as possible. In Section 2.1.2 the courses of the wave parameters in time are treated. The almost instant start of the wave should be approximated, considering the front of the overtopping wave is significant for the stability of the armour layer. Figure 3.9 shows the course of the desired layer thickness and velocity of an overtopping wave in time, where the parameter starts at zero and increases to its maximum (t_1) and decreases linearly to zero again (T_{ovt}). Where T_{ovt} is the total duration of the overtopping wave. A requirement is that the values of these parameters can be altered during the experiments. The device is able to alter the layer thickness between 0 cm and 10 cm. The ratio between t_1 and T_{ovt} is important. It should be sufficiently small if $t_1/T_{ovt} < 0.2$ to simulate an adequate representative wave.

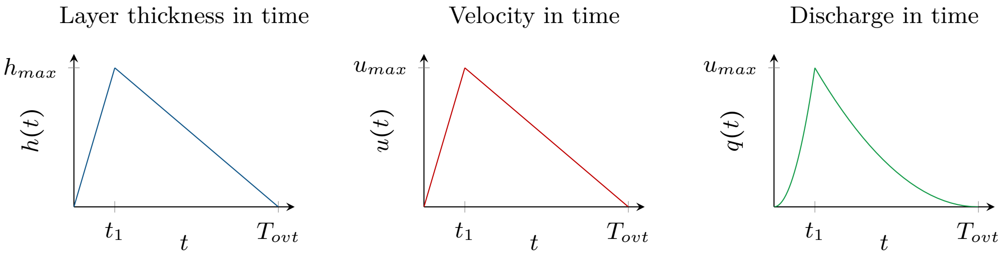

Figure 3.9: Idealised simulated overtopping flow parameters in time (as discussed in Section 2.1.2) (Hughes, 2011)

Physical boundary conditions. The physical boundary conditions are largely determined by the dimensions of the flume:

Flume width	The inside width of the flume is 76.6 cm.
Flume walls	The distance from the flume bottom to the top of the glass flume wall is 80 cm. The glass walls are not able to withstand any extra forces except water pressure. On top of the walls, a rail is installed. This rail is not capable of supporting heavy objects, solely measuring equipment.
Flume bottom	The bottom is made out of very weak concrete, not capable of holding any screws.
Crane	The distance between the maximum height of the crane in the Fluid Mechanics Laboratory and the top of the flume wall is about 2.5 m.

Performance boundary conditions. The performance boundary conditions are listed below:

Safety	The device has to be absolutely safe to use, both for visitors and the operator.
Adaptable feet	The flume bottom is not 100% horizontal. Therefore it has to be possible to execute adjustments to the feet to install the orifice of the device exactly horizontal.
Stiff	Large forces are exerted on the device. It has to be able to coop with these forces.
Repeatable waves	To increase the accuracy of the tests, the values of the wave parameters have to be able to stay constant.
Spillway	To overcome accidents with overflowing water, a spillway has to be installed.

Preferences

Next to the requirements, some preferences of the device are composed:

Frame width	To minimise the difference between the inner width of the simulators reservoir and the width of the flume, the frame of the simulator should be as slender as possible.
Simplicity	To minimise the risk of failure, the device should be designed as simple as possible.
Installation	Where possible, the fabrication and installation should be as straightforward as possible.
Scale	Considering all the boundary conditions, it is strived for to dimension the simulator as large as possible to minimise scaling errors.

3.2.2 Starting point of the design of the WOS

Concluding from the requirements, decisions were made about some basic design principles. Keeping in mind the demand to adjust the final opening sizes, a sliding valve was preferred over a butterfly valve as used in both the Dutch Overtopping Simulator and the US Overtopping Simulator. Relevant factors that have to be taken into account using sliding valves are leakage and friction.

The overtopping simulator had to be placed in an environment where a certain water level could be maintained. It was, therefore, opted to install the overtopping simulator inside of the 'sediment flume'.

As stated in Section 2.1.2, five main factors are incorporated in the description of an overtopping wave at the outer crest line (crest height, wave height and steepness, outer slope angle and slope friction). Considering it differs per situation which sea state generates a certain maximum wave, the dimensions of the reservoir and the valve of the simulator were determined iteratively and mainly by practical boundary conditions. The height of the bottom of the reservoir of the simulator was bounded by the flume walls. With a wall height of 85 cm and 30 cm of space for both the wave tongue and splashing water, the distance from the bottom of the flume to the base of the reservoir had to be 55 cm.

A reservoir height $h = 1$ m is taken as a practical maximum. Using Torricelli's equation this generates a theoretical water velocity of $u = \sqrt{2gh} = 4.43$ m/s. This is in theory too large, considering this creates a plunge which shoots over the rear side slope, missing the impact on the armour layer. The intention was to design the reservoir slightly over-dimensioned. As a starting point of the flume axial width of the reservoir, the formulas for the Dutch Overtopping Simulator (Van der Meer et al., 2006) describing the relation between the total volume of the overtopping wave and the front velocity were used, resulting in a width of 70 cm. This width can easily be adapted. Table 3.1 shows a summary of the starting points for the final design of the Wave Overtopping Simulator.

Table 3.1: Starting point

Reservoir height	1 m
Reservoir width in flume axial direction	0.70 m
Reservoir depth in flume width direction	large as possible
Valve mechanism	sliding valve
Distance from reservoir bottom to flume bottom	0.55 m

With these assumptions, three major elements had to be investigated. Namely the opening mechanism of the sliding door, the reservoir with its support and the door post. These the elements are discussed in the next sections.

3.2.3 Design elements

The most relevant considerations in the design process are discussed in this section

Basic door opening mechanism

To generate an overtopping wave with an almost instant start of the discharge, the valve has to be opened as quickly as possible. The inside water pressure in the reservoir generates large friction between the valve door and door post. This is minimised by applying polystyrene strips (POM-strips) on the door with a very low friction factor for contact with stainless steel. The door itself should be as light as possible so that the door could accelerate rapidly. By constructing the door with the same height as the reservoir, one possible leakage side is eliminated considering the water can not flow over the gate. With that in mind, four different valve opening principles were investigated and are discussed below.

Weights. By attaching a weight (W) via a rope and a pulley to the top of the sliding valve (Figure 3.10a), the door (D) is opened rather quick. Although, the acceleration has a defined maximum of 9.81 m/s. The friction will be significant and a counterweight with considerable mass would be required. This mass has to be stopped at the end of the

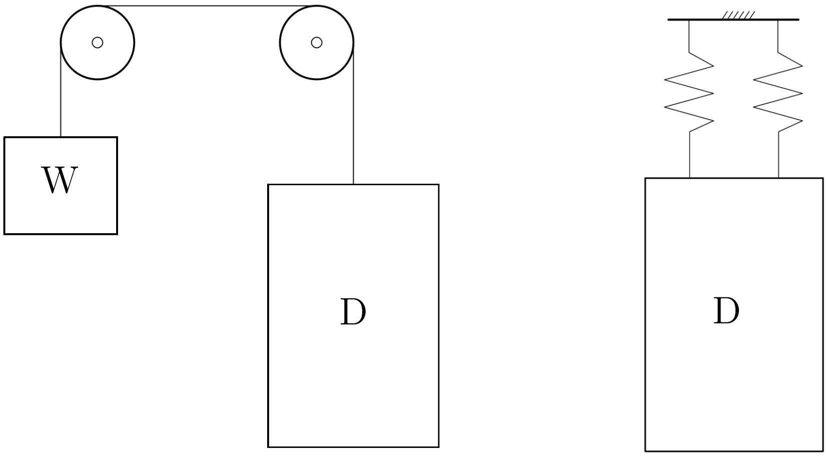

(a) Weights *(b) Springs*

Figure 3.10: Valve opening mechanisms

movement. It was estimated that letting the mass bang on a surface with every wave was not workable (for both the operator and personnel of the Fluid Mechanics Laboratory as well as the construction itself).

Spring. Using springs attached to the top of the door (D) and a construction on top could provide large upward accelerations (Figure 3.10b). A mechanism should be installed to keep the door down and releasing the door instantly. The valve has to be stopped as well, hence it would bang on a structure as well. Because the door was planned to be designed as light and slender as possible, the internal forces would be too large. Next to that, after every wave, the springs would have to be brought to tension again. This mechanism had too many drawbacks so this idea was cancelled.

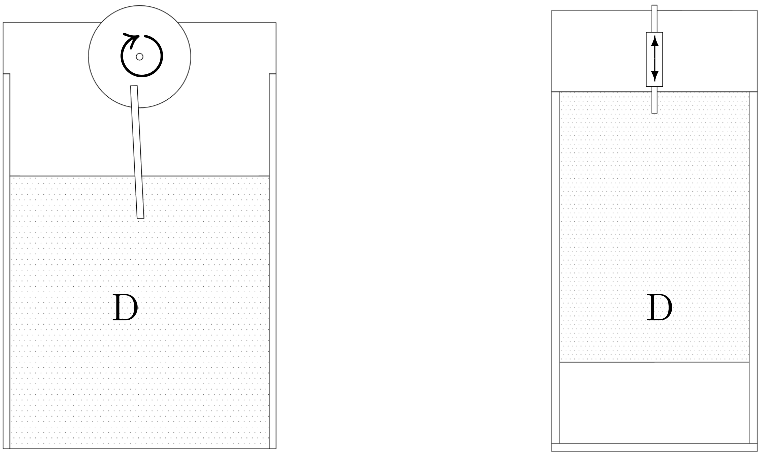

(a) Rotating engine *(b) Linear actuator*

Figure 3.11: Valve opening mechanisms

Rotating engine. Using an ordinary rotating electrical engine with a shaft attached to the door (D), the rotating movement converges to an up and downward movement of the door (Figure 3.11a). In this way, the movement of the valve could easily be controlled.

The shaft would generate horizontal forces to the door posts, which is not desired. Also, the availability of a linear motor made this principle abundant.

Linear motor. A system with a linear electrical actuator (Figure 3.11b) satisfies all of the requirements and preferences. Provided that it is capable of generating the forces needed, it can steer the valve very precise. The fact that the motor was already available was decisive to opt for this mechanism. The functioning of the linear actuator is discussed later.

Reservoir (support) principles

Different options were available for both the support of the reservoir and the construction of the reservoir itself. The fact that the reservoir should be positioned in front of a breakwater model was in this stage already taken into account. The principals are discussed below.

Outer side support. By installing the support of the reservoir outside the flume (Figure 3.12), the reservoir would hover above the breakwater model. This would save a lot of effort when altering the crest width of the breakwater model considering that only the simulator has to be moved back and forth. Unfortunately, the flume in the Fluid Mechanics Laboratory is not easily accessible on both sides. Therefore, installing legs on both sides appeared to be difficult. Next to that, with a hanging reservoir, large tensions could be found in the structure when the reservoir is filled. This option was cancelled.

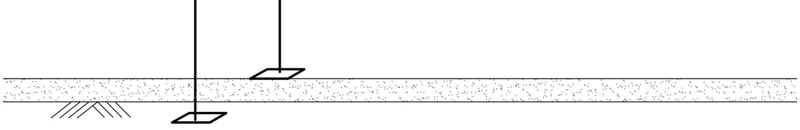

Figure 3.12: Concept design of simulator with support legs outside the flume

Wooden structure funded by structure inside the breakwater. Building a support structure inside the flume, the overtopping simulator reservoir could be placed on top. A complete wooden device would be easy to construct, but dilatation of moist wood would be significant. This would induce significant leakages at the door posts. In addition, the forces exerted by the linear actuator have to be transferred. It is estimated that the wooden structure could cope with the forces, but the wood structure would not be ideal for the shock aspect of the forces. A detailed drawing of the wooden structure is included in Appendix B.

Existing frame. Keeping in mind the total duration of the design and build process, the use of an existing ITEM-profile was put forward. This ITEM-profile is easily adjustable and can be mounted on top of the flume walls (Figure 3.13). In this way, the forces of the actuator are directly transferred to the flume walls. The drawback of the usage of this system was the connection of the system with the door posts and the reservoir. Little settlements would cause large tensions in the reservoir-doorpost connection and could lead to failure. Therefore this option eventually was not used. A detailed drawing is included in Appendix B.

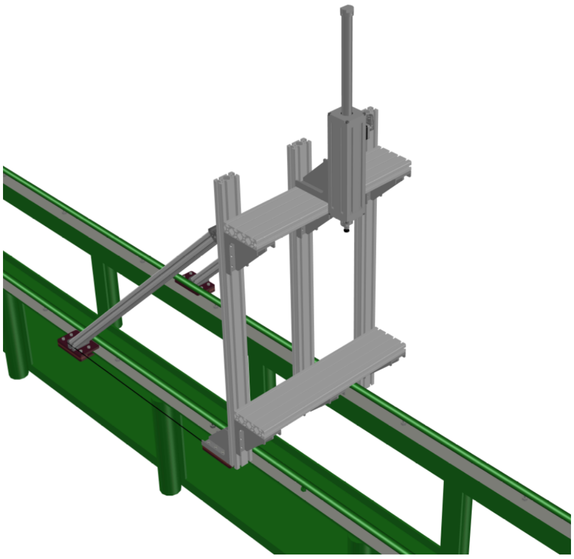

Figure 3.13: Concept design of available ITEM-frame with mounted linear actuator mounted on green flume walls (without reservoir and valve)

Completely steel device. By using a standalone device, which includes the doorpost and the reservoir, no settlement differences would occur between the door frame and the reservoir. A design was made from sole steel. With the reservoir constructed from a steel sheet. This steel sheet could be executed using a thin sheet with a supporting frame or using a thick plate which was able to handle the water pressure itself. This option was both quite costly (for the reason that the frame was a lot of welding work) and the thick plate uses a considerable amount of material. A detailed drawing is included in Appendix B.

Steel frame with a wooden reservoir. The best solution appeared to be a steel outer framework with a wooden reservoir. This was possibly the easiest and quickest to build, was capable of absorbing the forces exerted by the linear actuator and satisfies the other requirements. The design is elaborated in Section 3.3.

Door frame detailing

The detailing of the door frame appeared to be very significant. By trying several variations an optimum had to be found between stiffness, frame thickness and constructibility. Also, leakage and friction played a large role in the design decisions.

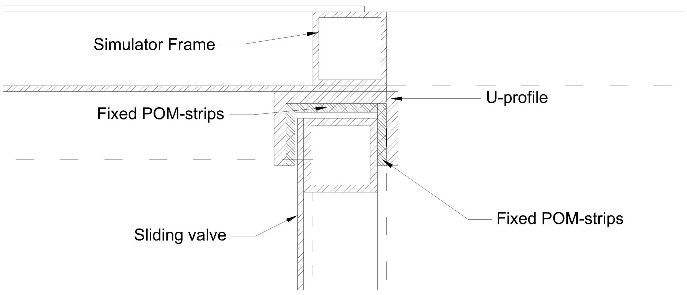
Simulator Frame
U-profile
Fixed POM-strips
Fixed POM-strips
Sliding valve

(a) Inside

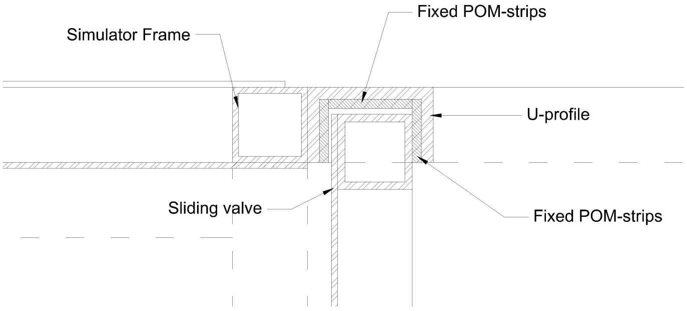
Fixed POM-strips
Simulator Frame
U-profile
Sliding valve
Fixed POM-strips

(b) Outside

Figure 3.14: Top-view detail of concept design of the valve inside and outside of the reservoir

The valve had to slide through a u-profile. This profile could be mounted at the inner side or on the front side of the reservoir. When placed inside (Figure 3.14a), the u-profile adds to the total thickness of the construction and enlarges the difference between the door width and the flume width. Placing the profile outside (Figure 3.14b) would take less space, but would be executed with large thicknesses of the u-profile and would be hard to connect to the frame (no room to screw a bolt or weld it together). Hence, it is opted to install the u-profile on the inside. The margins between the door and the doorpost on the side of the door had to be minimised to prevent leakage. An option was to fill the u-profile with rubber strips, this is discussed later.

3.2.4 Summary

Next to the starting points of section 3.2.2, from the above was concluded that the Wave Overtopping Simulator had to be constructed with:

- a sliding valve with a linear actuator,
- a steel frame with a wooden reservoir,
- an outlet guidance,
- and a door post at the inner side of the reservoir.

3.3 The Wave Overtopping Simulator (WOS)

The final design (Figure 3.15) is based on the conclusions from all the discussed design principles in the former section. This design is elaborated in combination with the device as built. Detailed technical drawings can be found in Appendix C.

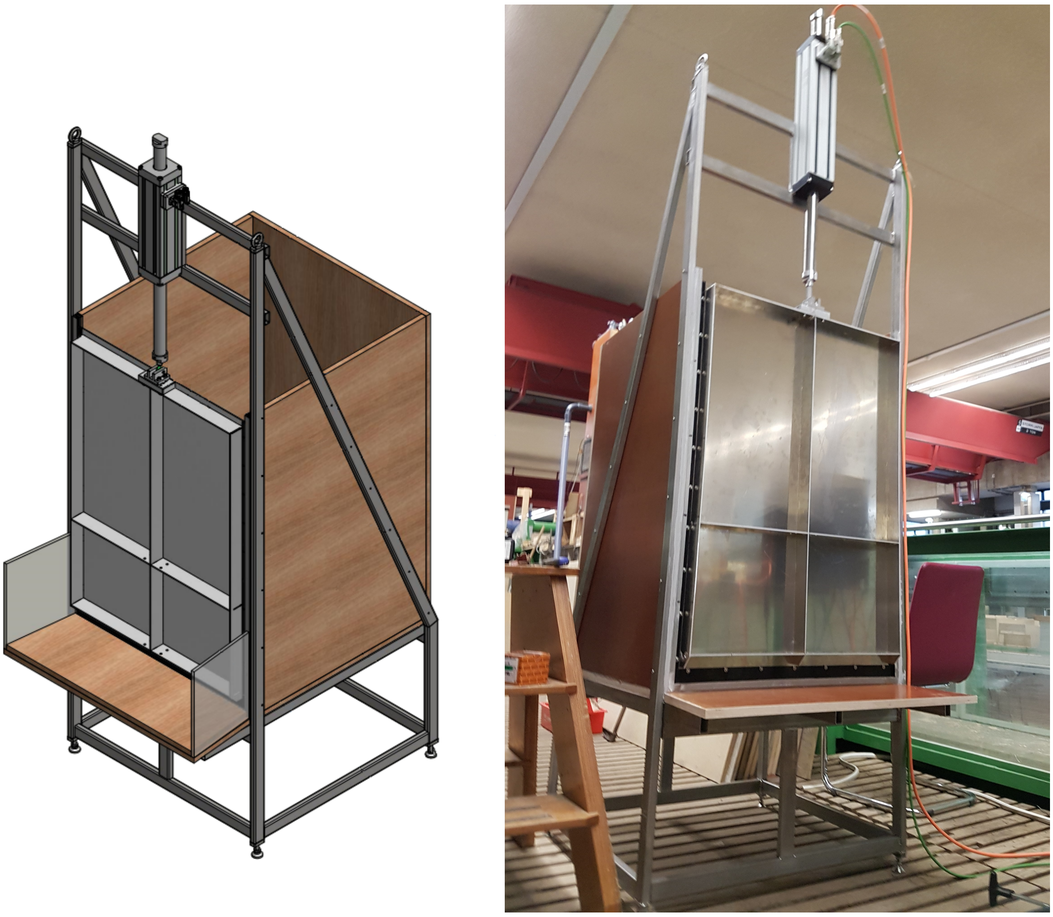

(a) Design *(b) As-built*

Figure 3.15: The Wave Overtopping Simulator (The WOS)

3.3.1 Support structure

The main structure of the WOS is constructed out of $40x20x2$ mm SAE304 stainless steel beams. The frame consists of a base with adjustable feet. Around the reservoir, a triangle like structure is designed. In this way, the moment forces exerted by the linear actuator are transferred to the base of the structure. On top of the steel frame two hooks are installed to facilitate the usage of the overhead crane. A detailed technical drawing is included in Appendix C.

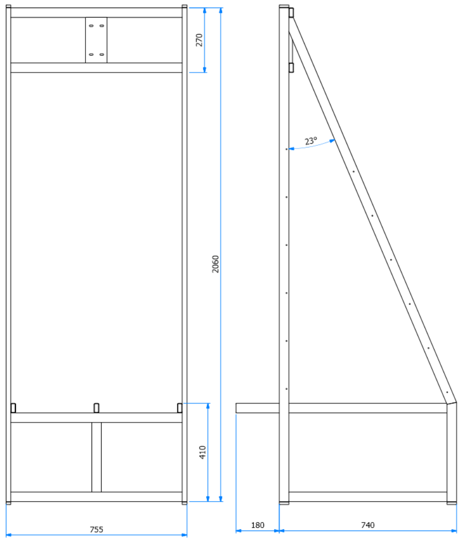

Figure 3.16: Side-views of stainless steel frame

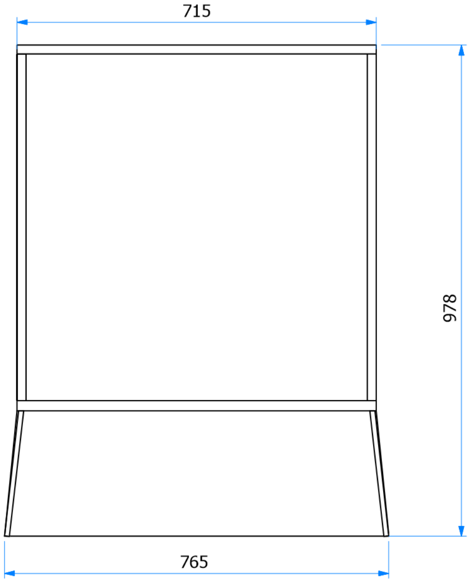

Figure 3.17: Top-view of wooden reservoir with (at the bottom) the outlet guidance

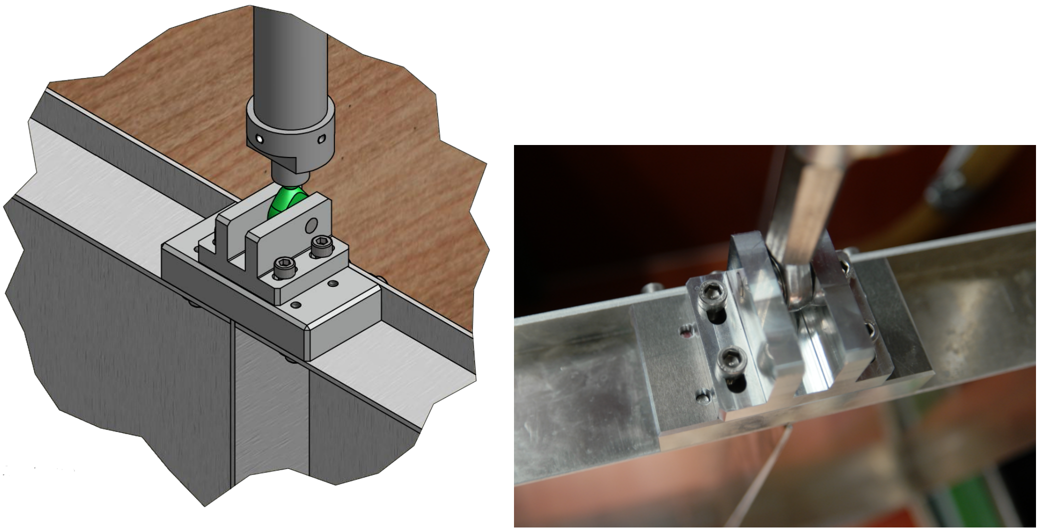

(a) Design

(b) As-built

Figure 3.18: Detail of device connecting actuator shaft to the valve

3.3.2 Reservoir

The reservoir itself is entirely made out of wood. The joints are closed using lute, so no leakage takes place at all from the joints of the screwed wooden sides. The reservoir is slightly higher than the door. In this way, a safety spillway is created and the water will always flow out the simulator at the front of the device. A detailed technical drawing can be found in Appendix C.

3.3.3 Valve and linear actuator

The door of the simulator is an important design element. The door is constructed as light as possible considering its inertia and the requirement to open as quick as possible. On the other hand, the maximum capacity of the linear actuator is as much as 1100 N. The door had to cope with this large although short duration force. In the first designs of the door, an aluminium frame was used covered with an aluminium plate. Later, it was opted to just use an aluminium plate with reinforcement plates on the back (Figure 3.19). By installing the reinforcement plates as much as possible to the outer sides, the moment force in the material at the door posts is minimised. The total weight of the 1 m high valve is less than 7 kg. To minimise the friction, POM-strips are installed on the sliding door. A detailed technical drawing is included in Appendix C.

To overcome extra unnecessary forces on the door (post), the centre of gravity of the door had to be aligned with the shaft of the actuator. Hence, it had to be possible to tune this alignment of the valve relative to the actuator shaft after construction. A special block was constructed to make this possible (Figure 3.18).

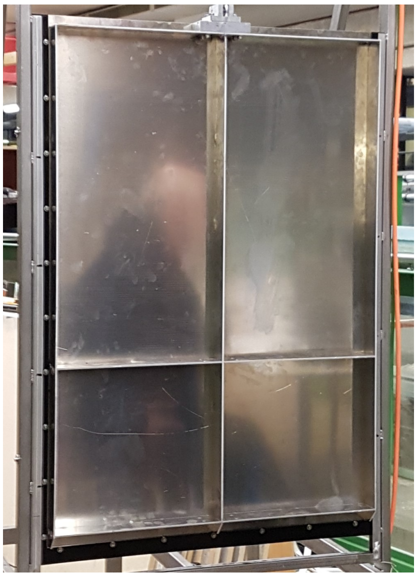

Figure 3.19: The valve

Using a software programme called SoMove from Schneider Electronics and the 'LXM32M AC Servo Drive', the actuator is controlled using 'PID control'. Where PID stands for 'Proportional, Integral and Derivative' and each of the three parts has a different effect on the behaviour of a system. The difference in stick-slip (of the doorpost and the valve) between a fully filled and semi filled reservoir, should not have an effect on the valve behaviour. The final values of those PID parameters are shown in Appendix D. In Figure 3.20, an actual opening sequence of the valve is shown, reaching a maximum velocity of more than 8 m/s.

3.3.4 Door post

The door posts are constructed as shown in Figure 3.21. For strength reasons, the u-frame is installed at the inner side of the frame. In this way, the momentum forces in the frame is reduced considerably. An extra metal strip is attached to the frame, using rivets at the outer side, to strengthen the door post, considering small deformations were seen.

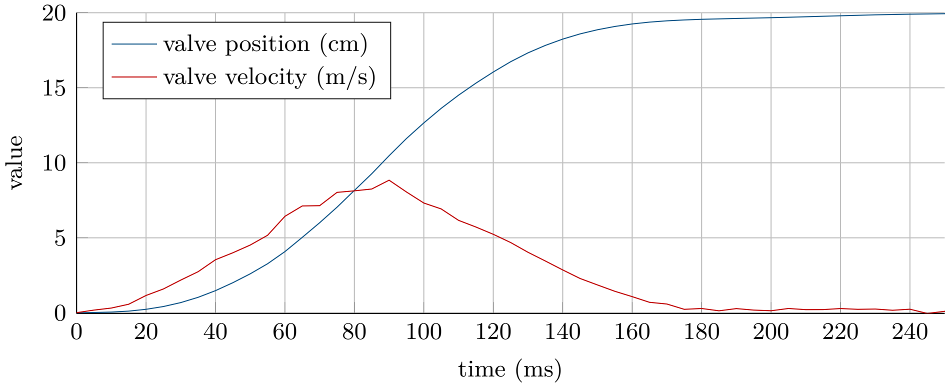

Figure 3.20: Measured valve movement (v_{max} > 8 m/s)

Moreover, the momentum exerted on the frame by the actuator is less with the door post on the inner side compared to the outer side, because the actuator can be installed closer to the frame. Figure 3.21a shows a rubber filled frame. This rubber strip was removed when appearing abundant. By designing the rubber strip in this way, different rubber strips can easily be exchanged. It appeared that the rubber strips, despite abundant lubrication, aided more than expected the friction. With the removal of the strips, still, an acceptable level of leakage was present. The bottom door post is constructed from a u-frame completely filled with rubber. When the valve is closed, the own weight of the valve deforms the rubber, hence the leakage is minimised. Detailed technical drawing can be found in Appendix C.

3.3.5 Outlet guidance

By installing the u-profile inside the frame, the total distance between the outlet and the glass flume wall is 4.5 cm. To overcome eddies and energy dissipation, a guidance structure is installed with a length of 25 cm.

3.3.6 Turbulence introduction

To introduce some rolling movements and air in the overtopping wave, the mock breakwater-crest with a certain width, covered with cubes, was placed at the orifice. It is difficult to quantify those phenomena, although, after 40 cm, air bubbles were seen over the full layer thickness. Hence, the turbulence induction zone was constructed for 40 cm.

3.3.7 Protection board

A protection board is installed to impede one could possibly put his or her hands under the valve door. With the board, the valve is out of reach for visitors and bystanders.

3.3.8 Depth-meter in reservoir

The course of the water level inside the simulator reservoir is directly linked to the volume of water that exits the simulator. The water level, therefore, had to be known as accurate as possible to quantify the discharge. A floating steel ball was fixed to a steel guidance rail in such way that it was able to move in the vertical direction only. The electrical resistance of the steel rod is influenced by the location of the floating ball. This influences

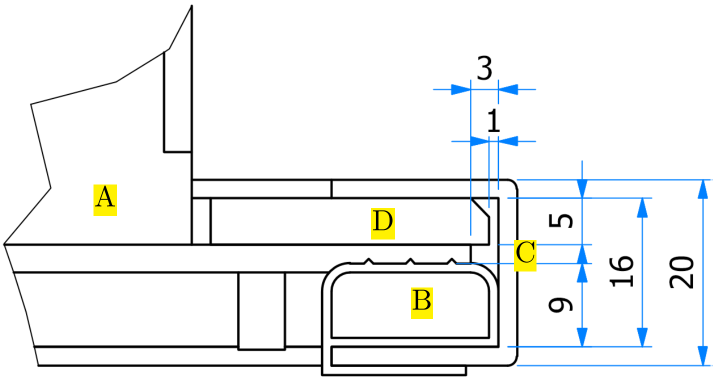

(a) Design

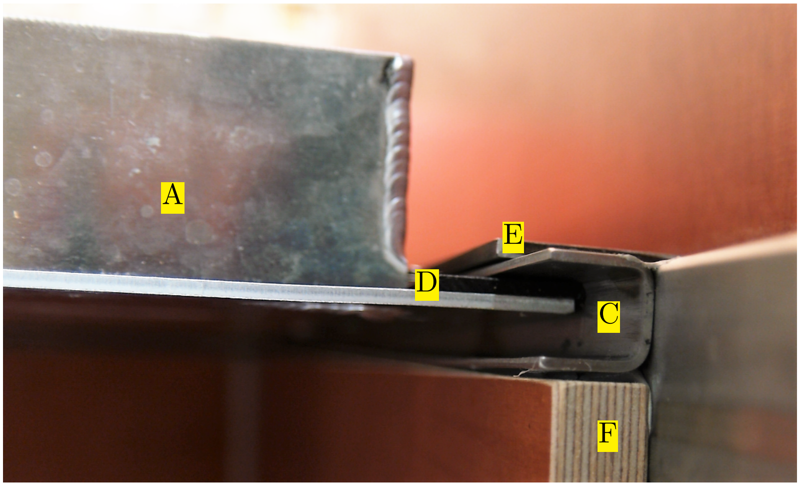

A = valve
B = rubber strip
C = u-profile
D = POM-strip
E = extra steel strip
F = reservoir wall

(b) As-built

Figure 3.21: Top view detail of door post

the electrical resistance of the steel rod. On top of the steel bar, the resistance was measured.

The float was influenced by waves inside the simulators reservoir, hence the accuracy is about 1.5cm. On the other hand, the required parameter is not the water level itself. The total water volume inside the reservoir is the desired parameter. Hence the error in the measured volume, depending on the water level, is $\sqrt[3]{E_{waterlevel}}$.

The raw output data from both the float and the laser distance meter mounted above the valve was saved using Dasylab in csv-files. The raw data (in volt) from those files was loaded into MATLAB and using calibration ratios converted into respectively water level and valve opening height. The data of the valve was used to exactly determine the moment of the valve opening and link this to the water level.

The lack of an analogue filter at the float (Appendix I) resulted in a water level signal with significant noise. A low-pass filter was used to remove this noise. When the gradient of the water level was taken, i.e. the velocity of the water level drop, gradient noise was introduced caused by fluctuations in the water level. This noise was removed using a stop-band filter, which resulted in a smooth signal.

3.4 Callibration of the Wave Overtopping Simulator

3.4.1 Properties of the Wave Overtopping Simulator

The characteristics the Wave Overtopping Simulator could be estimated, although were not exactly known beforehand. Therefore, it was useful to exactly quantify the magnitudes of the leakage, the orifice discharge coefficient, the effect of the guidance bulkheads, the emptying durations (i.e. wave periods of the simulated waves), and peak discharges. This was done in four steps, discussed in Table 3.2.

Pre-test	Purpose	Method	Conclusion
A	Leakage	Determined differences in water volume in the tank in given time intervals	0.1 L/s
B	Orifice discharge coefficient μ	Determined difference in orifice opening widths and water layer thicknesses at the end of the guidance bulkheads	0.5
C	Eddies	Investigated the turbulence at the edges of the gate posts and eddy lengths	31 cm
D	Reservoir waterlevel	Compared theoretical water level drop with actual water level course	-

Table 3.2: Pre-tests

Leakage

Due to the sliding valve mechanism, it can not be prevented that some leakage occurs. In Figure 3.22 the water level in time is shown without opening of the valve. At t=0 the reservoir is largely filled. In the line, a buckle is seen. The 'leakage test' is executed 3 times and every test showed the buckle on a similar water level. An explanation for this buckle could be that the valve is not 100% aligned to the door post. The magnitude of the leakage is before the buckle around 0.9 L/s. This is significant, although the water level in the reservoir is larger than used in the executed tests for reasons discussed before. After the buckle, the leakage is around 0.1 L/s. Which is less than 0.05% of the reservoir volume per second and results in a total empty duration of around 5000 s (1 hour and 25 min).

Orifice discharge coefficient

Due to the sharp edge of the bottom of the valve, the actual discharge from the simulator is different than the theoretical discharge calculated using the opening distance of the valve. This difference is denoted with the factor μ and is caused by the difference between the layer thickness and the door opening height. Figure 3.23 shows for all four different opening heights a water level around x=0 of respectively 2.5 cm, 5.0 cm, 7.5 cm and 10 cm. This concludes in $\mu = 0.5$ for the Wave Overtopping Simulator.

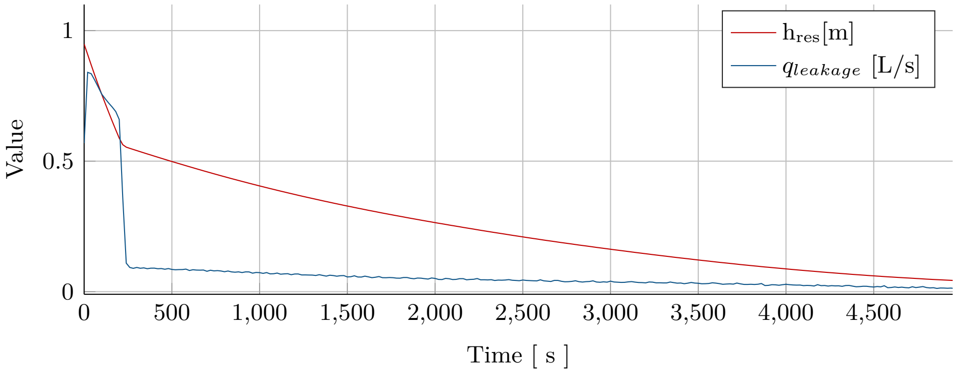

Figure 3.22: Water level inside the reservoir without opening of the valve

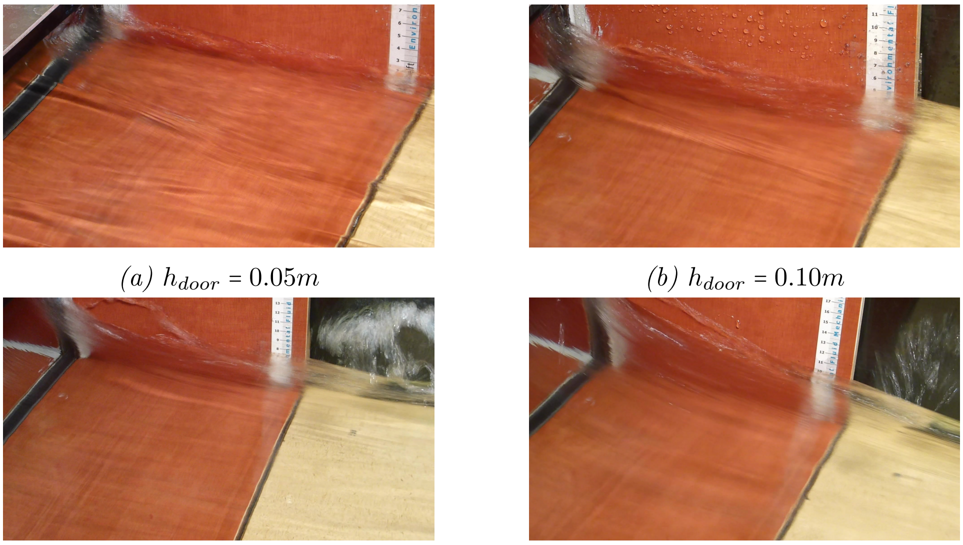

(a) $h_{door} = 0.05m$ *(b)* $h_{door} = 0.10m$

(c) $h_{door} = 0.15m$ *(d)* $h_{door} = 0.20m$

Figure 3.23: Orifice with different valve opening heights

Eddies

The width inside the reservoir of the simulator (0.679 m) is smaller than the width of the flume (0.767 m). This is caused by the fact that the whole simulator, including its frame, has to fit inside the flume. On both sides, there is a difference of 4.4 cm between the inside of the simulators reservoir and the flume wall. Although this difference is merely 11%, it causes a small difference in discharge per meter located at the orifice and the discharge per meter on top of the crest. To minimise energy losses by eddies, guidance bulkheads are installed. These reduce the difference from 4.4 cm to 1.8 cm. This resulted still in eddies and a slightly rounded wavefront instead of a straight front (3.24b).

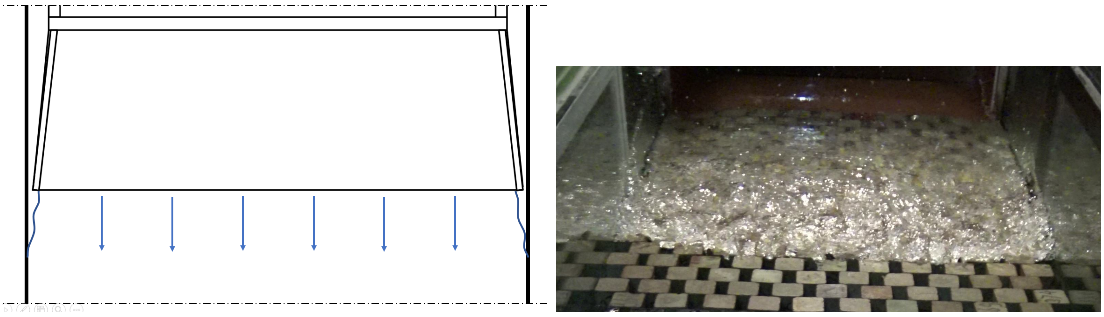

(a) Schematic top view of outlet indicating eddies caused by the difference in widths

(b) Front of a simulated wave

Reservoir water level (h_{res})

In Figure 3.25 a typical test cycle is displayed. In a test cycle, the water level in the reservoir rises due to the inflow of water by the pump. When the pump is switched off, the water level drops slowly due to the leakage at the valve. When the valve opens, the water level drops quickly till the reservoir is empty. Figure 3.25 and all the other figures in this thesis don't show a water level in the reservoir below 4.5 cm. This is caused by the fact that the float doesn't allow measurements below 4.5 cm. The red line in Figure 3.25 is the valve opening height, which is in this case 20 cm in opened position.

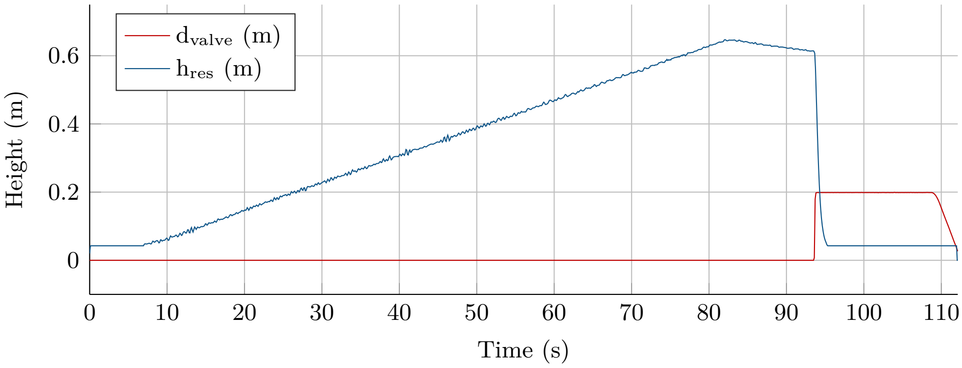

Figure 3.25: Typical course of the water level during a wave simulation cycle

The emptying duration is influenced by three different factors, namely the opening height of the valve, the water level in the reservoir, and the width of the reservoir. The influence of those parameters is discussed in the next subsections.

It is obvious that the water level in the reservoir of the Wave Overtopping Simulator (h_{res}) drops faster when d_{valve} is larger. This is shown in Figure 3.26. The emptying duration varied between 6.5 seconds and 2.4 seconds. It must be noted that the moment the water level is lower than the valve opening height, the situation can no longer be considered as a floodgate considering the gate does not have any influence on the stream anymore. In practice, the layer thickness does not rise at the moment $h_{res} < d_{valve}$ as a result of the fast decrease of h_res (this could differ with a very large flume-axial width of the reservoir (w_{res})). The consequence of this phenomena is therefore, next to the little relevance of the wave tail, neglectable.

The flume-axial width of the reservoir introduces a phenomenon which was not well measured using one single float. The float was positioned close to the valve opening, to enable boxes to be placed inside the reservoir (at the rear) to reduce the reservoirs width. By

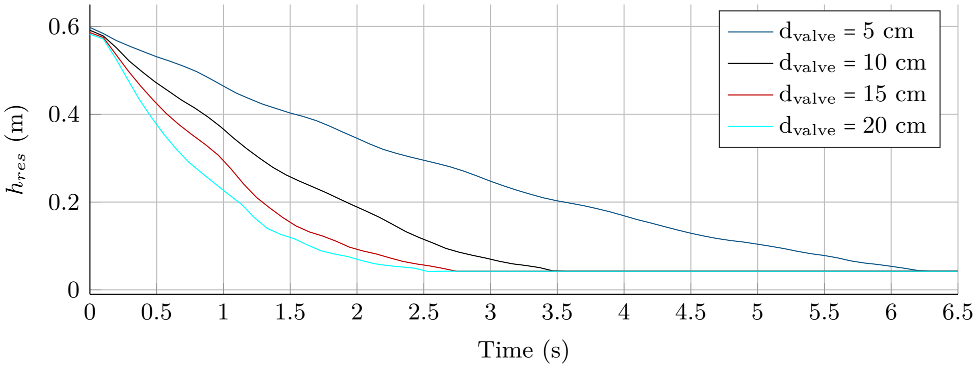

Figure 3.26: Water level inside the reservoir (h_{res}) in time with varying opening heights d_{valve} ($w_{res}(t = 0)$ = 0.60 m)

opening of the valve, the water level does not drop evenly over the reservoir. A translation wave is introduced. Figure 3.27 shows the location of a float and a schematization of the water level in time. This shows that multiplying the water level measured by the float by the horizontal dimensions of the reservoir does not give the actual volume in the reservoir! This error enlarges with wider reservoirs. Solely the measurements with w_{res} =0.4 m are taken into account in this thisis. In the recommendations the posibble solutions for this flaw are elaborated.

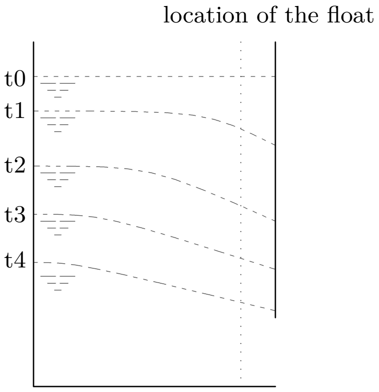

Figure 3.27: Water level in reservoir during emptying

3.4.2 Individual simulated wave volumes

Tested WOS settings

From initial tests it became clear that filling the reservoir of the simulator with a water level larger than 60 cm is redundant for tests in the scope of this thesis, considering a large velocity of the wave tongue generates a jet that shoots over the rear slope (an elaboration of the hydraulic properties is given in Section 4.5.1). This resulted in a test programme of 36 different waves generated by the WOS with the flume axial width of the reservoir (w_{res}) values of 0.4 m, 0.55 m and 0.7m, h_{res} values of 0.2 m, 0.4 m, and 0.6 m and d_{valve} values of 0.5 m, 0.10 m, 0.15 m and 0.20 m.

Simulated volumes

The gradient of the water level in the reservoir can, in theory, be converted to the discharge at the orifice by multiplying the water level gradient times the dimensions of the reservoir. The formerly mentioned translation wave, on the other hand, caused too large deviations in the found water level, hence only the data collected with $w_{res} = 0.4\ m$ is used. The noise of the measurements is removed by averaging three emptying cycles per wave configuration. In this way, little digital filtering was needed (using a low-pass filter), the precise discharge is known and the relevant phenomena are visible. In Figure 3.28 the discharge in time with different initial water levels and valve opening heights is shown.

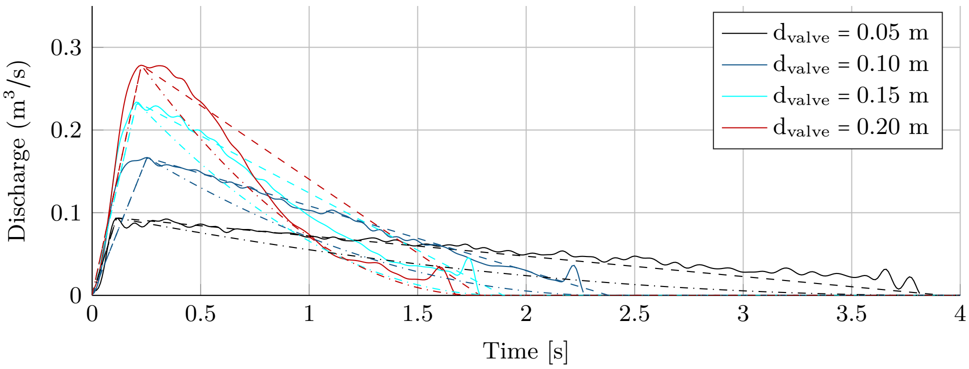

(a) $h_{res}(t=0) =$ *60 cm*

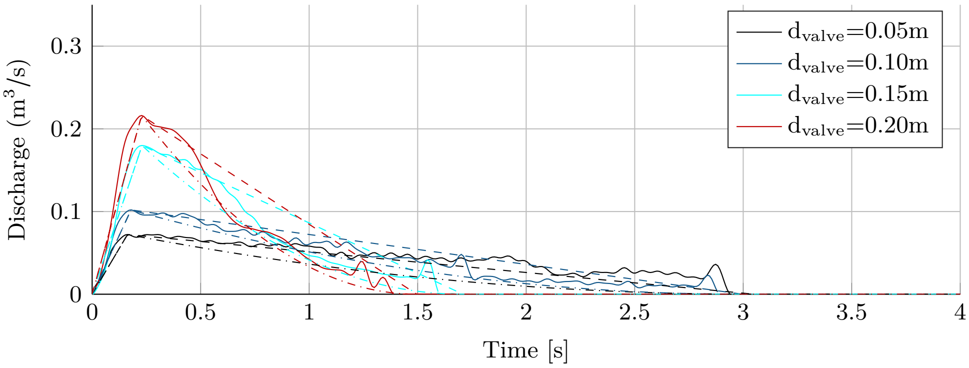

(b) $h_{res}(t=0) =$ *40 cm*

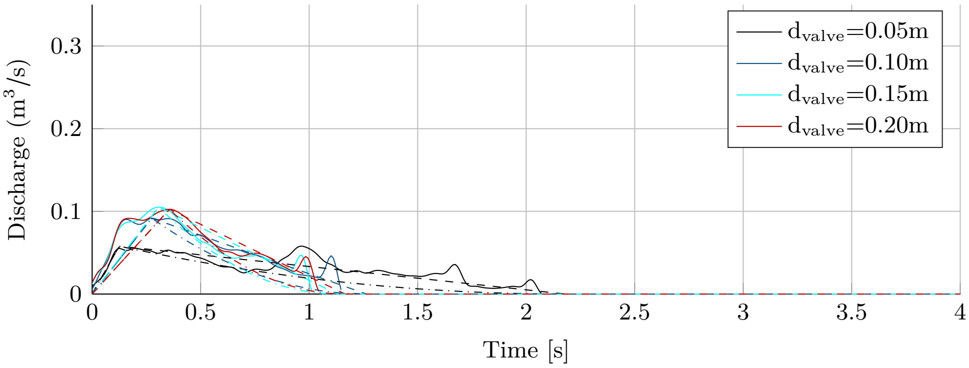

(c) $h_{res}(t=0) =$ *20 cm*

* The solid lines are the measurement results. The dashed lines represent the linear approximation, where the dash-dotted lines represent the exponential approximation (discussed in the next section).

Figure 3.28: Discharge in time (w_{res} = *0.40 m)*

From physical reasoning, it is assumed that the flume axial width of the reservoir w_{res} only influences the total volume and the duration of the wave (see duration difference between Figure 3.26 and Figure 3.29a), and not the peak discharge and peak velocity. The formerly mentioned deficit of measuring the water level correctly at the set-up with $w_{res} = 0.55$ and $w_{res} = 0.70$, caused the lack of verification of this statement. The velocity in time is derived from the discharge (Figure 3.29). To acquire the velocity, the discharge is divided by the water layer thickness: $u = \frac{q}{\mu\, d_{valve}}$. Considering this relation, the course of the magnitude of the velocity in time is exactly similar to the course of the magnitude of the discharge in time. The value of d_{valve} is not changed during an individual overtopping wave simulation.

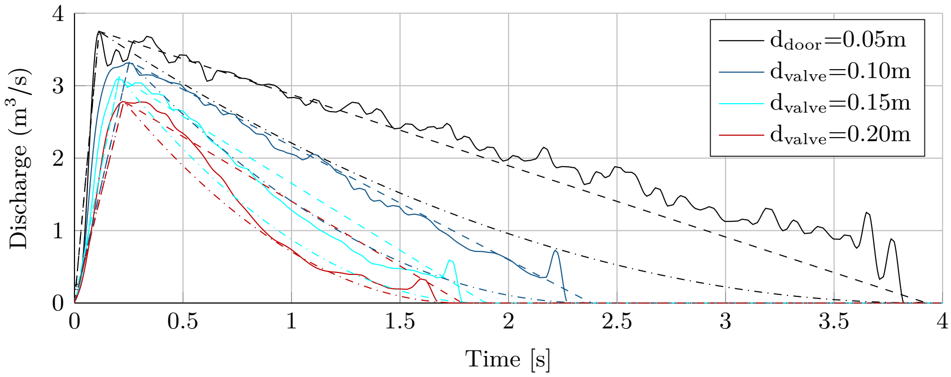

(a) $h_{res}(t=0)$ = *60 cm*

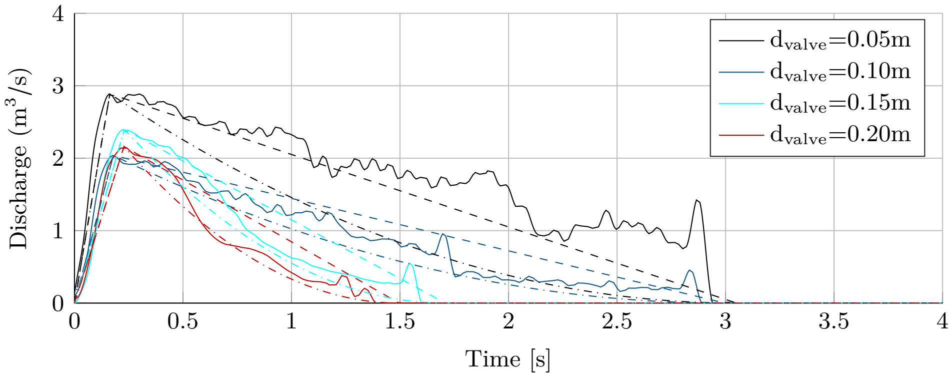

(b) $h_{res}(t=0)$ = *40 cm*

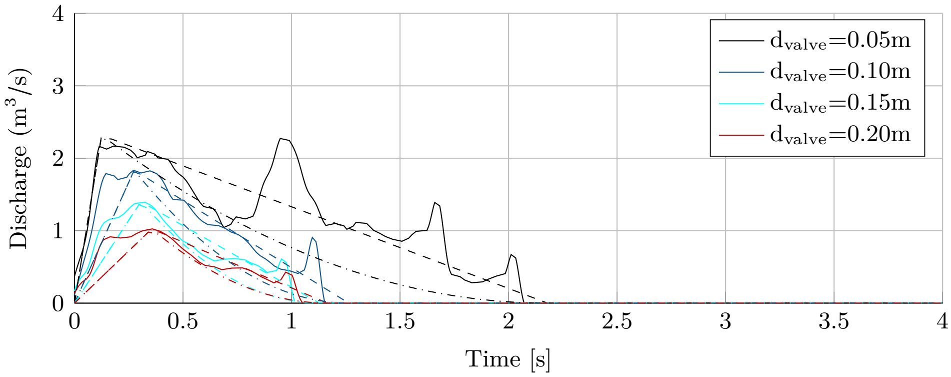

(c) $h_{res}(t=0)$ = *20 cm*

* The solid lines are the measurement results. The dashed lines represent the linear approximation, where the dash-dotted lines represent the exponential approximation (discussed in the next section).

Figure 3.29: Velocity in time (w_{res} = *0.40 m*)

It was visually observed that waves simulated with the reservoir water level of 20 cm behaved slightly different than waves generated with a reservoir water level larger than 20 cm. This is again seen in the measurements. This effect could be influenced by the ratio between the flume axial width of the reservoir and the (small) volume of the wave. Another difference with the waves generated with larger water volumes is the fact that a significant part of the duration of the wave, the water level is lower that the door opening height. This fraction is small for larger waves and therefore neglectable, although for smaller waves this can be significant.

Description of q_{peak} with h_{res} and d_{valve}

To describe the behaviour of the simulator expressed in the water level height inside the reservoir (h_{res}), the door opening height (d_{valve}) and the resulting peak discharge (q_{peak}) as shown in Figure 3.28, a polynomial equation is opposed with 1 (h_{res}) and 3 (d_{valve}) degrees. See Equation 3.1, with a rMSE of q_{peak} is 10.59 L/s/m. The values of the coefficients are noted in Appendix H. The settings for the w_{res} are not elaborated considering the measurements of the water level with w_{res} were not sufficiently accurate.

$$q_{peak} = c_1 + c_2 \cdot h_{res} + c_3 \cdot d_{valve} + c_4 \cdot h_{res} \cdot d_{valve} + c_5 \cdot d_{valve}^2 + c_6 \cdot h_{res} \cdot d_{valve}^2 + c_7 \cdot d_{valve}^3 \quad (3.1)$$

Course of parameter values compared to theory

In Section 2.1.2 the idealised courses of the parameter values at x=0 (see Figure 4.2) as generated by the WOS are discussed and in Section 3.2.1 the required parameter courses are elaborated. Section 4.5.1 elaborates the hydraulic behaviour of the generated volumes at the crest and rear slope. The parameters measured at the WOS are:

- $q(t)$ as shown in Figure 3.28,
- $h(t)$ related to d_{valve},
- $u(t)$ calculated from $q(t)$ and $h(t)$ shown in Figure 3.29.

As shown in the requirements at Figure 3.9, u(t) should decrease linearly, where q(t) decreases exponentially. During the tests, the valve opening height was kept constant (Figure 3.30). Hence, the h(t) remained constant (when $h_{sim} > d_{valve}$). Moreover, w_{res} is not changed during an individual wave simulation.

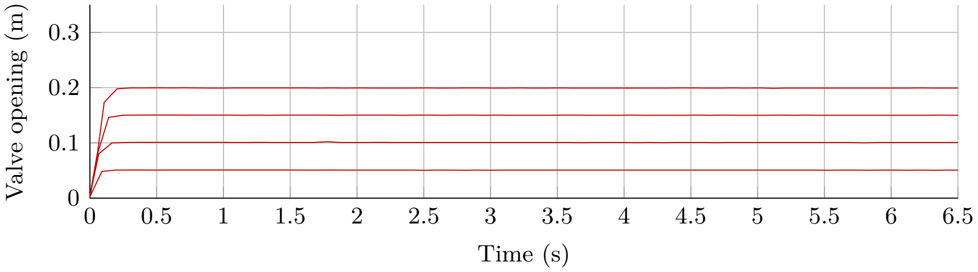

Figure 3.30: Valve opening distances (d_{valve}) in time. $h = \mu d_{valve}$ for the period where $h_{res} > d_{valve}$

The theoretical course (calculated numerically) is acquired considering the following relations:

- $h_{res}(i) = V_{res}(i)/w_{res}$ (m)
- $u(i) = \sqrt{2 \cdot g \cdot h_{res}(i)}$ (m/s)
- $q(i) = u(i) \cdot d_{valve} \cdot \mu$ (m^2/s)
- $V(i+1) = V(i) - q(i) \cdot \Delta t$ (m^2)

This results in a linear decreasing u(t) and q(t), as displayed in Figure 3.31.

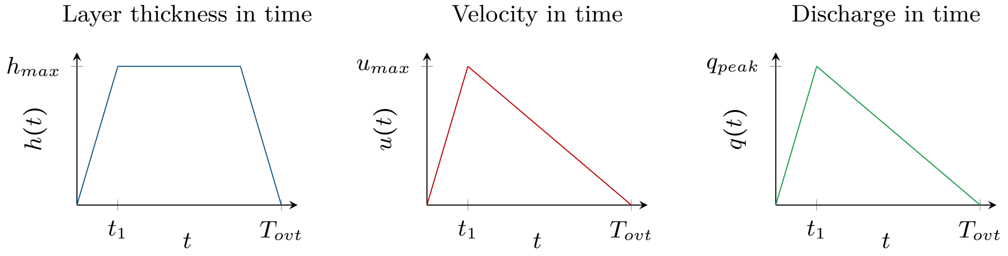

Figure 3.31: Theoretical parameter courses based on physical relation between the h_{res}, $u(t)$ and $q(t)$

Comparing the above Figure 3.31 with the previous requirements indicated in Figure 3.9 shows theoretical differences. In practice, comparing the measured discharge (Figure 3.28) and velocity (Figure 3.29) with the linear or exponential approximations shows that the parameters u(t) and q(t) decrease linearly. In situations where $d_{valve} > 0.1$ m, the course becomes more exponential. This is an improvement of simulating q(t). Figure 3.28 indicates that $t_1/T_{ovt} < 0.2$ for all the released volumes. In theory, the duration of the generated wave volume is:

$$T_{ovt,theory} = \frac{w_{res}}{d_{valve} \cdot \mu} \cdot \sqrt{h_{res}(t=0)} \cdot \sqrt{\frac{2}{g}} \tag{3.2}$$

The actual overtopping durations come close the theoretical values, in particular with smaller values of d_{valve}. Which can be explained by the lower values of t_1.The exact duration of the overtopping wave (T_{ovt}) is quite arbitrary, considering the exact end of the tail of the overtopping wave is hard to define. As mentioned before, the simulator is not able to measure water levels in the reservoir below 4.5 cm, hence no clear measurements could be executed concerning the exact emptying duration of the reservoir. Although, this last 'tail' is not significant for the hydraulic load on the breakwater revetment (elaborated in Section 4.5.1).

From above it is concluded that the WOS is able to simulate individual overtopping waves correctly within a specific range of the parameters. The unequal water level in the reservoir during an overtopping event hindered the exact measurements of the volume inside the reservoir, resulting in solely reliable measurements for the tests with the smallest width of the reservoir.

3.5 Storm Simulation Approach

The usability of the WOS is determined by the ability of the WOS to represent the hydraulic loads of real storms on a breakwater. The characteristics of real individual overtopping waves are discussed in Chapter 2. In this section, the simulation approach and range of the values of the parameters are discussed. This section uses the values of the parameters of this set-up, hence the test range is only applicable in this situation, although the approach is similar to other testable set-ups.

3.5.1 Determination of overtopping parameter magnitudes

In Chapter 2 the relevant formulas are discussed. Victor et al. (2012) and Zanuttigh (2013) were well capable of describing the distribution of volume magnitudes of overtopping waves at steep permeable slopes. Hughes (2015) succeeded to link the overtopping volumes to the peak discharges, using the slope angle and wave period. Hence, the approach indicated in Figure 3.32 is recommended. In blue, the final simulated parameters are indicated.

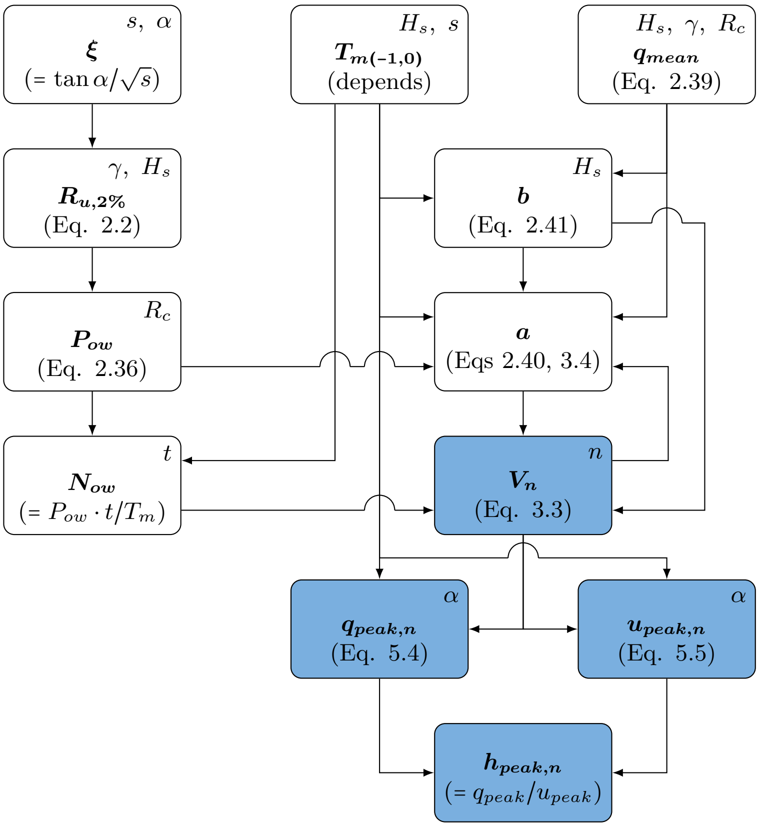
$s,\ \alpha$
$\boldsymbol{\xi}$
$(=\tan\alpha/\sqrt{s})$
$H_s,\ s$
$\boldsymbol{T_{m(-1,0)}}$
(depends)
$H_s,\ \gamma,\ R_c$
$\boldsymbol{q_{mean}}$
(Eq. 2.39)
$\gamma,\ H_s$
$\boldsymbol{R_{u,2\%}}$
(Eq. 2.2)
H_s
$\boldsymbol{b}$
(Eq. 2.41)
R_c
$\boldsymbol{P_{ow}}$
(Eq. 2.36)
$\boldsymbol{a}$
(Eqs 2.40, 3.4)
t
$\boldsymbol{N_{ow}}$
$(= P_{ow}\cdot t/T_m)$
n
$\boldsymbol{V_n}$
(Eq. 3.3)
α
$\boldsymbol{q_{peak,n}}$
(Eq. 5.4)
α
$\boldsymbol{u_{peak,n}}$
(Eq. 5.5)
$\boldsymbol{h_{peak,n}}$
$(= q_{peak}/u_{peak})$

Figure 3.32: Interdependencies of parameters for calculating simulated overtopping characteristics (in blue), with the used boundary conditions indicated in the right corners

3.5.2 Distributions of parameter values in storm simulation

The distribution of the different parameter values is significant for representative storm simulation. Where the run-up is best described by a Rayleigh distribution, the volumes of overtopping waves is two-parameter Weibull distributed (Hughes et al., 2012). Rewriting Equation 2.42 and using $P_V = n/N_{ow}$ gives:

$$V_n = a \cdot \exp\left(\frac{ln(-ln(\frac{n}{N_{ow}}))}{b}\right) \tag{3.3}$$

Figure 3.33 shows an fictive example storm simulation assuming 100 overtopping volumes ($N_{ow} = 100$) using the Weibull distribution with fictive values of a=0.35 and b=0.8. It shows the significant volume difference between the largest volume and the volumes with larger probabilities.

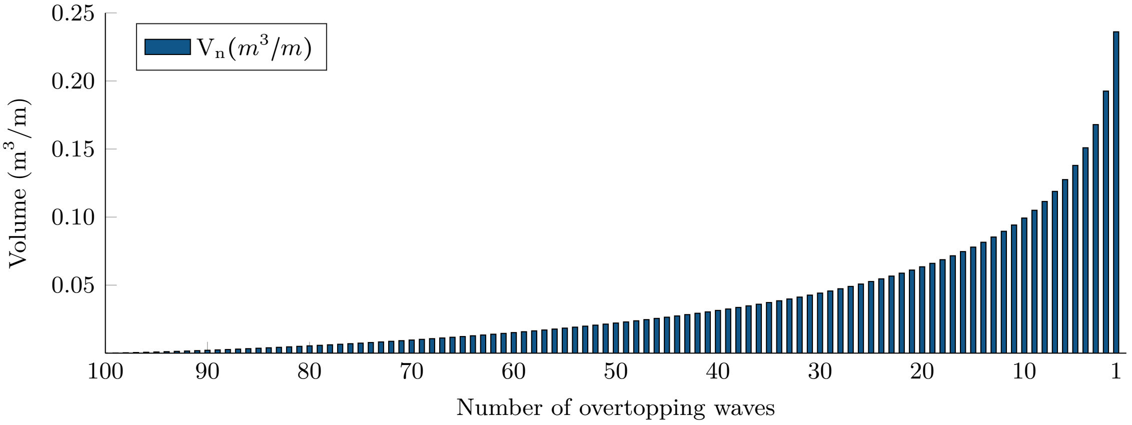

Figure 3.33: Overtopping volumes in a fictive storm ordered in magnitude, using Eq. 3.3 (N_{ow} = 100, a=0.35 and b=0.8)

3.5.3 Boundary conditions and parameter ranges

Three types of boundary conditions determine the workable range of the simulator. The hydraulic boundary conditions set by the test range, the structural boundary conditions set by the size of the experimental set-up (discussed in Chapter 4) and the boundaries of the simulator itself.

Set-up boundary conditions

The experimental set-up is discussed in Section 4.2. The freeboard (R_c) is set in the range of 0.1 m to 0.35 m. The outer slope is set to tan(0.5) with a friction coefficient of $\gamma = 0.53$ for single-layer cube revetment.

WOS boundary conditions

The WOS is able to generate a peak velocity of $u_{peak} = 3.6\ m/s$ (Figure 3.29), a layer thickness of $h_{peak} = 0.1\ m$ and a peak discharge of $q_{peak} = 0.28\ m^3/s/m$ (Figure 3.28).

Hydraulic boundary conditions

A 3-hour storm duration (t=10800 s) and surging waves with a wave steepness in the range of s=0.015 to 0.039 (similar to the tested range in Hellinga (2016)) are assumed. The simulated wave height H_s depends on α, R_c, γ, t and s. With $R_c = 0.35\ m$ and s=0.039 the maximum simulated wave height is bounded by the layer thickness of $h_{peak} = 0.1\ m$. This results in a maximum simulatable wave height of $H_s = 0.24\ m$.

Table 3.3: Tested waves

	Hs (m)*	s*	q_{peak} $(L/s/m)$	u_{peak} (m/s)	h_{peak} (cm)
Wave 1	-	-	55	2.2	2.5
Wave 2	0.18	0.039	91	1.8	5.0
Wave 3	0.18	0.014	105	1.4	7.5
Wave 4	-	-	101	1.0	10
Wave 5	-	-	72	2.8	2.5
Wave 6	0.19	0.040	102	2.1	5.0
Wave 7	-	-	180	2.4	7.5
Wave 8	0.22	0.025	216	2.2	10
Wave 9	-	-	94	3.4	2.5
Wave 10	-	-	164	3.3	5.0
Wave 11	-	-	233	3.1	7.5
Wave 12	0.24	0.039	278	2.8	10

* Not all volumes represent a 'real' maximum overtopping volume in a sea state according to the formulas of Hughes (2015) (Equations 5.4 and 5.5), elaborated in Section 2.1.2. With $R_c = 0.35$, $t = 3$ hours, $\tan\alpha = 0.5$.

3.5.4 Application of the WOS

Approaching a stability study using the WOS will first require assumptions on the boundary conditions of the parameters (s, α, t, γ, R_c and H_s). With this set, the parameters can be calculated as indicated in Figure 3.32. A distribution of the individual overtopping wave volumes is acquired.

Considering the distribution describes an 'unlimited' amount of waves, it is not directly applicable to a fixed number of waves (van der Meer et al., 2011). The following equation does not hold for a limited number of waves with the same value of a in Equation 2.40:

$$\sum_{n=N_w}^{n=1} V_n = q_{mean} \cdot t \tag{3.4}$$

Enlarging the scale factor a iteratively in such extent that the sum of the volumes equals the mean period times the storm duration, will generate correct volumes.

To simulate a relevant storm, the smaller volumes could possible be insignificant, hence for practicality, it could not be required to simulate those volumes. Next to that, keeping in mind the test duration, it is beneficial to avoid simulating every individual wave size. A possible better approach is to collect several waves together and simulate those x times (Van der Meer et al., 2006). In Figure 3.34 a plot is shown with an fictive example of a possible outcome of such a procedure with (in red) the actual simulated waves. The five largest waves could be simulated in this case and 3 other types of waves are used to represent all the other volumes. It can be questioned if the smallest volumes are significant, although it is safe to test smaller waves as well keeping in mind smaller waves can increase the strength of a slope (elaborated in Chapter 4). An example of such a simulation is shown in Appendix G.

In this thesis solely single overtopping volumes are tested. It is assumed that those single volumes represent the largest wave in a storm and is largely representative for the normative load during a storm. This assumption is supported by the fact that single layer cube revetment has a mostly brittle failure (Chapter 2).

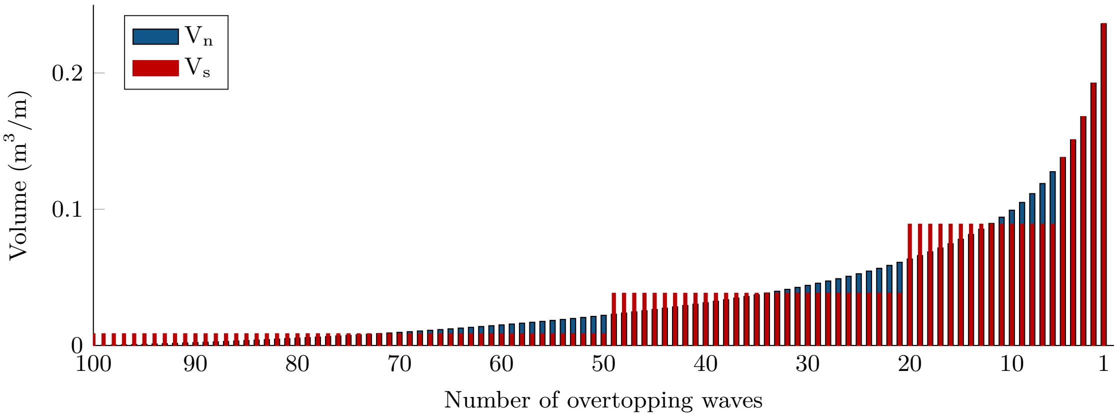

Figure 3.34: Simulated overtopping volumes

3.6 Discussion on (the applicability of) the Wave Overtopping Simulator

3.6.1 Properties of the Wave Overtopping Simulator

Leakage

With sliding valves, leakage can not be prevented totally. Although, the maximum leakage of the WOS with $h_{res} < 0.6$ is 0.1 L/s/m. This is acceptable, considering the leakage of one second is 0.05% of the reservoir volume.

Guidance bulkheads

The effect of the difference in width between the inside of the reservoir and the inside of the flume was significant. Not only did the wavefront deform, splashing up of the water hitting the sides complicated the detection of the water line by video analysis which introduced extra scatter.

Turbulence intensity

The turbulence introduction was a disputable point. Especially the air entrapment of an overtopping wave tongue could influence the impulse exerted on the slope during impact. The determination of this length and the turbulent movements have a possibly significant influence on the forces exerted by the overtopping wave. Detailed knowledge of the vector field inside the wave tongue could solve this uncertainty.

Valve

The valve opening control is configurated in such a way that a robust simulation can be done with different stick-slip situations (depending on the water level inside the reservoir). A safety margin is taken between the used maximum opening distance and the maximum displacement distance of the linear actuator. Considering the valve is the limiting boundary condition, decreasing this margin will directly result in larger simulatable storms.

Maximum layer thickness

The orifice discharge coefficient of the valve is 0.5. This small value generated relative low water layer thickness. A streamlined valve could increase the orifice discharge coefficient. Considering the layer thickness is the leading boundary conditions, this enables the WOS to simulate larger velocities. Additionally, the duration of reaching a certain water level thickness will decrease, considering the valve has to open a smaller distance.

Water level at x=0

The water layer thickness at x=0, assumed as a fixed boundary condition, was influenced by the water layer thickness on the crest. This influence was especially large where small volumes were tested and large fractions of the volume infiltrated in the slope, resulting in quickly decreasing water layer thicknesses on the crest.

Measurement of the reservoir water level

The water level in the reservoir was measured by a float fixed to a rod. The incapability of the float to measure water levels below 4.5 cm is not negligible for waves generated with a reservoir water level smaller than 20 cm (>22.5% deviation).

During an emptying cycle, the water level is not equal all over the reservoir. This deviation caused a non-reliable calculation for both the discharge and velocity with large flume-axial reservoir widths. The float was installed close to the valve, suggesting a larger discharge as actually created. Considering no secondary discharge peaks resulting from resonance inside the reservoir were detected, together with the fact that the integral of the discharge was equal to the initial volume, the results from simulations with small reservoir widths were considered reliable.

3.6.2 Storm simulation

Supporting formulas

The formulas of Hughes (2015) are used to link the volumes to a certain peak discharge and peak velocity. Although these formulas include the slope angle, the data used for the determination of the empirical formula is not originating from slopes steeper than 1:3. Moreover, an increase in scatter was observed with an increase in slope steepness inside the tested range (Hughes, 2015). This suggests that even steeper slopes (as assumed in this experiment) generate more variations in the relation between overtopping volume and corresponding discharge.

Wave generation order

The reservoir of the WOS needs a certain time to fill. Therefore, it is not capable of simulating a wave train with several large volumes within a short time interval. The significance of this deficiency for this experiment is questioned since the influence of the duration of the interval between subsequent loads on single-layer cube revetment is disputed.

Chapter 4

Breakwater Experiments

The application of the Wave Overtopping Simulator is tested in the investigation in the stability of single-layer cube revetment at the crest and rear slope of a low-crested breakwater. The tests were performed in the sediment flume at Fluid Mechanics Laboratory at the Delft University of Technology. This chapter will elaborate the approach of the experiments, the test set-up is explained and the executed tests are discussed including the results of these experiments.

4.1 Test Outline

Delimiting the scope on solely the crest and inner slope is the main starting point of this experiment. The method used in these experiments is based on elimination of the variables depending on the sea state and the outer slope. The experiments can be divided into two parts. The first tests were executed on a mock breakwater to acquire data for the calibration of the Wave Overtopping Simulator and the rest of the tests were executed to discover the damage levels of the single-layer cube revetment depending on different variables (discussed in Chapter 2).

In Chapter 2, a large number of relevant parameters for this research are treated. Although, not all influencing factors could be included in the scope of this research. The main variables excluded from this thesis are listed below:

Wind: Although wind can have a great contribution to wave overtopping volumes, especially with very steep or vertical slopes it is not included in these experiments.

Incident wave angle: The incident wave angle has a significant influence on wave overtopping. The tests are executed in a flume. Therefore, the angle can not be taken into account.

Roundhead: Inherent to the conclusion above, solely the trunk of a breakwater is tested.

Transmission: Albeit the transmission could be a significant factor for the stability of the inner slope, with the proposed method using an overtopping simulator it is not possible to test this factor.

Berm: The presence of a berm at the front of a breakwater is highly significant for the wave breaking and run-up height. Nevertheless, this is not in the scope of this experiment.

Foreshore: The bathymetry of the foreshore in front of a breakwater determines the distribution of incoming waves. This is important for the determination of the maximum overtopping wave. Despite this significance, it is not taken into account in this research.

Crest width: Despite the significance of the crest width (due to friction and infiltration), it is not included in the scope.

Rear slope angle: Concluding from Hellinga (2016), minor changes in the slope steepness around 2:3, are not significant for the stability.

4.2 Experimental Set-Up

The experimental set-up is discussed in this section. In Figure 4.1 the test set-up is shown including the Wave Overtopping Simulator (Chapter 3), a configuration of the breakwater model (Section 4.2.1) and the measurements instruments (Section 4.2.2).

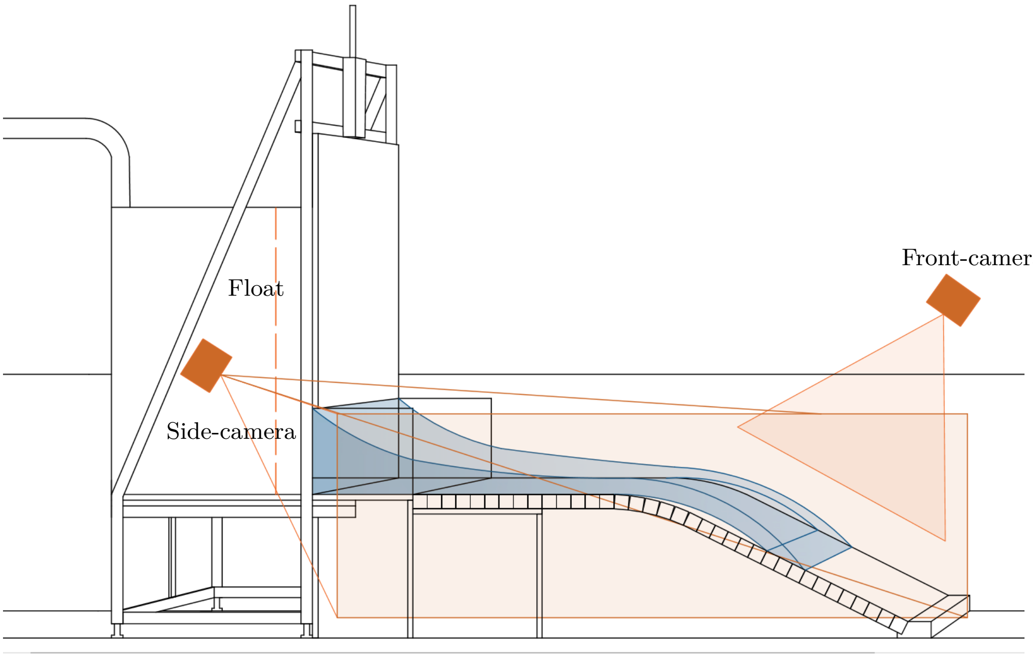

Figure 4.1: Schematisation of the test set-up

4.2.1 Breakwater model

Elements of the breakwater model were altered several times during the experiments, however, the general dimensions were kept the same. The exact tested breakwaters are discussed in Section 4.4.2. In this section, the main elements are discussed.

Outer dimensions

The flume has a height of 0.85 m. With a breakwater height of 0.55 m, there is another 0.30 m left for the wave tongue. This is more than sufficient. With a fixed slope of 1 in 2, the slope will be 1.1 m wide. The 'front side' of the breakwater will be constructed with a wooden plate, preventing the core to collapse.

Inner crest line transition

Relevant for the stability is the transition of the crest to the rear side slope. This can be a rounded transition or a transition with a sharp edge. This is varied in several configurations.

Armour layer

The armour layer tested in this experiment is a single layer cubic armour layer. The size of the used cubes differed per test configuration varying from a $D_n = 2.1$ cm up to $D_n = 5$ cm. Some tests were executed with configurations with a crest armour size different than the slope armour size. The placement densities of the configurations varied between 25% and 30%.

Underlayer and core

With an armour layer of cubes in a single layer on a rubble mound breakwater, a contradiction arises (Van Gent et al., 2002). The underlayer is more under attack by incoming waves when a single layer of armour is applied, than using multiple layers. Therefore, the filter layer should consist of stones with a larger diameter to prevent washing out of material. On the other hand, using large stones gives a highly irregular surface to place the armour blocks on to. The cubes rising above the surrounding cubes encounter more wave attack than those who have the same top level as the neighbouring cubes. A ratio of $D_{cubes}/D_{n50-filter} = 1.8$ (i.e., $M_{cubes}/M_{n50-filter} = 10$) is proposed (Van Gent et al., 2002).

Two aspects are not taken into account here. First, this ratio is an optimisation for slopes under direct wave attack, which is not the case at the crest and inner slope. Secondly, using geometric scaling, the permeability of the core is not scaled correctly. One could argue that at the crest high permeability is preferred, to minimise the volume of water that arrives at the lee side of the crest generating a jet at the inner slope (e.g. lower loads on the armour layer). On the other hand, as mentioned before, the larger rocks will generate an uneven bed to support the cubes. At the inner slope, the impinging jet could be compared as a plunging wave, which supports the size ratio of 1.8.

Little is known about the tolerances of the underlayer for single layer cubic revetment. A starting point could be the underlayer tolerance applied to Accropodes. This is set for generalised deviations of the underlayer to ± H/10 as the mean value calculated from measurements on 3 profiles spaced no more than 10 m apart, with H as the size of the Accropode. For local defects in the underlayer, the tolerance is larger using ± H/6 (CLI, 2015). In this thesis, no exact measurements of the underlayer are performed. However, the resulting irregularities in the surface of the placed armour blocks are surveyed by measuring the largest deviations.

Turbulence induction

To induce 'realistic' turbulence in the simulated waves, a longer impermeable preamble covered with cubes is used. From initial tests, it appeared that after 40 cm the visible air bubbles were developed over the full water layer. It is argued that air entrapment has a significant influence on the impact generated by the front of the impinging jet. Therefore, the preamble length is taken as 40 cm.

4.2.2 Instruments and measurements

In order to acquire data to describe the wave tongue and armour damage, different instruments were used both inside the Wave Overtopping Simulator and at the breakwater model. Figure 4.2 shows the schematic overview of the measured parameters. Details on the exact dimensions of the simulator are discussed in Chapter 3.

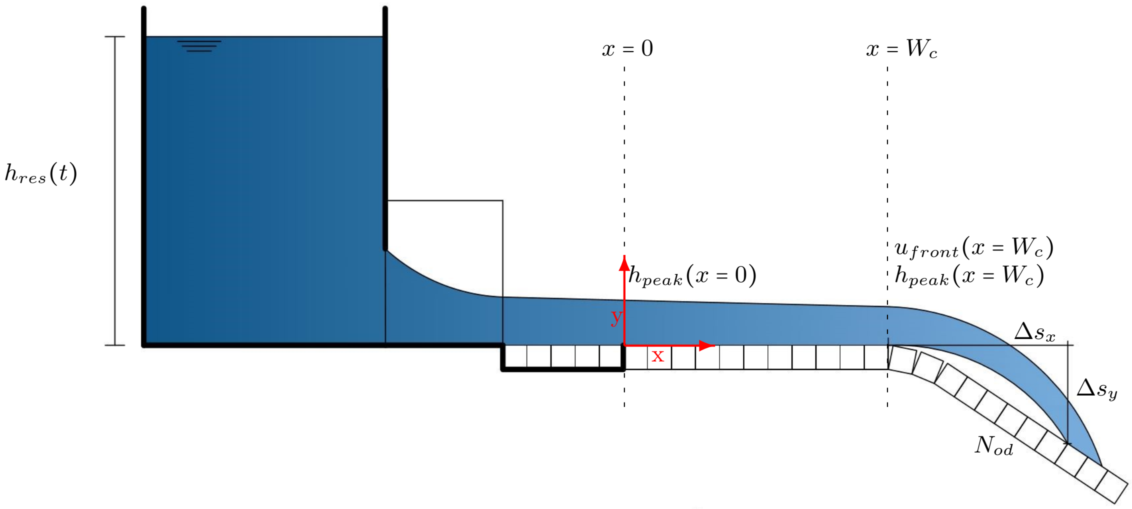

Figure 4.2: Measured parameters (not on scale)

In Figure 4.1 the used measurement instruments are indicated in orange. The output of the measuring devices is sent to a computer and saved using software programme Dasylab. The output from the cameras is processed using FFmpeg and MATLAB. This process is elaborated in the next section. This section elaborates the measurement devices. The final set-up is the end result of an iterative process, which is briefly discussed as well.

Side-view video camera

The front velocity and the course of the wave tongue at the transition between the crest and the slope is not well known. To investigate these elements of the wave, a camera was installed on the side of the breakwater model. A cross section of the slope was illuminated with lamps and the 4k camera filmed with 24 fps during an overtopping event. This film was analysed using FFmpeg and MATLAB to find the layer thickness and front speed of the wave tongue. This information was desired considering it relates to the forces of the potential impinging jet.

The lens of the camera generates distortion in the picture. To give an accurate, picture wide, the definition of the distance one pixel represents, the distortion had to be removed. To determine the exact distortion of the lens, a checker-board and software were used. By making 20 pictures from the checker-board from all different angles, the software is able to detect the distortion and is able to correct all the pictures taken from that camera. Keeping in mind the calibration is only valid for that single lens/camera combination and the selected amount of zoom.

To enhance the contrast between the water layer and the background, a black background was installed. For the camera an optimum was found using a shutter speed of 1/1600 s and installing extra lights.

Top-view camera for damage

The eventual damage on the slope was measured with a camera above the slope. This camera took a picture before and after the wave. Former research by Hellinga (2016) noted that the contrast between the pores has to be enhanced to analyse the photos properly. This was reached by adding two lights above the flume. Two photos per test were taken, one before and one after the test. With a flume width of 76.5 cm, and a camera with 6.1MP (3008x2008 pixels) 1 pixel equals about 0.25 mm which is 0.32% of the width of the flume.

Laser distance meter

In order to link the exact opening moment to the measurements of the reservoir's water level, a laser distance meter was installed above the valve of the Wave Overtopping Simulator. The scope of the laser distance meter is 20 cm, similar to the maximum opening height of the valve.

Data processing

In the experiments, two main topics were investigated. The first one was the ability of the simulator to generate overtopping waves which are comparable to 'real' overtopping waves, and the second was the research in the stability of single-layer cubic revetment at the rear slope. The data processing and the results of the experiments in those two topics are discussed in the next sections.

The measurement data from the tests consisted in the basis of two types of data: videos and voltage outputs. The measurement instruments are discussed in the former chapter. In this section, the processing of this data will be discussed, next to the analysis of the data. The goal of the processing is to visualise and sort the data in such a way that conclusions can be drawn from the measured data. This section elaborates the different data and their processing.

To analyse the videos, the videos are processed to separate stills. Those stills are saved individually as jpg-files. The videos shot from the side are 4K (4096 x 2160 pixels) videos with a frame rate of 24 fps. This holds that every 1/24 of a second a picture is taken, which results in a time between the pictures of 1/24=0.042 s. With for example a wavefront with a velocity of 2 m/s, the front has moved 8.3 cm in this period.

To detect the exact position of the wavefront, a script is written (Appendix E) which detects the contrast difference between the dark background and the light water. Small droplets are filtered out. By analysing two photos in a row, the distance in the amount of pixels is known in which the wavefront is moved. To relate a pixel size to a certain length in millimetres, known points are pointed out in the distorted images. For the water layer thickness in time, the same procedure is followed. Figure 4.3 shows a wave overtopping the crest with a green line as detected water line.

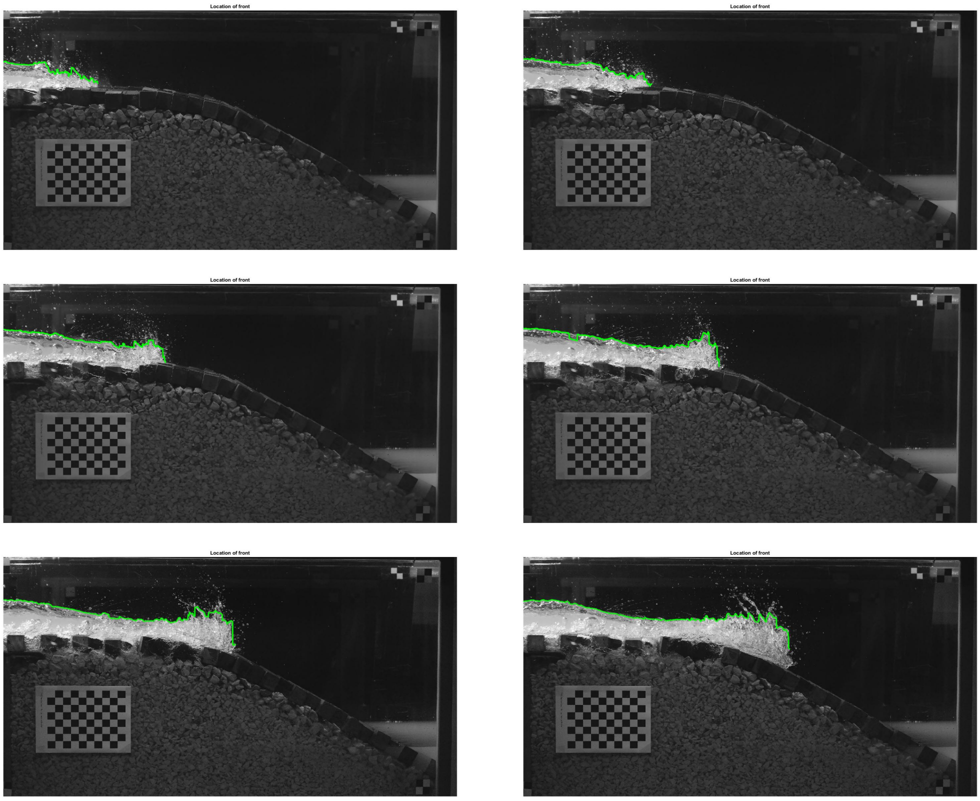
Location of front
Location of front
Location of front
Location of front
Location of front
Location of front

Figure 4.3: Wave tongue propagating on crest with green line as detected waterline

4.3 Test Approach

The breakwater configurations are exposed to waves generated by the Wave Overtopping Simulator. The test programme per configuration consisted out of 12 generated waves (when no failure occurred). Table 3.3 gives an overview of the generated waves. These waves are similar to the volumes discussed in Section 3.4.2. The volumes were released starting from the smallest up to the largest volume. In this way, little settlement of the revetment during the smaller waves generated extra stability for the impact resulting from the larger waves. The waves tested ($s = 0.014 - 0.04$) all represent surging waves ($\xi = 2.53 - 4.23$), similar to tested in the experiments of Hellinga (2016).

4.4 Tested Configurations and Results

The tested configurations are discussed in this section, including the observations and results of the tests.

4.4.1 Impermeable breakwater model

The dimensions of the configurations used for the tests with an impermeable core were similar to the configurations of the tests with a permeable core. The breakwater tested here was a ‘mock’ breakwater made out of impermeable wooden plates. The purpose of these tests was, next to calibrate the WOS, to find the influence of the crest friction and permeability. The WOS is elaborated in Chapter 3.

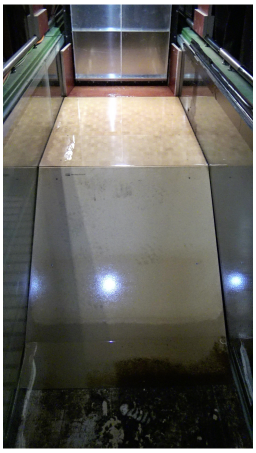

Figure 4.4: Front view of Configuration 0a

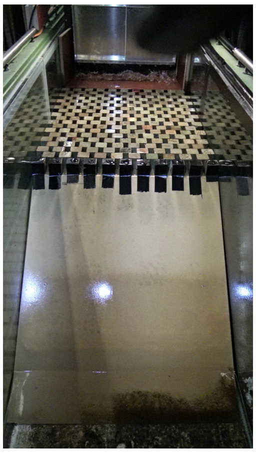

Figure 4.5: Front view of Configuration 0b

Smooth wooden breakwater

The first tests were executed with a theoretical set-up using a wooden ’breakwater’, excluding friction and infiltration. The goal of using this test set-up was to quantify the hydraulic parameters which should be comparable to a grass dyke, which is likewise smooth and impermeable. By installing a sharp edge, the possible effect of water ’sticking’ to the slope of a round edge is diminished. This should show the Δs_x and Δs_y very clearly. The wooden breakwater was 1 m long and had a slope of 1:1.5 (Figure 4.6). Figure 4.7 shows an overtopping wave tongue.

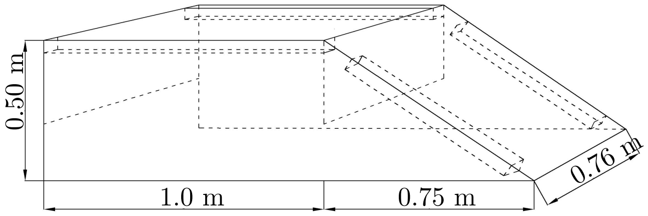

Figure 4.6: Wooden mock breakwater

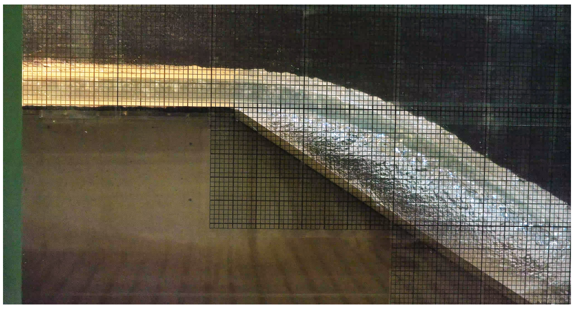

Figure 4.7: Wave tongue on top of wooden breakwater

Wooden breakwater covered with cubes

To examine the influence of cubes on the friction of the crest, tests were executed with 5 cm cubes placed on top of the wooden breakwater crest. The cubes at the crest line were fixed with duct-tape to prevent flushing away. The influence of the surface difference between a concrete cube and a cube covered with duct-tape is assumed negligible compared to the overall roughness of the crest. The slope was not covered with cubes, considering these tests were not stability tests and a detached jet (as seen in Figure 4.7) would not be influenced by cubes on the slope.

4.4.2 Permeable breakwater models

This subsection describes the tested permeable-core configurations and its observations. The determination of the layout of a configuration is well substantiated by the results from the former configuration, taking into account failure mechanisms, cube size, underlayer, transition, and factors as availability and test pace. For the underlayer gradation the ratio between the cube size and the underlayer D_{n50} of $D_{cube}/D_{n50,f}$ = 1.8 (Van Gent et al., 2002) was the design starting point. An overview of the structural parameters is given in Table 4.1. A short summary of the observations is shown in Table 4.2, together with the largest value of the stability number tested (limited by failure or total wave programme).

Table 4.1: Tested configurations

	Conf 1	Conf 2	Conf 3	Conf 4	Conf 5	Conf 6	Conf 7
Cube size slope (mm)	50	31	40	40	40	40	20
Cube density (kg/m^3)	2600	2200	2400	2400	2400	2400	2400
Placement density slope	0.3	0.25	0.3	0.3	0.3	0.3	0.25
Filter layer slope - grading (mm)	20/40	-	-	16/25	16/25	16/25	-
Filter layer slope - thickness (mm)	60	-	-	40	40	40	-
Ratio $D_{cube}/D_{n50,f}$ slope	1.66	-	-	1.95	1.95	1.95	-
Transition	round[1]	sharp	sharp	sharp	sharp	sharp	sharp
Cube size crest (mm)	50	50	50	50	50	50	40
Filter layer crest - grading (mm)	20/40	20/40	20/40	20/32	20/32	20/32	-
Filter layer crest - thickness (mm)	60	60	60	50	50	50	-
Ratio $D_{cube}/D_{n50,f}$ crest	1.66	1.66	1.66	1.92	1.92	1.92	-
Core grading (mm)	11/22	11/22	11/22	11/22	11/22	11/22	11/16
Toe	fixed	rubble[2]	fixed	fixed	rubble	fixed[3]	fixed[2]

[1] Arc diameter of 0.7 m
[2] Toe constructed higher on the slope
[3] Toe allowed a settlement of 3 mm

Table 4.2: Result overview

	Observations	$\frac{H_s}{\Delta \cdot D}$[1]	$\theta^{1,2}$
Conf 1	no damage, rocking of cubes at crest and transition	3.0	6.27
Conf 2	toe failure	5.1	5.66
Conf 3	no failure, out-wash of rock material at transition	4.2	9.37
Conf 4	no failure, rocking of last row of cubes at the crest	4.2	9.37
Conf 5	toe failure, out-wash of rock material at the toe	4.2	9.37
Conf 6	removal of cube below waterline	4.2	9.37
Conf 7	removal of cube below waterline	8.5	13.35

[1] Maximum value tested; The theoretical values of $H_s aredeterminedbytheapproachshowninFigure3.32$
[2] $\theta = \frac{q_{peak,max}}{\sqrt{g \cdot \Delta \cdot D^3}}$ (Andersen, 2006), elaborated in Section 4.5.2

Configuration 1

The in the former section elaborated initial tests showed the impressive velocities and forces of an overtopping wave. Together with the fact that other failure mechanisms were seen (Appendix I) it was estimated that the armour layer constructed out of cubes with D = 5 cm would likely fail.

On the other hand, keeping in mind the conclusions of Hellinga (2016) concerning the tested cube sizes and their remarkable high stability, this was an uncertainty. The advantage of testing with larger cubes is the declination of scaling errors, which adds to the eventual decrease in reliability of the test results. With this in mind, the cubes with a size of D = 5 cm were installed (Figure 4.8b). An underlayer of 20/40 mm was applied with a thickness of 60 mm. This is on the large side (the calculated underlayer using (Van Gent et al., 2002) gives $D_{n50,f}$ = 2.78 cm), especially the largest stones of the underlayer were hard to place in such a way that a smooth underlayer was created. The other parameters of the configuration are shown in Table 4.1, a side view is drawn in Figure 4.8a.

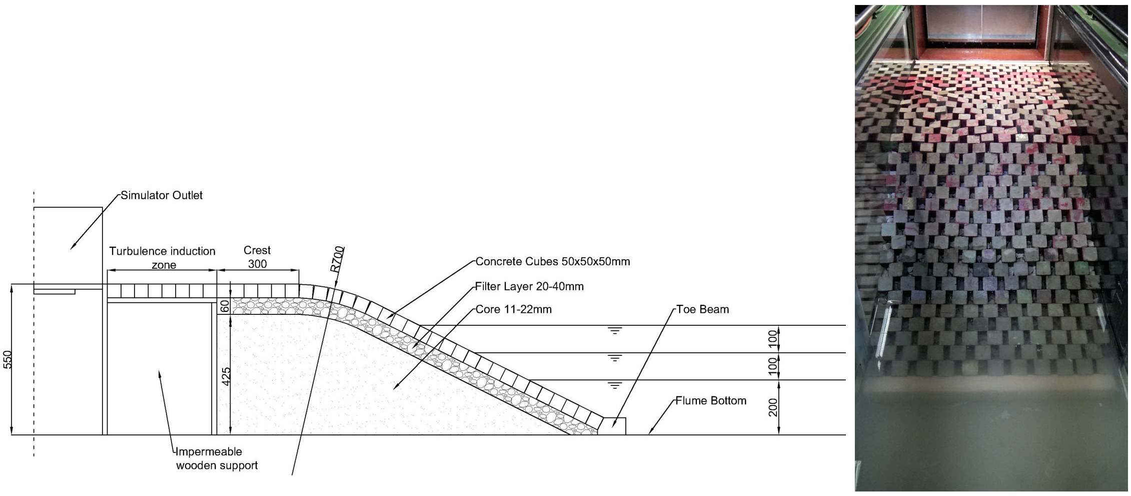

(a) Cross-section (in mm) *(b) Front view*

Figure 4.8: Configuration 1

No damage was observed at the slope during overtopping tests with this configuration. Rocking and displacement of the cubes were noticed on top of the crest. Starting from Wave 5 (q_{peak} = 72 L/s/m), the rocking on top of the crest intensified with enlargement of the simulated waves. Displacement of the cubes was seen solely on top of the crest. Wave 12 did not result in any damage nor displacement of the cubes at the slope at all, although the rocking of the cubes at the transition during the release of the volume was significant.

Configuration 2

Concluded from the tests with Configuration 1, an armour layer constructed out of cubes with D_n = 5 cm is very stable. Cubes with a D_n = 3.1 cm were installed (Figure 4.9b), despite the mass difference of factor 5 ($M_{D_n=5cm}/M_{D_n=3.1cm}$ = 5). The placement density was increased with n=0.25 considering the large mass difference compared to the 5 cm cubes. Cubes with a diameter of 5 cm were used on top of the crest considering rocking was observed at Configuration 1. Moreover, rocking was observed at the transition of Configuration 1. Hence, a sharp-edged transition was installed similar to the tests of Hellinga (2016). It was concluded from the experiments of Hellinga (2016) that the stability of the rear slope increases with the cubes of the slope placed in the 'shadow' of the rear crest line. Hence the placement of the slope cubes in the lee of the crest, as can be seen in Figure 4.9a.

Installing 3.1 cm cubes from the bottom of the slope upwards would result in an armour layer of 34 rows of cubes. This is significant more rows as tested by Hellinga (2016), were 23 rows were used. More rows could lead to larger displacements due to settlements. To overcome this issue, a toe higher up the slope was constructed, using the same material as used for the underlayer of the crest with an additional metal strip to ensure all cubes were lined up accordingly (similar construction as used in Hellinga (2016)). The side view is drawn in Figure 4.9a. The toe, constructed in this way, is not infinitely stable. Although, it is still more stable than a toe used in a 'real' situation without the steel rod. Hence, it was foreseen that the failure mechanism (failure of the slope stability) would not alter.

The Waves 1 to 4 resulted in no damage. This was caused by the large amount of infiltration in the core at the crest, ergo no water jet impinged on the slope. The cube at the crest line started rocking at Wave 5. Wave 6 (q_{peak} = 106 $L/s/m$) caused next to significant rocking of the outer row of cubes on the crest, a sudden rupture of the toe on the slope (Figure 4.9c). At the right bottom of the figure, the supporting rod is visible sticking out of the slope.

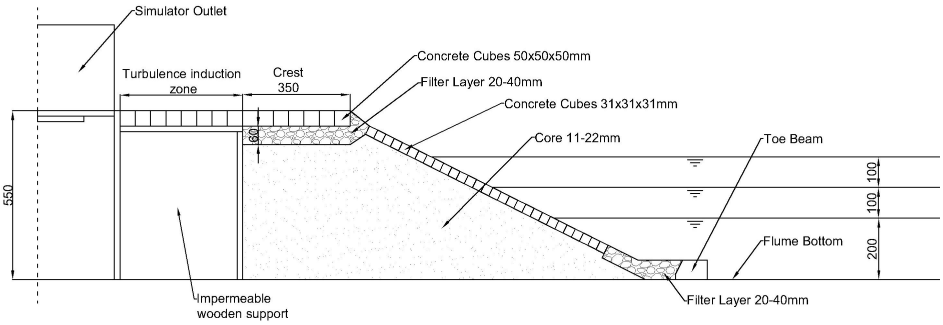
Simulator Outlet
Turbulence induction zone
Crest
350
Concrete Cubes 50x50x50mm
Filter Layer 20-40mm
Concrete Cubes 31x31x31mm
Core 11-22mm
Toe Beam
60
550
100
100
200
Flume Bottom
Impermeable wooden support
Filter Layer 20-40mm

(a) Cross-section (in mm)

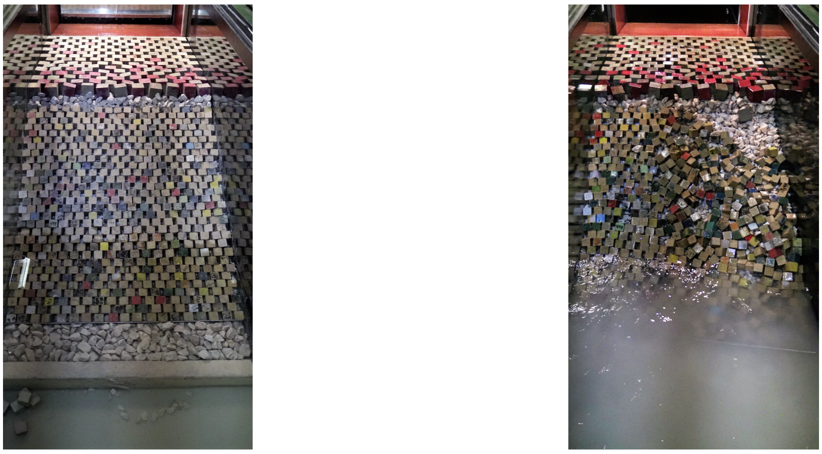

(b) Front view *(c) Front view failure*

Figure 4.9: Configuration 2

Configuration 3

Configuration 3 was changed compared to Configuration 2, for the reason that: (1) considering the toe of Configuration 2 was constructed slightly too stable for a 'real' situation (using the metal strip to align all the cubes), (2) the fact that the rupture was so severe and (3) the large step from D_n = 5 cm to D_n = 3.1 cm. Therefore, it was opted to install an armour layer using cubes with a diameter of 4 cm on the slope with n=0.3. The 4 cm cubes were placed directly on top of the core, hence little protrusion between next laying cubes was present (Figure 4.10b) due to the small grading of the core (Figure 4.10a). The transition was filled with the same material as used for the underlayer of the crest.

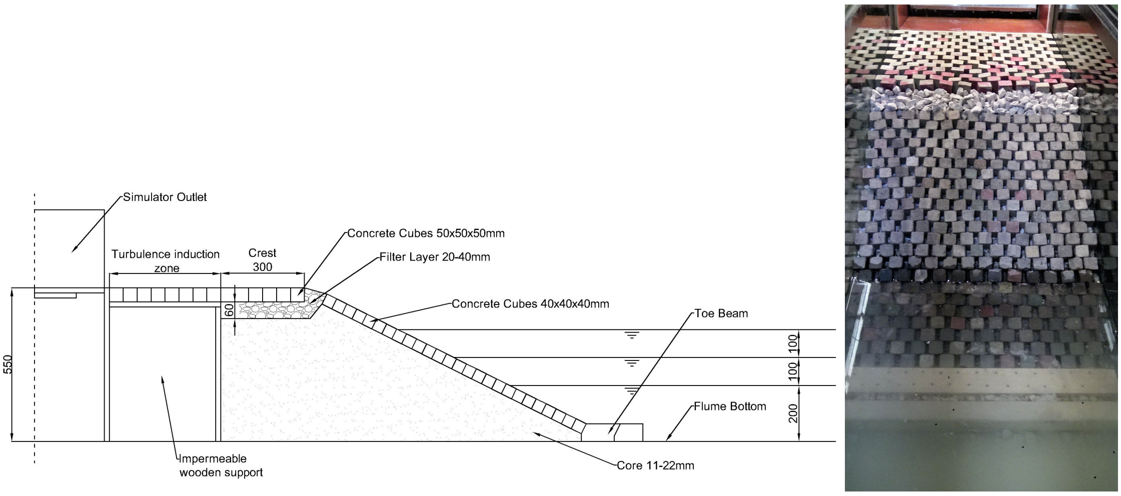
Simulator Outlet
Turbulence induction zone
Crest 300
Concrete Cubes 50x50x50mm
Filter Layer 20-40mm
Concrete Cubes 40x40x40mm
Toe Beam
60
550
100
100
200
Flume Bottom
Impermeable wooden support
Core 11-22mm

(a) Cross-section (in mm)

(b) Front view

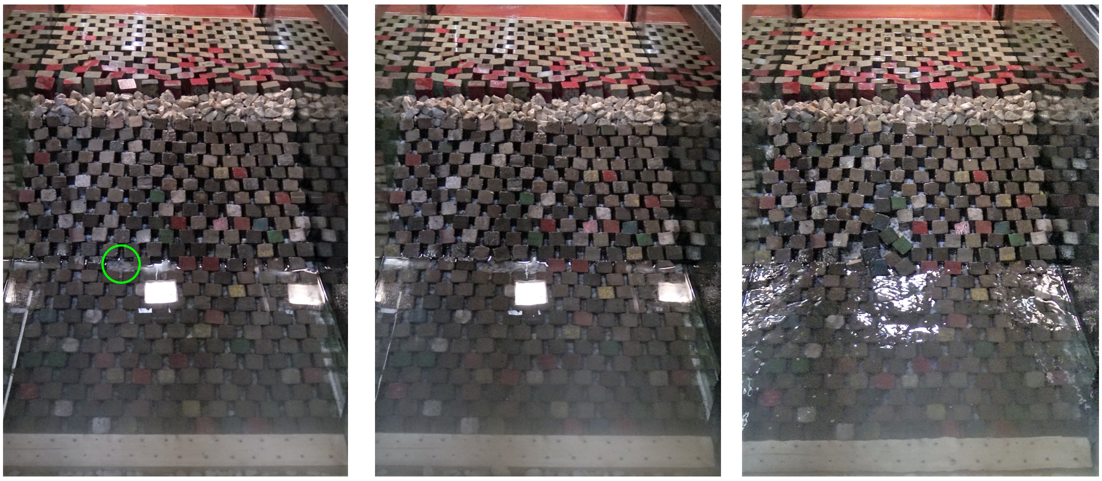

(c) Front view (one cube removed manually)

(d) Front view (three cubes removed manually)

(e) Front view failure

Figure 4.10: Configuration 3

This configuration better enclosed the last row of cubes of the crest compared to Configuration 3. This caused less rocking of that row of cubes, however, the rubble material at the transition (equal to the underlayer of the crest) was in the discharge stream. Flushing out of the rubble material was observed directly at the smallest waves. Where after little out-wash took place till Wave 10 (q_{peak} = 164 $L/s/m$). At Wave 10 larger amount of the rock fill at the transition flushed out, and cubes at the inner crest line were no longer supported sideways, hence rocking was observed. After the 12 waves, no damage at the cubes was found. The cubes appeared to be very stable. This could have been caused by the underlayer (short leakage length) and the taut placement of the cubes.

Extra tests were executed with a cube manually extruded from the slope at the waterline (at the green circle in Figure 4.10c). While pulling out one cube, the significant clamping was observed by the lifting of 3 rows of cubes both upwards and downwards of the slope (as shown in Figure 2.13b). The cubes settled slightly around the gap, however, no difference in settlement was seen after 3 times Wave 7. Next to the gap, two other cubes were removed manually (Figure 4.10d). This caused the above two cubes to have no lateral support at all, hence the slope collapsed (Figure 4.10e).

Configuration 4

This configuration was similar to Configuration 3, except for the underlayers (Figure 4.11a). This difference should create larger leakage lengths and less precise placed cubes. The latter was not the case because the precise placement was still very well possible (Figure 4.11b). For the filter layer for the crest $D_{n50,f} = D/1.8 = 2.78$ cm is available. The formerly used fraction of 20/40 mm was slightly too large, hence a different layer (20/32 mm) was installed on the crest. The slope required an underlayer of $D_{n50,f} = D/1.8 = 2.22$ cm, hence a filter layer of 16/25 mm was installed on the slope.

Another difference between Configuration 3 and 4 was the number of rows, an extra row was installed to prevent removal of the fill of the transition (see the difference between Figure 4.10b and Figure 4.11b). It was estimated that the alteration of the filter layers should cause (1) less infiltration in the crest and (2) larger leakage lengths, hence more loads on the armour layer.

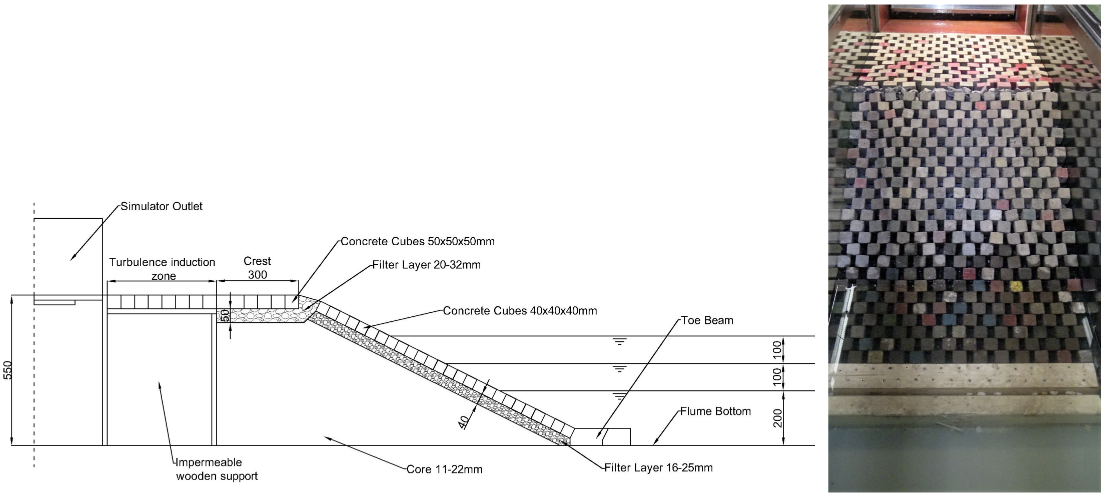
Simulator Outlet
Turbulence induction zone
Crest
300
Concrete Cubes 50x50x50mm
Filter Layer 20-32mm
50
Concrete Cubes 40x40x40mm
Toe Beam
550
100
100
100
200
40
Flume Bottom
Impermeable wooden support
Core 11-22mm
Filter Layer 16-25mm

(a) Cross-section (in mm) *(b) Front view*

Figure 4.11: Configuration 4

In this configuration, a smaller area at the transition which had to be filled was used, compared to Configuration 3. This transition appeared to be very stable and no out-wash of the fill was seen. It is possible that this changes when the slope settles. No damage was found during this test cycle. The water level was increased to observe the stability effect of the buoyancy forces. After the whole test cycle, no damage nor rocking was found. Similar as in former tests, no damage was realised at the armour layer after all twelve waves. It was again observed that large clamping forces were present in the armour layer.

Configuration 5

It was considered that clamping is of major influence of the stability. To 'loosen up' the layer, a rock material toe (20/40 mm) was constructed considering the toe would slightly settle (Figure 4.13a and 4.13b). The settlement, in this case, is not controlled and highly dependent on the placement of the rubble and the length of this section on the slope.

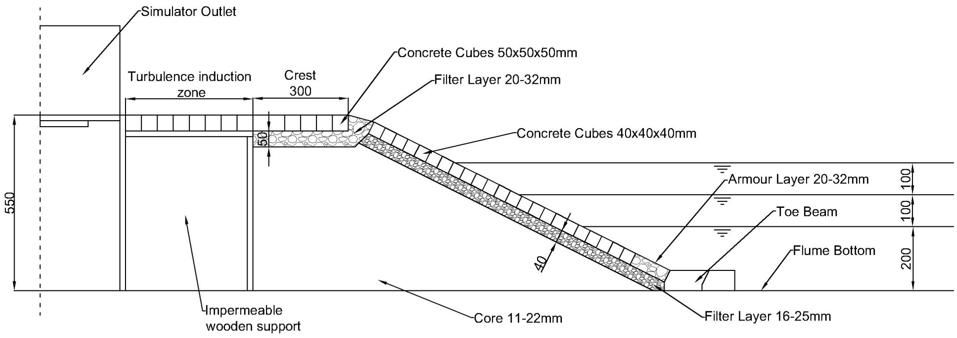
Simulator Outlet
Turbulence induction zone
Crest
300
Concrete Cubes 50x50x50mm
Filter Layer 20-32mm
Concrete Cubes 40x40x40mm
50
550
40
Armour Layer 20-32mm
Toe Beam
Flume Bottom
100
100
200
Impermeable wooden support
Core 11-22mm
Filter Layer 16-25mm

(a) Cross-section (in mm)

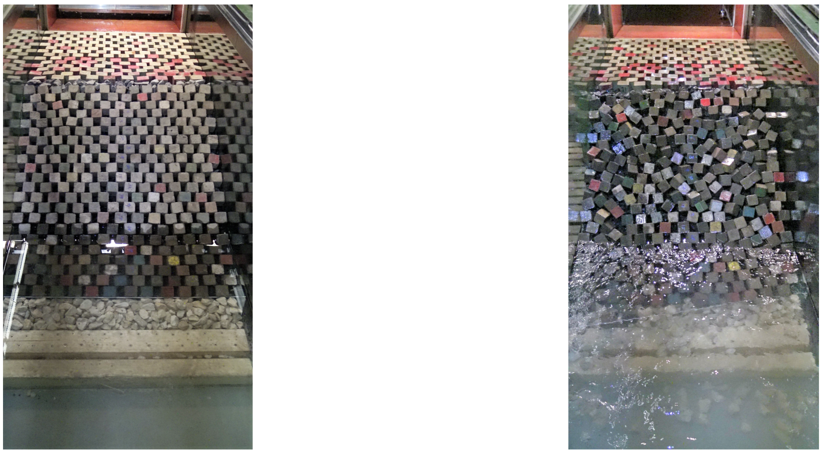

(b) Front view *(c) Front view failure*

Figure 4.12: Configuration 5

Starting again with the smallest wave, after Wave 7 the whole cubic armour layer collapsed (Figure 4.13c). This configuration showed significant flushing of the armour layer under the toe during Wave 6 and Wave 7. At the bottom of Figure 4.13c the large amount of rock material is visible on the flume bottom. This flushing was presumably introduced by the influence of the bottom of the flume. Large turbulence was seen around the toe. Considering the D_{n50} of this armour layer of rock was relatively large and still failed, it was assumed that the flume bottom was influencing the water current at the lower part of the slope, creating large forces on the rubble to such extent that this washed out. After Wave 7, the rubble was removed in such extent that the cubic armour layer collapsed.

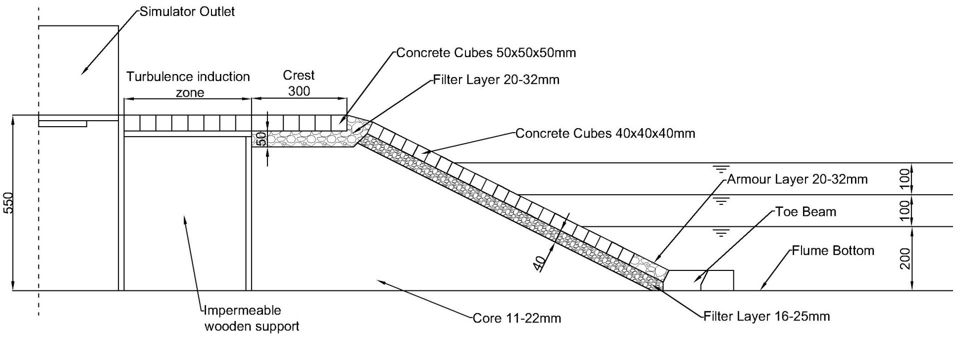
Simulator Outlet
Turbulence induction zone
Crest 300
Concrete Cubes 50x50x50mm
Filter Layer 20-32mm
Concrete Cubes 40x40x40mm
Armour Layer 20-32mm
Toe Beam
Flume Bottom
Filter Layer 16-25mm
Core 11-22mm
Impermeable wooden support
550
50
40
100
100
200

(a) Cross-section (in mm)

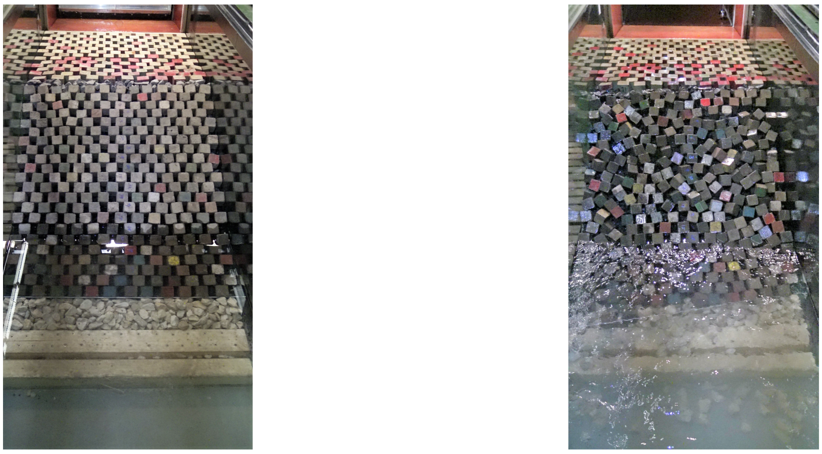

(b) Front view *(c) Front view failure*

Figure 4.13: Configuration 5

Configuration 6

In Configuration 6, the rubble toe of Configuration 5 is replaced by steel plates of 3 mm thick (Figure 4.14b). In contrary to the situation with a toe constructed of rubble (with an unpredictable settlement), by extruding one or multiple plates a known available settlement was created. With removing one plate a settlement capability of 3 mm was available at the bottom row of cubes.

After the first waves, settlement was observed in the armour layer. This settlement loosened particularly the cubes at the bottom. In Wave 9 indeed one cube was removed, due to the fact that no mutual contact was present between the cubes. This removal did not show any further failure during the test programme. Figure 4.14c shows (in the green circle) the removed cube. Later, in the middle, 4 rows above, two cubes were extruded manually. Figure 4.14d shows the eventual failure, after one load of Wave 7.

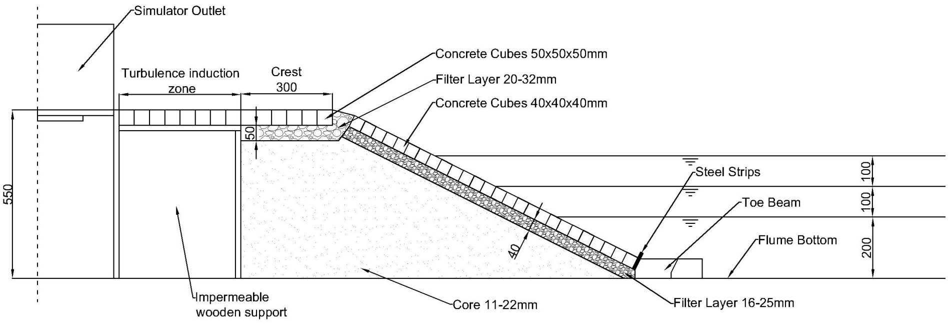
Simulator Outlet
Turbulence induction zone
Crest
300
Concrete Cubes 50x50x50mm
Filter Layer 20-32mm
Concrete Cubes 40x40x40mm
50
550
40
Steel Strips
Toe Beam
Flume Bottom
100
100
200
Impermeable wooden support
Core 11-22mm
Filter Layer 16-25mm

(a) Cross-section (in mm)

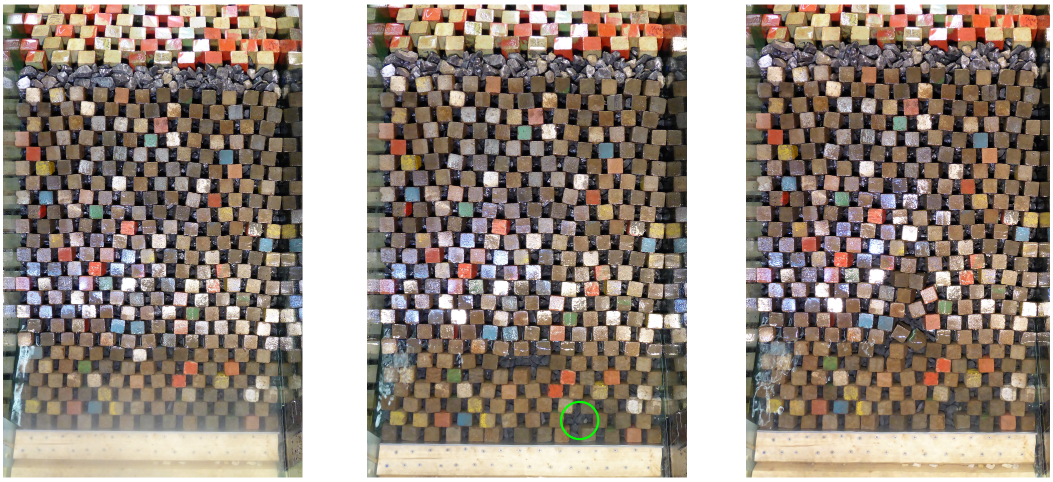

(b) Front view

(c) Front view with one cube removed by wave load (green) and two cubes removed manually

(d) Front view failure

Figure 4.14: Configuration 6

Configuration 7

Considering the obvious cause of the failure at Configuration 6 and the lack of stability failure found in the above-mentioned tests at the slope, the slope armour layer with 2 cm cubes with n=0.25 was constructed. To limit the number of rows of cubes, a toe was installed (with similar permeability yet without the ability to settle) higher up the slope. See Figure 4.15a and Figure 4.15b. The toe was constructed by drilling 915 holes with a diameter of 10 mm (no core material could flush through the holes) in a 2 cm thick plate. On both sides of the plate a couple of millimetre space was left, hence no holes had to be drilled directly on the border. In this way the permeability was equal to a slope covered with cubes placed with n=0.25 and no settlement of the lower row of cubes could occur.

The simulation programme was refined with smaller intermittent water levels inside the reservoir as used in former tests. During the 6th wave (H_s = 18 cm), a piston-like failure was seen at the lowest row (the green cirle in Figure 4.15c), 5 rows under the water level. This is likely caused by the smaller friction between the wooden toe support and the concrete cube. The subsequent waves did not cause any other damage at the revetment.

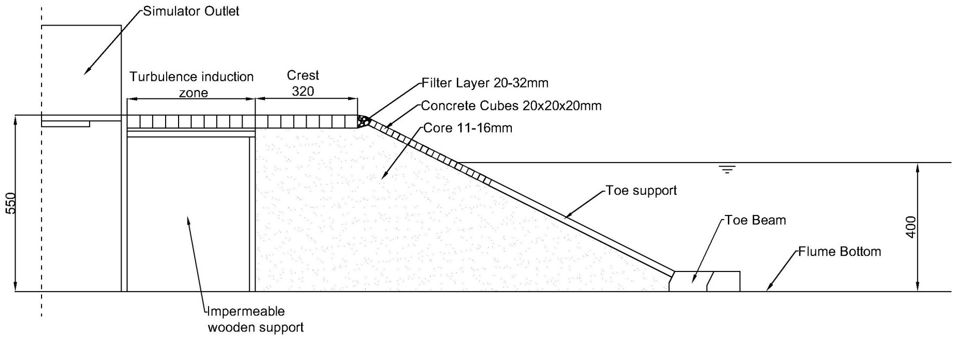
Simulator Outlet
Turbulence induction zone
Crest
320
Filter Layer 20-32mm
Concrete Cubes 20x20x20mm
Core 11-16mm
Toe support
Toe Beam
Flume Bottom
550
400
Impermeable wooden support

(a) Cross-section (in mm)

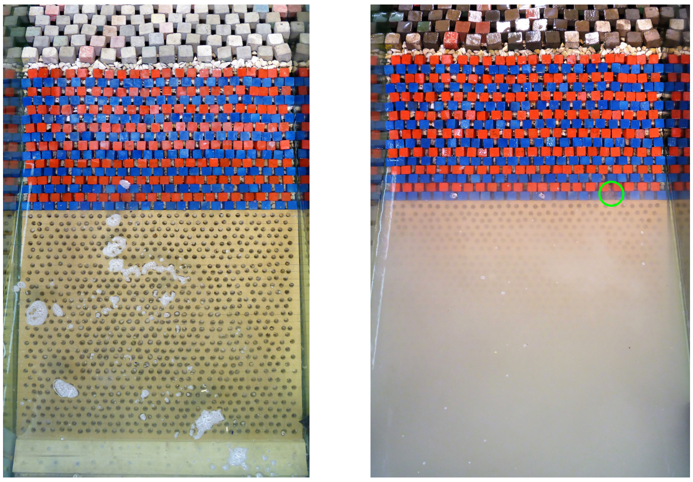

(b) Front view *(c) Front view damage*

Figure 4.15: Configuration 7

4.5 Breakwater Experiments Analysis and Discussion

4.5.1 Hydraulic (load) aspects

Simulated wave on top of the crest

Regarding overtopping wave volumes at the crest, several interesting phenomena were seen, which are discussed below.

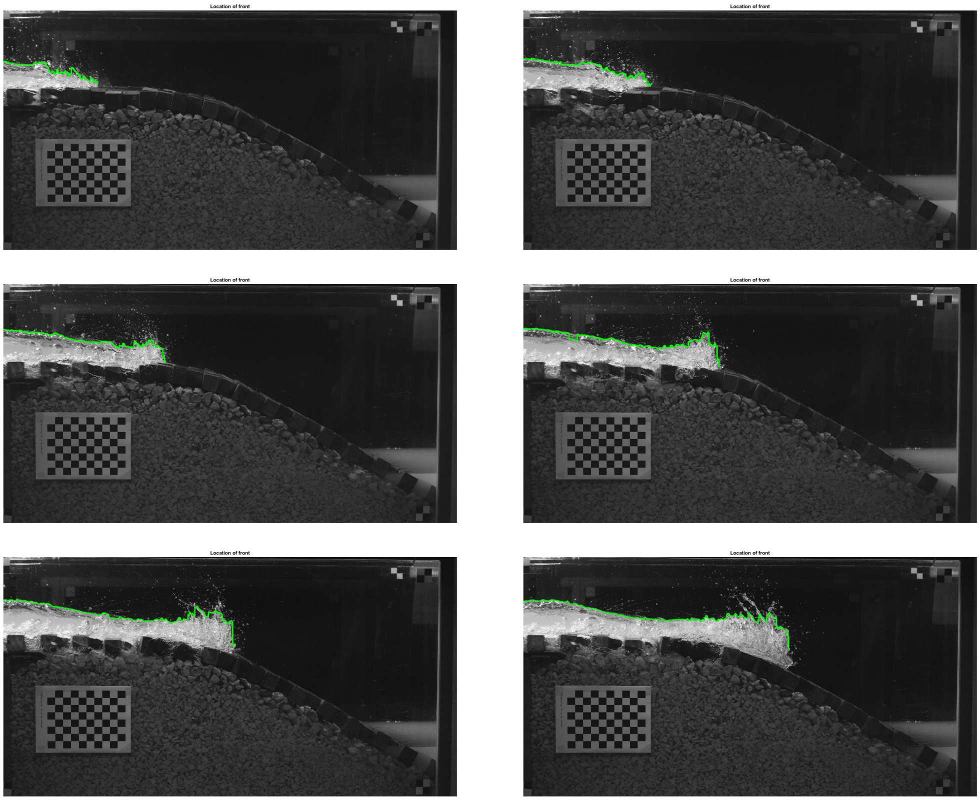

Figure 4.16: Wave tongue propagating on crest with green line as detected waterline

Infiltration. The effect of infiltration is clearly visible in Figure 4.16 by the decrease in layer thickness. A relatively large fraction of the smaller wave volumes is able to infiltrate in the crest compared to larger volumes.

Front Steepness. As the wave propagates on the crest, the steepness of the wavefront increases. This is visible in Figure 4.16. One could argue that the ‘real’ front is not the splashing water. Although on a rough crest with high turbulence intensities ‘real’ wave is not determinable. With a smooth crest, the wavefront steepness does not increase. This increase in steepness is resulting from the friction of the crest. The steepness of the wavefront could be relevant for the impulse of the impinging jet at the slope, where a steeper slope enlarges the initial impact. How the steepness of a ’real’ overtopping wave at the outer crest line propagates is likely similar.

Velocities. With the used set-up of instruments, solely the averaged u_{front} was measured. The exact location of the wavefront was hard to determine, considering the significant splashing droplets at the front of the slope (hence large scatter was found per velocity interval). Averaged velocities over the crest were established by averaging the four velocities found with five subsequent pictures (Figure 4.17). Several trends are visible in the table:

- The impermeable configurations (Configuration 0a and Configuration 0b) show larger velocities compared to the permeable configurations. Especially with the higher velocities.
- The difference between Configuration 0a and Configuration 0b is caused by the friction of the cubes, which is substantial.
- No trend is visible between Configuration 1 and Configuration 4. Although Configuration 4 has a smaller graded underlayer.
- The measured front velocities differ from the peak velocities generated by the WOS. Where small layer thicknesses have a lower front velocity, and large thicknesses have a higher front velocity compared to the peak velocity. This difference could be explained by the fact that the peak velocity exerted by the WOS is from such short duration that it has little effect on the averaged front velocity at the crest.

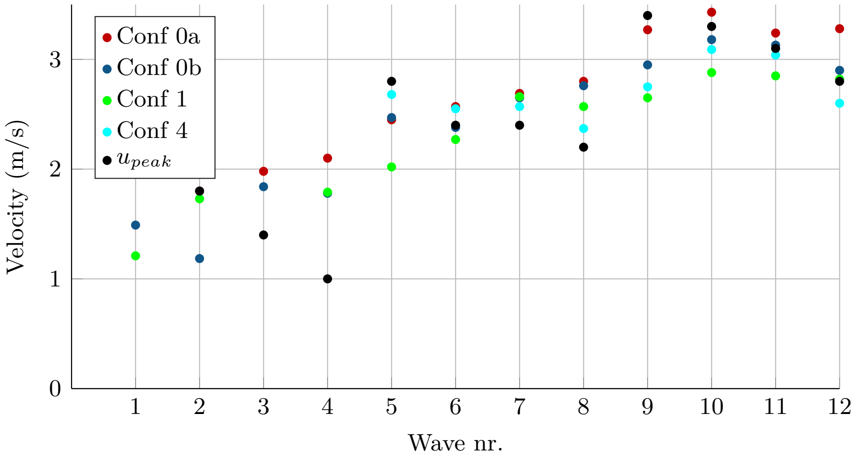

Figure 4.17: Averaged front velocities on the crest

Not only the wavefront(velocity) is relevant for the load on the cubes. Indicated by the movements of the cubes seen during the overtopping wave tongue. The inner slope of a low-crested breakwater, in contrary to a dyke, is mainly loaded by the wave front of the impinging jet.

Turbulence. The turbulence intensities in the overtopping wave itself are hard to determine. Air bubbles indicated rolling movements, likely similar to the rolling movements in a ‘real’ overtopping wave considering the run-up at the outer slope.

Simulated waves at the slope

Figure 4.18 shows Wave 7 propagating on different crest and transition configurations. Figure 4.18a clearly shows a separate jet, wherein Figure 4.18b the jet is less distinguishable although a large part still detaches from the slope. Figure 4.18c shows a rounded transition, where a jet is present as well. Although, not that well able to indicate. Figure 4.18d shows a jet created by a rocking cube acting as a ramp.

The velocity at the transition of the crest determines the location of impact of the jet on the slope. The formulas of Kudale and Kobayashi (1996) can be used to determine the shape of the jet (Equation 2.31 and 2.32). It is likely that if the jet exactly hits the waterline the combination of jet impact and buoyancy will be least favourable stability wise for the cube layer. Consequently, the formula determining Δs_x of Kudale and Kobayashi (1996) has to equal $R_c/\tan\beta$ to predict the most vulnerable combination of u_{front}, h, β and R_c. Rewriting gives:

$$u_{front} = \frac{\sqrt{g} \cdot R_c \cdot \cot\beta}{\sqrt{h + 2R_c}} \tag{4.1}$$

This effect is elaborated in the next section.

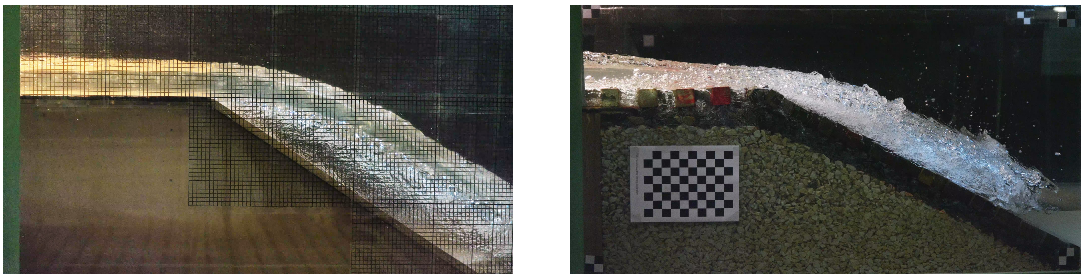

(a) Impermeable crest; sharp transition; slope 1:1.5 (Configuration 0a)

(b) Permeable crest; sharp transition; slope 1:2 (Configuration 4)

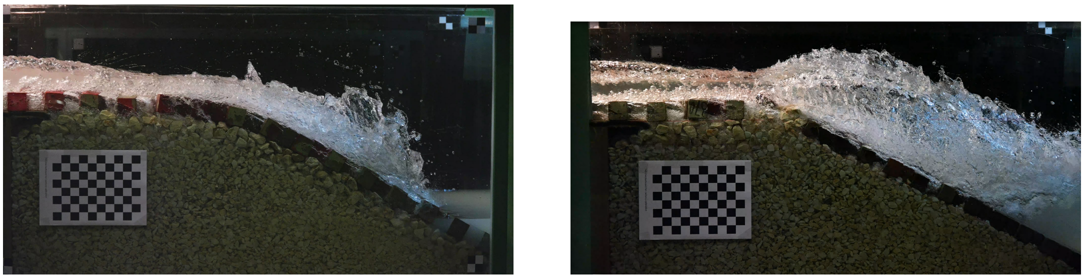

(c) Permeable crest; round transition; slope 1:2 (Configuration 1)

(d) Permeable crest; sharp transition with rocking cubes; slope 1:2 (Configuration 3)

Figure 4.18: Side view of overtopping volumes using Wave 7

4.5.2 Stability aspects

The stability of the cubes on the rear slope is not well described by the dimensionless stability parameter $\frac{H_s}{\Delta \cdot D}$. Figure 4.19 shows the values of the parameters, where the filled dots represent the failing cases and the empty dots represents the maximum values tested. The dimensionless rear-slope mobility number $\theta = \frac{q}{\sqrt{g \cdot \Delta \cdot D^3}}$ proposed by Andersen (2006) gives, in theory, a better representation of the stability. Especially at the rear slope where the duration of the wave is likely to have less influence on the stability compared to the stability at the crest. For q, $q_{peak,max}$ should be used. Instead of the term D, W_c or R_c could be used as well. The magnitude of W_c is not changed during the experiments and only the largest R_c is tested, hence no conclusions can be drawn regarding these factors.

This dimensionless number θ combines the most relevant load parameters (the maximum peak discharge in the storm $q_{peak,max}$) and the most relevant strength parameters (Δ

and D). The parameter H_s would not provide enough significant information at the rear slope considering the slope angle, slope friction and freeboard influence the wave tongue. The stability numbers found in the research of Hellinga (2016) were not very accurate. Table 4.2 showed the maximum mobility/stability numbers tested. No trend is visible here. The possible explanation of this lack of trend is the third power of the cube dimension in the number, which greatly influences the value.

The stability formula of van Gent and Pozueta (2004) (Equation 2.53) for rock revetment at the rear slope can not be used to compare the found rock damage at the transition and toe with the theoretical values. This formula uses the $R_{u,1\%}$, where the simulated volumes by the WOS represent the maximum overtopping volume found in a storm. The maxima of the simulated storm are relatively very large (Figure 3.33). This results in $R_c > R_{u,1\%}$ and consequently no useful stability values can be calculated using Equation 2.53. Smaller values of the outer slope friction than used in the rest of the thesis ($\gamma = 0.53$) still result in low $R_{u,1\%}$.

The excess of work theory of Hughes and Thornton (2016) as shown in Figure 2.14, with a certain critical q_c, applied to the observed rocking at the crest and transition, did not show any trend.

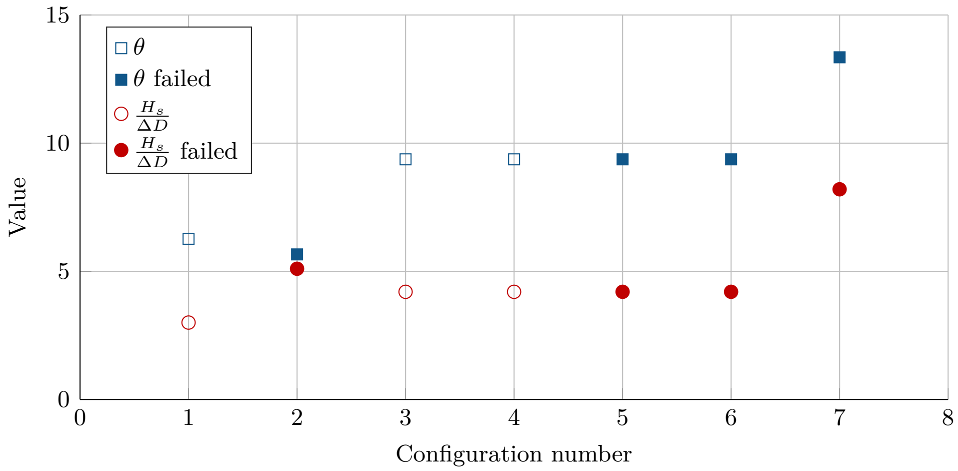

Figure 4.19: Damage numbers $\frac{H_s}{\Delta \cdot D}$ *and* θ

Figure 4.20 shows that the theoretical most vulnerable velocity (Equation 4.1) is a very reasonable estimation of the weakest situation. All configurations where damage was seen, failed during the waves where the front velocity on the crest was around the velocity which generated a jet landing at the waterline.

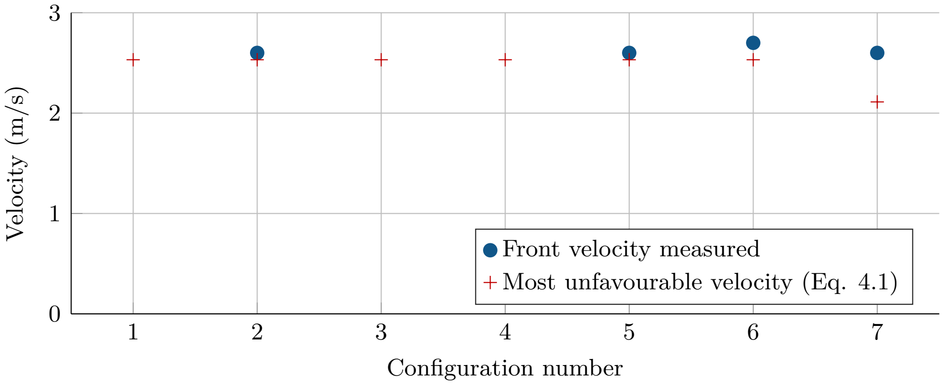

Figure 4.20: Most unfavourable front velocity vs. front velocity measured of damaging wave

Crest

Clamping. The lack of sideways support of the cubes placed at the crest resulted in lower revetment stability compared to the cubes placed on top of the slope. During the test, solely rocking of the cubes on top of the crest was observed. Especially during larger waves in the test range.

Underlayer and protruding cubes. The underlayer appeared to have a significant influence on the stability as well. This was caused by the fact that an underlayer consisting of larger stone sizes, results in an ill-placed top layer (as can be seen at the crest of Configuration 3 (Figure 4.10b)). Two factors play a role here. First is the fact that with ill placement, more blocks protrude from its next-laying cube. The second reason is the formerly mentioned lack of horizontal support or clamping with ill-placed cubes. In a layer of cubes which are all a bit tilted, space exists for the blocks to rock during an overtopping wave.

Stability-wise, it is crucial that the cubes are supported by three points of the underlayer. Figure 4.21 shows four different support mechanisms. 'A' is the favourable position, using 3 stones from the underlayer to support the cube. 'B' shows a cube which is supported by 2 cubes. This results automatically in a cube which leans against a next laying cube. Cube 'C' is supported by stones from a large gradation which results rapidly in too large height differences, and hence ill placed cubes. 'D' shows the cube supported by 4 stones. This is hard to exactly align and little rocking is likely to occur. This analysis shows the importance of a flat underlayer.

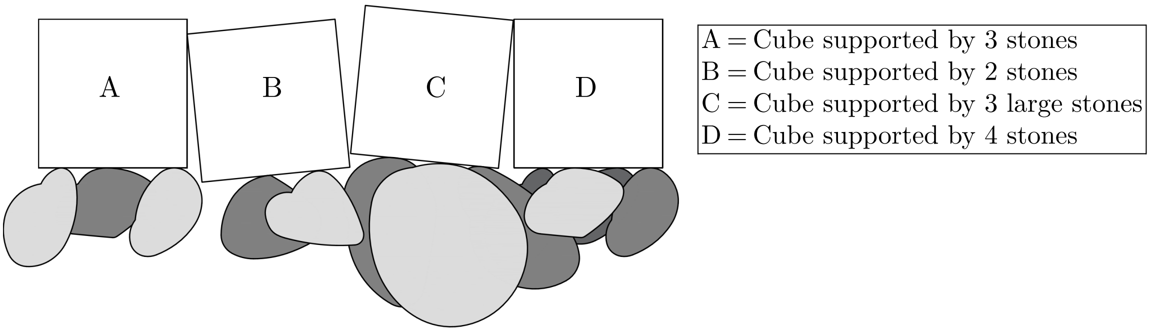
A
B
C
D
A = Cube supported by 3 stones
B = Cube supported by 2 stones
C = Cube supported by 3 large stones
D = Cube supported by 4 stones

Figure 4.21: Cubes placed on top of a crest

Stability-wise, it is crucial that the cubes are supported by three points of the underlayer. Figure 4.21 shows four different support mechanisms. 'A' is the favourable position, using 3 stones from the underlayer to support the cube. 'B' shows a cube which is supported by 2 cubes. This results automatically in a cube which leans against a next laying cube. Cube 'C' is supported by stones from a large gradation which results rapidly in too large height differences, and hence ill placed cubes. 'D' shows the cube supported by 4 stones. This is hard to exactly align and little rocking is likely to occur. This analysis shows the importance of a flat underlayer.

Not only the positive deviation but also the local negative deviations, where space is left for vertical settlement of the cube . Especially on the crest, where no clamping occurs, this is significant (see crest difference in Figures 4.10b and 4.10c). A good starting point is the tolerances used for Accropodes. The protrusion distance of one cube next to the other should then be limited to the tolerances applied to the underlayer.

Crest width. In the tests of Hellinga (2016) the width of the crest was varied to investigate the significance of the crest width to the rear slope stability. The crest stability itself was not in the scope of that study, hence no comparison in results can be made.

Transition

Concluded from the tests of Hellinga (2016) was the significance of the crest-slope transition to the rear slope stability. It was stated that placing the cubes in the shadow of the crest would increase the slope stability. Two types of transitions were tested in this study: the rounded transition, as generally applied on the outer crest line, and the sharp-edged transition wherein the lee of the last row of cubes of the crest, the slope cubes are placed. The gap was filled with differently sized rubble, similar as the underlayer on the crest. Both types of transitions are discussed below.

Rounded transition. Cubes placed in a rounded transition have in theory only at the bottom support from the next laying cubes (Figure 4.22a). Small fluctuations in the underlayer quickly result in cubes resting with the full sides on each other (Figure 4.22b). This mutual support generates more resistance for rocking, although the distance to the cube in front of those aligned cubes enlarges, hence this cube is more sensitive for rocking. The rocking of the cubes at the rounded transition during the tested configuration started from Wave 6 and intensified up to Wave 12 without further damage of the armour layer.

When settlement takes place, the gap between the cubes will expand, hence the rocking will intensify. It is thought that the cubes not only give direct support to each other but also streamline the water flow behind the cube (Figure 4.24). This minimises the vortex trailing the cube and hence minimises the pressure difference behind the cube. This effect is stronger with the sharp transition between the crest and the slope, which is discussed in the next section.

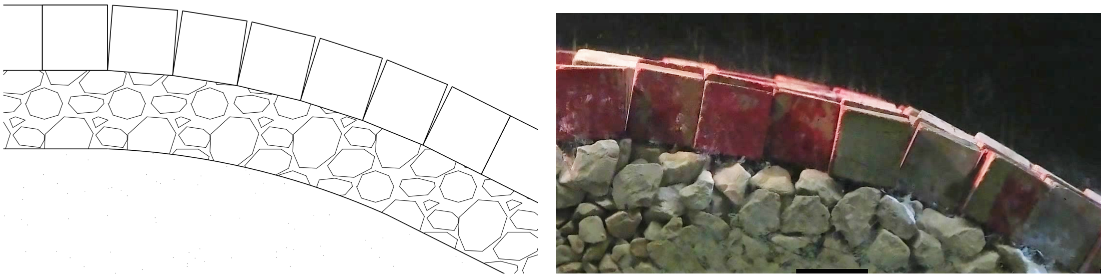

(a) Technical drawing *(b) As-built*

Figure 4.22: Transition Configuration 1

Sharp transition. A sharp transition has several benefits over a rounded transition at the rear side. A sharp inner crest line transition between the crest and the slope is less vulnerable to settlement and displacement of the toe (discussed in a next subsection). The last cube on the crest, on the other hand, appeared to be very sensitive for rocking. The horizontal support was lacking when the slope was settled a bit. Moreover, the amount of washing out of the filling material was significant in Configurations 3 and 6. The transition detailing appeared to be very important. This result is in agreement with the findings by Hellinga (2016).

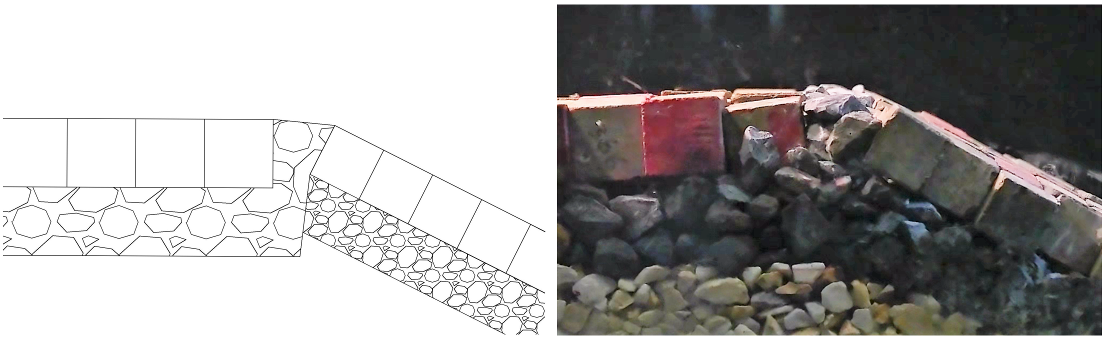

(a) Technical drawing *(b) As-built*

Figure 4.23: Transition Configuration 5

With a sharp transition, the last cube on the crest appeared to be the weakest link. Where the round edge ensures a streamlined behind the crest cubes, a sharp transition lacks this kind of shape. In the basis 4 different sharp transitions are possible, 2 non-filled and 2 filled. In Figure 4.24 these four possibilities are schematized.

Figure 4.24a shows the slope placed in the lee of the crest cube. This generates large forces on the last cube of the crest. Figure 4.24b shows, on the other hand, a configuration where the slope cubes are placed higher. Although this generates a smaller vortex, the cube slope is more exposed to the forces of the overtopping wave tongue. Figure 4.24c displays the transition with fill material. Although this is placed in the lee of the cubes of the crest, the fill is not well supported and will presumably flush away. The configuration shown in Figure 4.24d is favourable considering the fill streamlines the crest, and prevents the occurrence of a vortex causing drag forces. The relative 'high' placement of the slope compared to the crest, enables a good support for the fill material.

The last cube of the row would not be stable without any horizontal support. When the cubes on the rear slope settle, the rock fill will move downwards as well and the potential horizontal support is disappeared. It is relevant to take into account the settlement of the slope considering this is one of the leading causes of failure. This is discussed in the next subsection.

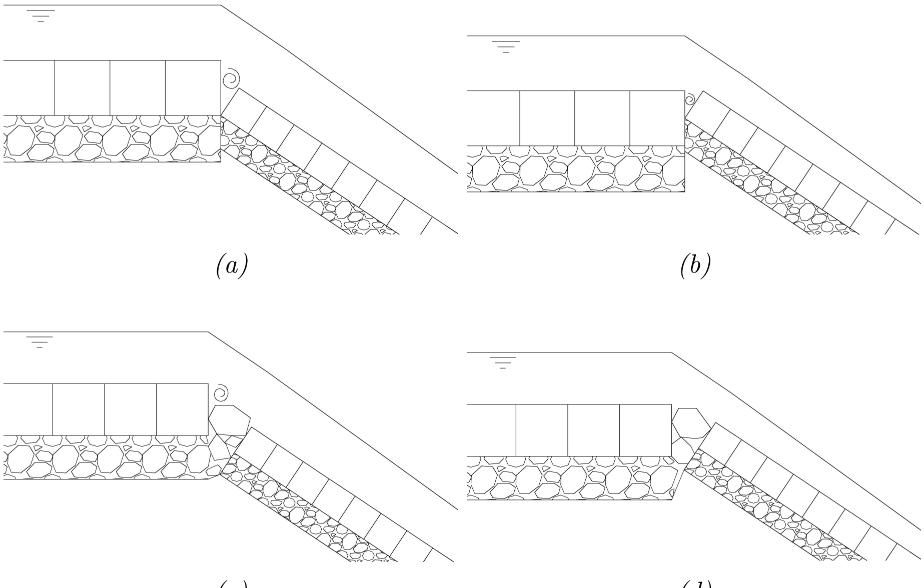
(a) (b)

(c) (d)

Figure 4.24: Schematisation of inner crest line transition possibilities

Slope

A single-layer cubic revetment rear-side slope is highly stable compared to similar sized cubes placed randomly on a slope. The study of Hellinga (2016) resulted in stability numbers $H_s/\Delta D$ for the rear crest between 2.5 and 6.5. Likewise, as shown in Figure 4.19, no clear stability numbers are determined in this study although the found stability numbers have similar magnitudes as found by Hellinga (2016). A minimum of $H_s/\Delta D = 4.2$ was found. Figure 4.20 shows indirectly the influence of the jet. This suggests that the normative design wave is the wave generating a jet impacting exact the waterline. Elements contributing to the revetment stability are discussed below.

Clamping. Concluding from the tests, clamping appeared to be one of the governing stability mechanisms. When trying to remove a cube manually, buckling of 3 rows below and above was observed. This shows the presence of large normal forces in the rows. The stability difference of the cubes with mutual interaction and the cubes without mutual interaction, such as placed on the crest and transition, is large. This indicates again that clamping, and not directly the own weight of the cubes, is an important stability mechanism of single-layer cube revetment. This own weight, on the other hand, does add to the normal forces generating the clamping on the slope.

The placement of the cubes in a stretching pattern results in a statical indeterminate system. Where in theory all cubes are well-clamped (without theoretical noise), practice shows that there are areas with well-clamped cubes and cubes with zero clamping. If this ill clamped cube is located at the waterline, the probability of extruding of that cube is significant. Similar as in the situation with placed-block revetment. The number of rows should be kept to a minimum, considering with every row small deviations are introduced.

This results in a slope where not all cubes are clamped with similar forces, and where some cubes are not clamped at all.

After tests with a manually removed cube in a well-clamped area, the cubes around that gap stayed stable (as in Figure 4.10c). Together with the slope failure with tests with two removed cubes in one row (as in Figure 4.10d), this suggests that clamping even generates enough stability for cubes only clamped at one side. In the case of a removed cube, washing out of the underlayer was seen, hence, in the end, the slope would fail. Configuration 6 did show a piston-like failure, although this is caused by the available settlement space at the toe. This again shows that the own weight of the cube is not the leading stability mechanism at single-layer cube revetment.

The stability mechanisms of single-layer cubic revetment could best be compared to placed revetment. Especially the stability mechanisms are highly comparable, whereas the load mechanisms differ considering the large porosity and hence the large leakage lengths of the single-layer cube revetment.

In general, the single-layer cube rear-slope armour is more stable than single-layer front-slope armour (at the front side unacceptable damage occures at $H_s/\Delta D = 2.9$ (van Gent et al., 2001)). Two major reasons can be provided to explain these findings. The first, and obvious, reason of the increased stability is the lack of impact of incoming waves. Solely overtopping waves, where already a lot of energy is dissipated, impinge on the inner crest. The second reason is that in situations with single-layer cubic revetment, upward movement ('swelling') of the armour unit is a possibility (Hofland and van Gent, 2016), which is not the case with rear side slope revetment: Almost all the forces exerted on the cubes on the rear side are downwards directed. This intensifies the clamping of the cubes. Only the forces generated by the overpressure in the underlayer are exerted in all directions. Due to the large porosity of single-layer cubic revetment (typically between 0.25 and 0.3) these forces are not considered significant, as in the case of placed revetment (typical porosity of 0.12).

Toe. The normal forces seen during clamping, have to be transmitted to the toe. The toe had to be able to cope with these large normal forces, otherwise, the toe will fail (as observed at Configuration 2 and 5).

The settlement of the toe is very relevant. If this settlement occurs equally over the slope, the normal forces, and hence its stability, will stay present. If the settlement is uneven, the clamping will deviate over the slope and ill-clamped areas will arise. Moreover, the formerly discussed transition will alter with a settled slope.

Underlayer and protruding cubes. The permeability of the underlayer plays a different role for the stability of cubes at the crest compared to the slope. A high permeable underlayer at the crest enlarges the amount of overtopping water infiltrating in the core, and hence reducing the hydraulic load on the rear slope. A high permeable underlayer at the rear slope enlarges the pressure differences between the inside and outside of the cube revetment. The delay in the outflow of water at the rear slope strongly indicates that transmission through a breakwater is not significant for the lee-side armour stability. Likewise, as the cube stability around a removed cube, it is assessed that protruding cubes have little influence on the stability in well-clamped areas.

Chapter 5

Conclusions and Recommendations

5.1 Conclusions

This research was intended to develop a different approach to study single-layer cube revetment on the crest and rear slope as used in the research of Hellinga (2016). In that study significant uncertainties and contradictions were found. By using an overtopping simulator the number of influencing factors is decreased. The introduction stated research questions which are answered below, starting with the two main research questions.

Is the Wave Overtopping Simulator an appropriate tool to investigate the failure mechanisms of single-layer armour units which are loaded by overtopping waves?

The WOS is an appropriate tool to investigate rear-slope failure mechanisms. The approach limits the number of influencing factors and enables tests at larger scales which reduces scaling errors (especially significant for cores with high permeabilities). Improvements on the device could be made enhancing the ability to simulate the characteristics of a realistic overtopping wave volume and to give a more detailed evaluation of the magnitudes of the overtopping characteristics.

What are the significant single-layer cube rear-slope stability mechanisms of low-crested breakwaters?

The normal forces between the cubes are very important for the stability of the cubes placed on the slope. The lack of interaction between the cubes on top of the crest results in a significantly lower tolerance for the hydraulic loads. The configuration with a sharp inner crest-line transition, if well designed, showed a stable alternative for a rounded transition.

Which hydraulic parameters are relevant for the description of the normative individual overtopping waves?

The five parameters determining the eventual magnitude of the individual wave overtopping volume with its characteristics are:

- the incoming significant wave height H_{m0};
- the incoming mean wave period $T_{m-1,0}$;
- the outer slope angle α;
- the outer slope friction factor γ;
- the storm duration t; and
- the crest height relative to the water level R_c.

The influence of a berm, the wind, and the influence of the angle of the incident waves are not included in the scope of this research. The characteristic parameters describing an individual overtopping wave are:

- the peak discharge q_{peak};
- the peak velocity u_{peak};
- the peak layer thickness h_{peak};
- the overtopping volume V_n; and
- the overtopping wave duration T_{ovt}.

Where h_{peak} is redundant assuming the peaks of the discharge and velocity occur simultaneously. From an extensive literature survey a set of equations was derived that can be used to calculate this second set of parameters based on the first set of parameters.

How should the overtopping simulator function, in order to generate waves with these hydraulic parameters?

The parameters noted above should all be steered individually assuming the peaks of the parameter values coincide. The distribution of the simulated volumes representing a storm could be determined by a two-parameter Weibull distribution (Hughes et al., 2012):

$$P_V = P(\underline{V} \geq V) = \exp\left(-\left(\frac{V}{a}\right)^b\right) \tag{5.1}$$

with (non-dimensional) (Zanuttigh, 2013)

$$b = 0.73 + 55\left(\frac{q_{mean}}{gH_sT_{m-1,0}}\right)^{0.8} \tag{5.2}$$

and (dimensional) (Victor et al., 2012)

$$a = 1.13 \cdot \tanh(1.32 \cdot b)\frac{q_{mean} \cdot T_m}{P_{ow}} \tag{5.3}$$

The corresponding individual overtopping characteristics were determined by (Hughes, 2015):

$$q_{peak} = 7.405 \cdot \frac{V\sqrt{\tan\alpha}}{T_{m-1,0}} \tag{5.4}$$

$$u_{@qpeak} = 25.99 \cdot \frac{\sqrt{V\tan\alpha}}{T_{m-1,0}} \tag{5.5}$$

and $h = q/u$.

The velocity can be controlled by the water level in the simulator's reservoir. The layer thickness can be steered by the opening height of the valve, and the volume and duration of the overtopping wave can be regulated by adjusting the flume axial width of the reservoir.

The orifice discharge coefficient was determined to link the opening of the valve to the layer thickness generated. The turbulence was intensified by installing a rough and impermeable zone directly next to the orifice. Visible rotating movement in the wave tongue was introduced, although to what extend this approach is correct representation of the 'real' turbulence intensities was not verified.

Is it possible to simulate wave overtopping volumes with accurate water layer thicknesses, turbulence intensities and wavefront velocities using a small scale wave overtopping simulator?

It is possible to simulate individual overtopping waves with their characteristics based on empirical overtopping formulas. The turbulence is introduced by a rough, impermeable section after the WOS outlet. The in this thesis suggested approach of storm simulation could be used to simulate a representative storm by the use of individual generated overtopping waves. An elaborating study is required to give a decisive conclusion about this statement.

How does an overtopping wave propagate on a low-crested breakwater crest, transition and inner slope?

The infiltration in the crest of the smaller wave volumes is significant. Additionally, the inner crest line transition has a large influence on the propagation the wave tongue. A rounded transition shows a more attached wave tongue, whereas a sharp-edged transition showed a more separate jet. Considering the short length of the inner slope of the low-crested breakwater, the rear slope itself has no influence on the propagation of the wave tongue, apart from getting impinged by the jet itself (in contrary to grass dykes).

How does an overtopping wave influence the single-layer cube revetment?

Seven different configurations with different cube sizes were tested in this research. During the executed experiments, the wave tongue induced significant rocking of the cubes placed on the crest and transition. Additionally, washout of the fill of the sharp transition crest line was seen in configurations where the area filled with rocks was more than $2D_{n,50}$. No exactly quantifiable stability relation was found during the executed experiments. Athough the stability number $H_s/\Delta D$ appeared to give little significant information of the stability at the rear slope, with stabiltiy tests resulting in a mininum $H_s/\Delta D$ of 4.2, the range is similar is in the tests of Hellinga (2016) (and larger as found for stability numbers at the front side by van Gent et al. (2001)).

The dimensionless rear-slope mobility number $\frac{q_{peak,max}}{\sqrt{g \cdot \Delta \cdot D^3}}$ (Andersen, 2006) includes more significant parameters, although no trend was visible in the results. The minimum value of $\frac{q_{peak,max}}{\sqrt{g \cdot \Delta \cdot D^3}}$ found was 5.6.

Which mechanisms are responsible for the stability and damage of the revetment, and what is the governing mechanism?

From the tests, two main hydraulic loading mechanisms are detected. The detached jet at the slope is most likely to generate large loads on the slope itself. On the crest and transition, both the front and the rest of the overtopping wave tongue generated relevant hydraulic loads on the cubes and rubble.

For the revetment stability, clamping is more significant than the own weight of the cube, hence the ill clamped areas appeared to be significantly less stable. Moreover, contrary to front slope revetment all hydraulic loads are directed downwards, increasing the normal forces between the cubes. The toe has to be able to cope with these large normal forces in single-layer cube revetment. In the present tests toe failure was mostly the governing failure mechanism.

5.2 Recommendations

From the discussions and the conclusions, several recommendations are stated below for further research on the topic of evolving the WOS itself and the relevant research on the stability of low-crested breakwater rear-slope single-layer cube revetment.

5.2.1 Wave Overtopping Simulator

Increase number of water level measurement devices

To overcome the problem with the lack of knowledge regarding the exact volume in time inside the reservoir when the valve is opened, multiple floats should be installed next to each other in flume-axial direction in the reservoir. The devices should be placed next to each other with small intervals (12 cm). This will significantly increase insight of the water level in time and consequently the applicability of the results.

Wall guidance

Another evident imperfection on the experimental set-up is the limitation of the flume width. It is recommended to install 4.5 cm thick (Plexi-)glass or perspex plates on both sides resulting in a decrease of the width downstream of the WOS. This adjustment helps to get a straight flow by cancelling the anomalies introduced by the width difference of the simulators reservoir and the flume, such as eddies, deformed wavefront, and splashing up of the water on the side walls.

Orifice discharge coefficient

The straight valve generates an orifice discharge coefficient of $\mu = 0.5$. This low value of μ limits the generated water layer thickness (which appeared to be the limiting boundary condition), and consequently the capacity of the WOS. A streamlined door will increase the value of μ and therefore the capacity of the WOS.

Different reservoir sizes

The reservoir of the WOS is constructed in such a way that it is easily removable and adaptable. Installing a reservoir with a larger width in flume-axial direction (w_{res}) will generate overtopping volumes with lower velocities compared to volumes generated with a small w_res. At that moment, the device could also be used for tsunami research or other experiments were sudden gusts of water volume are required. It must be kept in mind that the streamlines inside the reservoir alter with a different size reservoir. This could also alter the value of the orifice discharge coefficient μ.

5.2.2 Hydraulic research

Wave tongue velocities

A full research into the velocities inside an overtopping wave volume is recommended. The frame rate of the side camera has to be increased, considering 24 frames per second is not sufficient for a precise study. A comparison of the velocity field inside a simulated overtopping wave and the velocity field of a ‘real’ overtopping wave influenced by the outer slope, is very useful, especially considering turbulence intensities. These results should also indicate the significance of the turbulence induction. This information can be used to solve the issue with the water layer thickness on the crest influencing the water layer thickness of x=0.

Relation peak velocity and wavefront velocity

The measured wavefront velocities are mean values of the front velocity over the crest using photo-analysis. The relation between the front velocity and the measured peak velocity is therefore complicated to find. An in-depth research with the discussed absence of eddies and a camera capable of high-speed filming will give detailed insight in this phenomenon.

5.2.3 Single-layer rear-slope cube revetment

Extrusion tests

As further elaborated upon Chapter 4, the normal forces are significant for the stability of single-layer cube revetment at the rear slope. Similar extrusion tests as executed during placed-block revetment tests, to check if the cubes are well clamped, are recommended. If the well and ill clamped areas of a slope are clarified, a link may be made between the location of the found damage and the amount of clamping.

In-depth transition tests

The executed tests showed the significance of the transition between the crest and the rear slope at the inner crest line. Keeping in mind the in this thesis stated analysis of the transition, the suggested design approaches could be tested.

Toe and settlement research

The toe is very important for the single-layer cube revetment stability at the rear slope. Especially in the case of brittle single-layer cube revetment. Further research into the settlement and, especially, the effects of those settlements on clamping and stability is recommended. The use of a type of spring with a known behaviour, acting as a toe, would be relevant. This could link the normal forces to the stability.

Bibliography

Andersen, T. L. (2006). *Hydraulic Response of Rubble Mound Breakwaters.* Phd thesis, Aalborg University.

Ang, K. H., Chong, G., and Li, Y. (2005). PID control system analysis, design, and technology. *IEEE Transactions on Control Systems Technology*, 13(4):559–576.

Bosman, G. (2007). *Velocity and flow depth variations during wave overtopping.* Msc thesis, Delft University of Technology.

Bosman, G., van der Meer, J., Hoffmans, G., Schuttrumpf, H., and Verhagen, H. (2008). Individual Overtopping Events At Dikes. In *Coastal Engineering*, pages 1–13, Hamburg. International Conference on Coastal Engineering (ICCE).

Bruce, T., van der Meer, J. W., Franco, L., and Pearson, J. M. (2009). Overtopping performance of different armour units for rubble mound breakwaters. *Coastal Engineering*, 56(2):166–179.

CIRIA (2007). The Rock Manual. *Construction*, pages 15–62.

CLI (2015). Abstract of Accropode Technical Specifications. Technical Report 2.

Coeveld, E. and Klein Breteler, M. (2003). Invloed klemming: statistische analyse trekproeven.

Coticone, R. (2015). *Reconstruction of flow characteristics over the crest of a breakwater with PIV technique.* Msc thesis, Delft University of Technology.

De Vries, M. (1982). Scale Models in Hydraulic Engineering. (January):415.

Dean, R. G., Rosati, J. D., Walton, T. L., and Edge, B. L. (2010). Erosional equivalences of levees: Steady and intermittent wave overtopping. *Ocean Engineering*, 37(1):104–113.

Delta Marine Consultants (2014). Guidelines for Xbloc Concept Desings. Technical Report March.

Frostick, L. E., McLelland, S. J., and Mercer, T. G. (2010). Users Guide to Physical Modelling and Experimentation.

Hai Trung, L. (2014). *Overtopping on grass covered dikes.*

Hellinga, L. (2016). *Stability of Single Layer cubes on Breakwater Rear Slopes.* Master thesis, Delft Univerisity of Technologies.

Hofland, B. and van Gent, M. (2016). Automatic Settlement analysis of single-layer armour layers. In *6th International Conference on the Application of Physical Modelling in Coastal and Port Engineering and Science (Coastlab16)*, number May, pages 10–13, Ottowa, Canada.

Hughes, S. (2015). Hydraulic Parameters of Individual Overtopping Wave Volumes. (February).

Hughes, S., Thornton, C., van der Meer, J., and Scholl, B. (2012). Improvements in Describing Wave Overtopping Processes. *Coastal Engineering Proceedings*.

Hughes, S. A. (2008). Combined Wave and Surge Overtopping of Levees : Flow Hydrodynamics and Articulated Concrete Mat Stability. *U.S. Army Corps of Engineers - ERDC\CHL TR-08-10*, (August).

Hughes, S. A. (2011). Adaptation of the Levee Erosional Equivalence Method for the Hurricane Storm Damage Risk Reduction System (HSDRRS) Coastal and Hydraulics Laboratory Adaptation of the Levee Erosional Equivalence Method for the Hurricane Storm Damage Risk Reduction Syste. Technical Report May.

Hughes, S. A. and Thornton, C. I. (2016). Estimation of time-varying discharge and cumulative volume in individual overtopping waves. *Coastal Engineering*, 117:191–204.

Klein Breteler, M., Mourik, G., and Bosters, M. (2014a). Stabiliteit van steenzettingen bij golfaanval. Technical report, Deltares, Delft.

Klein Breteler, M., Mourik, G., and Provoost, Y. (2014b). Stability of placed block revetments in the wave run-up zone. *Coastal Engineering*, pages 1–12.

Kudale, M. D. and Kobayashi, N. (1996). Hydraulic Stability Analysis of Leeside Slopes of Overtopped Breakwaters. *Coastal Engineering Proceedings*, pages 1721–1734.

Kuiper, C., Klein Breteler, M., Booster, L., and Eysink, W. (2006). Stabiliteit van gezette steenbekleding op havendammen. Technical report, Deltares, Delft.

Le Méhauté, B. (1976). *An Introduction to Hydrodynamics and Water Waves.* Springer, New York, springer s edition.

Molines, J. and Medina, J. R. (2015). Calibration of overtopping roughness factors for concrete armor units in non-breaking conditions using the CLASH database. *Coastal Engineering*, 96:62–70.

Nederpel, A. (2002). Stabiliteit van het Achtertalud van een Rubble Mound Golfbreker.

Pearson, J., Bruce, T., Franco, L., van der Meer, J., Falzacappa, M., and Molino, R. (2004). D24 Report on additional tests. Technical report, The University of Edinburgh, Edinburgh.

Peters, I. D. J. (2003). Placed revetments under wave attack Study of structural mechanics. Technical report, TU Delft, Delft.

Ponsioen, L. (2016). *Overflow and wave overtopping induced failure processes on the landside slope of a dike.* PhD thesis.

Schiereck, G. J. (2012). *Introduction to Bed, bank and shore protection.* VSSD, Delft, 2nd edition.

Schuttrumpf, H. and van Gent, M. R. A. (2003). Wave Overtopping at Seadikes. In *In Coastal Structures 2003*, volume 40733.

Schüttrumpf, H. F. R. (2001). *Wellenüberlaufströmung bei Seedeichen-Experimentelle und theoretische Untersuchungen*. PhD thesis, Technischen Universität Carolo-Wilhelmina zu Braunschweig.

Taveira-Pinto, F., Almeida, L., and Luis, L. (2015). Experimental evaluation of a rubble mound with one layer cubic blocks using video image analysis. In *Factors affecting the performance and cost efficiency of sand storage dams in South Eastern Kenya*, number 3, pages 1–14, The Hague.

Trung, L. (2014). *Velocity and water-layer thickness of overtopping flows on sea dikes*. Phd-thesis, Delft University of Technology.

van Broekhoven, P. (2011). *The influence of armour layer and core permeability on the wave run-up*. Msc thesis, Delft University of Technology.

van Buchem, R. V. (2009). *Stability of a single top layer of cubes*. Msc thesis, Delft University of Technology.

van der Meer, J. (1995). Conceptual Design of a Rubble Mound Breakwater.

van der Meer, J. (2002). Technisch Rapport Golfoploop en Golfoverslag bij Dijken. pages 15–25.

van der Meer, J. (2006). Design, construction and calibration of wave overtopping simulator. Technical report.

van der Meer, J., Allsop, N., Bruce, T., De Rouck, J., Kortenhaus, A., Pullen, T., Schüttrumpf, H., Troch, P., and Zanuttigh, B. (2016). EurOtop Manual on wave overtopping of sea defences and related structures. Technical report.

Van der Meer, J., Bernardini, P., Snijders, W., and Regeling, W. (2006). The wave overtopping simulator. *Asce, Icce 2006*, pages 1–13.

van der Meer, J. and Bruce, T. (2014). New Physical Insights and Design Formulas on Wave Overtopping at Sloping and Vertical Structures. *Journal of Waterway, Port, Coastal, and Ocean Engineering*, 04014025(18):1–18.

van der Meer, J., Thornton, C., and Hughes, S. a. (2011). Design And Operation Of The U.S. Wave Overtopping Simulator. *ASCE, Proc. Coastal Structures 2011, Yokohama, Japan.*, pages 1–13.

van der Meer, J. W. and Janssen, J. P. F. M. (1994). *Wave run-up and wave overtopping at dikes and revetments*. Delft Hydraulics, Delft.

van der Meer, J. W., Steendam, G. J., de Raat, G., and Bernardini, P. (2008). Further Developments On The Wave Overtopping Simulator. *ASCE, Proc. ICCE 2008, Hamburg.*, pages 2957–2969.

van Dijk, B. (2001). *The rear slope stability of rubble mound breakwaters*. Msc thesis, Delft University of Technology.

Van Gent, M. and Luis, L. (2013). Application of cubes in a single layer. In *6th SCACR âĂŞ International Short Course/Conference on Applied Coastal Research*.

van Gent, M. R. A. (1999). Wave run-up and wave overtopping for double-peaked wave energy spectra. Technical report, Delft Hydraulics, Delft.

van Gent, M. R. A. (2001). Wave Runup On Dikes With Shallow Foreshores. *Journal of Waterway, Port, Coastal, and Ocean Engineering*, 127(5)(September/October):254–262.

van Gent, M. R. A. (2002a). Low-exceedance wave overtopping events. Technical report, Delft Cluster, Delft.

van Gent, M. R. A. (2002b). Wave overtopping events at dikes. In *Coastal Engineering Conference*, volume 2, pages 2203–2215.

van Gent, M. R. A., D'Angremond, K., and Triemstra, R. (2001). Rubble mound breakwaters : Single armour layers and high-density concrete units. (January 2001):1–12.

Van Gent, M. R. A., D'Angremond, K., and Triemstra, R. (2002). Rubble mound breakwaters: Single armour layers and high-density concrete units. In *Breakwaters, coastal structures and coastlines*.

van Gent, M. R. A. and Pozueta, B. (2004). Rear-side stability of rubble mound structures. In *Coastal Engineering Conference. Vol. 29. No. 4. ASCE American Society of Civil Engineers*.

Verhagen, H. J., Steenaard, J., and Tuan, T. Q. (2004). Infilitration of Overtopping Water in a Breakwater Crest. pages 1–11.

Verhagen, H. J., van Dijk, B., and Nederpel, A. (2003). Riprap Stability on the Inner Slopes of Medium-Height Breakwaters. *Coastal Structures*, pages 213–222.

Victor, L. (2012). *Optimalisatie van het hydrodynamische gedrag van golfenergieconvertoren gebaseerd op golfoverslag : experimentele studie van optimale geometrie en kansverdeling van overslagvolumes Optimization of the Hydrodynamic Performance of Overtopping Wave Energy Co.* PhD thesis.

Victor, L., van der Meer, J. W., and Troch, P. (2012). Probability distribution of individual wave overtopping volumes for smooth impermeable steep slopes with low crest freeboards. *Coastal Engineering*, 64:87–101.

Wescott, T. (2016). PID Without a PHD. *Embedded Systems Programming*, pages 86–108.

Zanuttigh, B. (2013). Statistical Characterisation of Extreme Overtopping Wave Volumes The Procedure for Data Elaboration at Low-Crested Breakwaters.

Appendix A

Parameter Scaling

The purpose of this experiment was to reproduce the phenomena that are entrapped in an overtopping wave on a single-layer cube revetment. Executing the tests in prototype scale is not feasible from a practical point of view, therefore scaling of the model and its input is obliged. When scaling rubble mount structures including roughness and permeability, scale effects are likely to introduce. Especially viscous-, surface tension- and elastic scale effects are significant compared to smooth impermeable structures (Andersen, 2006). The occurring phenomena should be similar to the ones on prototype scale in three forms: geometric, kinematic and dynamic. These similarities will be treated in this subsection, as well as the applicability of these laws in the experiments. The last subsection will compare the used method in this experiment to the method used with wave scaling in a wave flume.

A.1 Similarity

A.1.1 Geometric Similarity

The model should have the same shape as the prototype when representing the original situation: all the linear dimensions should have the same scale ratios ($L_p/L_m = n_L$). When this requirement is met the model is geometrical similar to the prototype.

A.1.2 Kinematic Similarity

The ratios of the velocities should be equal. This similarity should be the case for all time dependent processes ($t_p/t_m = n_t$). A circular movement in prototype scale has to be a circular movement in model scale. When this relation is met, kinematic similitude is reached.

A.1.3 Dynamic Similarity

Dynamic similarity implies that the ratio between the forces on the prototype and the model have a constant relation ($F_p/F_m = n_t$). Different scaling rules apply when scaling wave overtopping experiments. For true dynamic similarity scaling conditions from Froude, Reynolds and Weber should all be met (Frostick et al., 2010). Those ratios are discussed below.

Froude Conditions

The ratio between inertia and gravity forces is called the Froude number and is defined by Equation A.1.

$$Fr = \frac{Inertia\,Forces}{Gravitational\,Forces} = \frac{F_i}{F_g} \infty \frac{\rho \cdot U^2 \cdot L^2}{\rho \cdot g \cdot L^3} = \frac{U}{\sqrt{gL}} \tag{A.1}$$

The Froude condition requires similar Froude numbers in model- and prototype scale, eg:

$$Fr_m = Fr_p = \frac{U_m}{\sqrt{gL_m}} = \frac{U_p}{\sqrt{gL_p}} \tag{A.2}$$

Equation A.2 shows the main scaling law in small scale wave overtopping experiments, since the influence of gravity and inertia dominate the wave fields (Frostick et al., 2010). This condition must hold if vertical accelerations are in the same order as as the gravitational acceleration, which is the case with propagating waves.

Reynolds Conditions

The Reynolds number is the ratio between inertia forces and viscous forces. Reynolds similitude will become more important when modelling flow through a structure and forces on structures (Frostick et al., 2010) (Equation A.3).

$$Re = \frac{Inertia\,Forces}{Viscous\,Forces} = \frac{F_i}{F_v} \infty \frac{\rho_w \cdot U^2 \cdot L^2}{\mu \cdot U \cdot L} = \frac{\rho_w \cdot U \cdot L}{\mu} = \frac{U \cdot L}{v_k} \tag{A.3}$$

With μ as and v_k as kinematic viscosity (for water $v_k = 10^{-6}$). For fully dynamic similarity the Reynolds condition must hold:

$$Re_m = Re_p = \frac{U_m \cdot L_m}{v_k} = \frac{U_p \cdot L_p}{v_k} \tag{A.4}$$

As can be seen, it is not possible to meet and the Froude condition and the Reynolds condition when using water as a model fluid. It is general assumed that when $Re_D > 30000$ the drag coefficient is constant. Flow will be fully turbulent in the primary armour layer. When this condition is met, Froude scaling will be sufficient.

Weber Conditions

The ratio between surface tension and inertia is called the Weber number (Equation A.5).

$$We = \frac{Inertia\,Forces}{Surface\,Tension} = \frac{F_i}{F_\sigma} \infty \frac{\rho_w \cdot U^2 \cdot L}{\sigma} \tag{A.5}$$

Surface tension and hence Weber similitude is negligible when water depths are larger than 2cm, wave periods >0.35s and wavelengths >2cm (Le Méhauté, 1976). With all the normative waves produced by the overtopping simulator this will be the case.

A.2 Scaling Conditions

When using the Froude law the following relationships can be derived in terms of the length scale factor n_L:

Wave height [m]	$n_h = n_L$
Time [s]	$n_t = n_L^{0.5}$
Velocity [m/s]	$n_u = n_L^{0.5}$
Acceleration [m/s^2]	$n_a = 1$
Mass [kg]	$n_M = n_\rho \cdot n_L^3$
Pressure [kN/m^2]	$n_P = n_\rho \cdot n_L$
Force [kN]	$n_F = n_\rho \cdot n_L^3$
Discharge [L/(s m)]	$n_q = n_L^{1.5}$

Appendix B

Reservoir (Support) Principles

Before the final design was developed, some relevant design elements were investigated. The first design was designed solely with wood (Section B.1). For the next design, an existing frame was used to mount the reservoir onto (Section B.2). Next a design was made using solely steel (Section B.3). The detailed drawings of those elements are shown in this Appendix.

B.1 Wooden structure

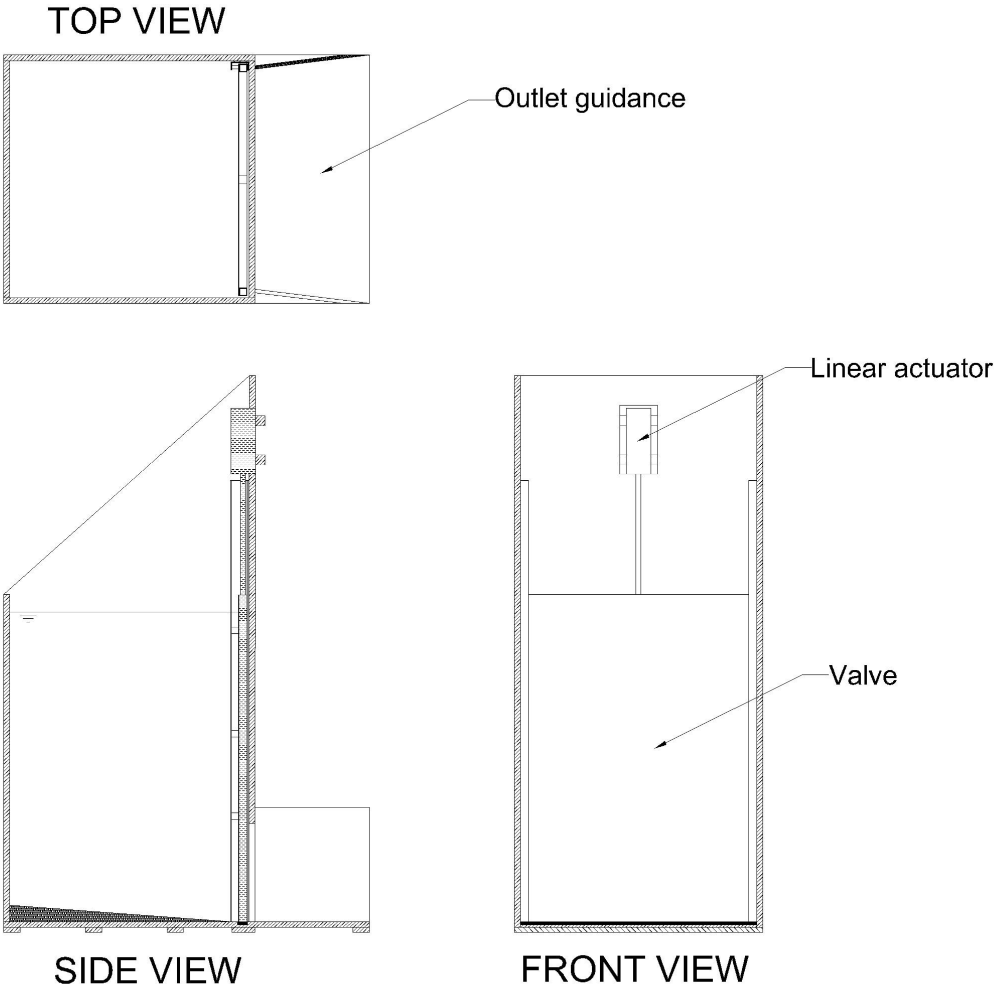
TOP VIEW
Outlet guidance
Linear actuator
Valve
SIDE VIEW
FRONT VIEW

Figure B.1: Wooden disign

B.2 Existing frame

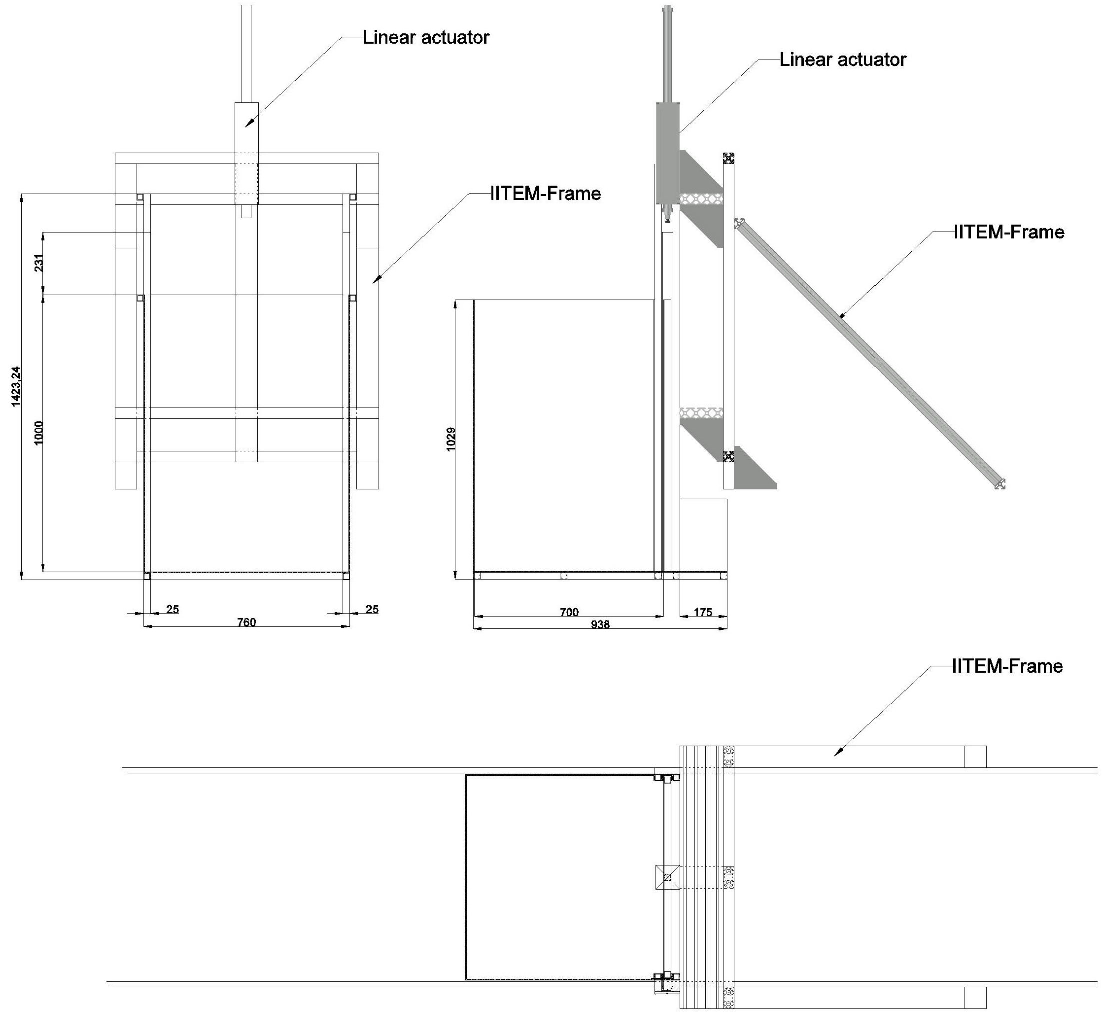
Linear actuator
IITEM-Frame
231
1423,24
1000
25
760
25
Linear actuator
IITEM-Frame
1029
700
938
175
IITEM-Frame

Figure B.2: ITEM-frame with steel reservoir

B.3 Completely steel

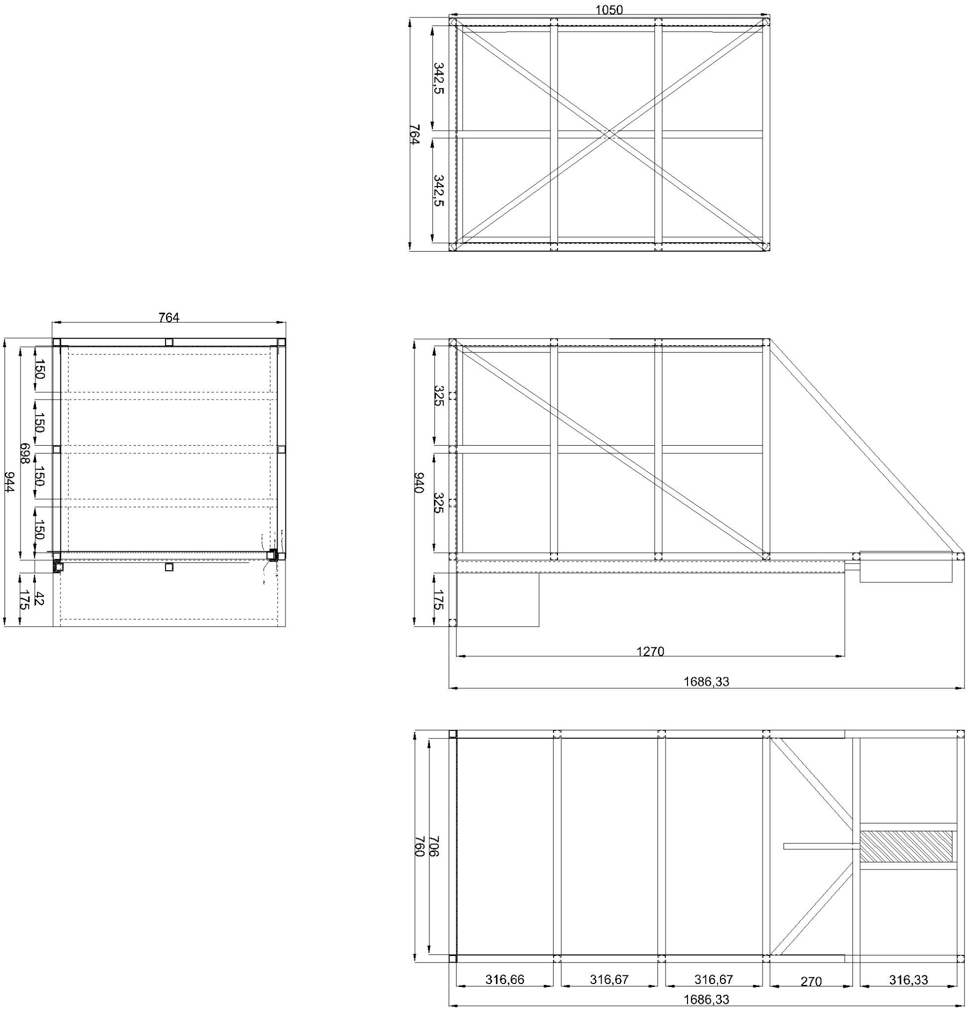
1050
342,5
764
342,5
764
150
150
150
150
698
944
42
175
325
940
325
175
1270
1686,33
706
760
316,66
316,67
316,67
270
316,33
1686,33

Figure B.3: Stainless steel frame and reservoir

Appendix C

Technical Drawings of the WOS

This Appendix shows the final technical drawings of the WOS:

- GEL709-S001: Overtopping Simulator
- GEL709-S002: Overtopping Deur
- GEL709-S003: Overtopping Frame
- GEL709-S004: Overtopping Hout

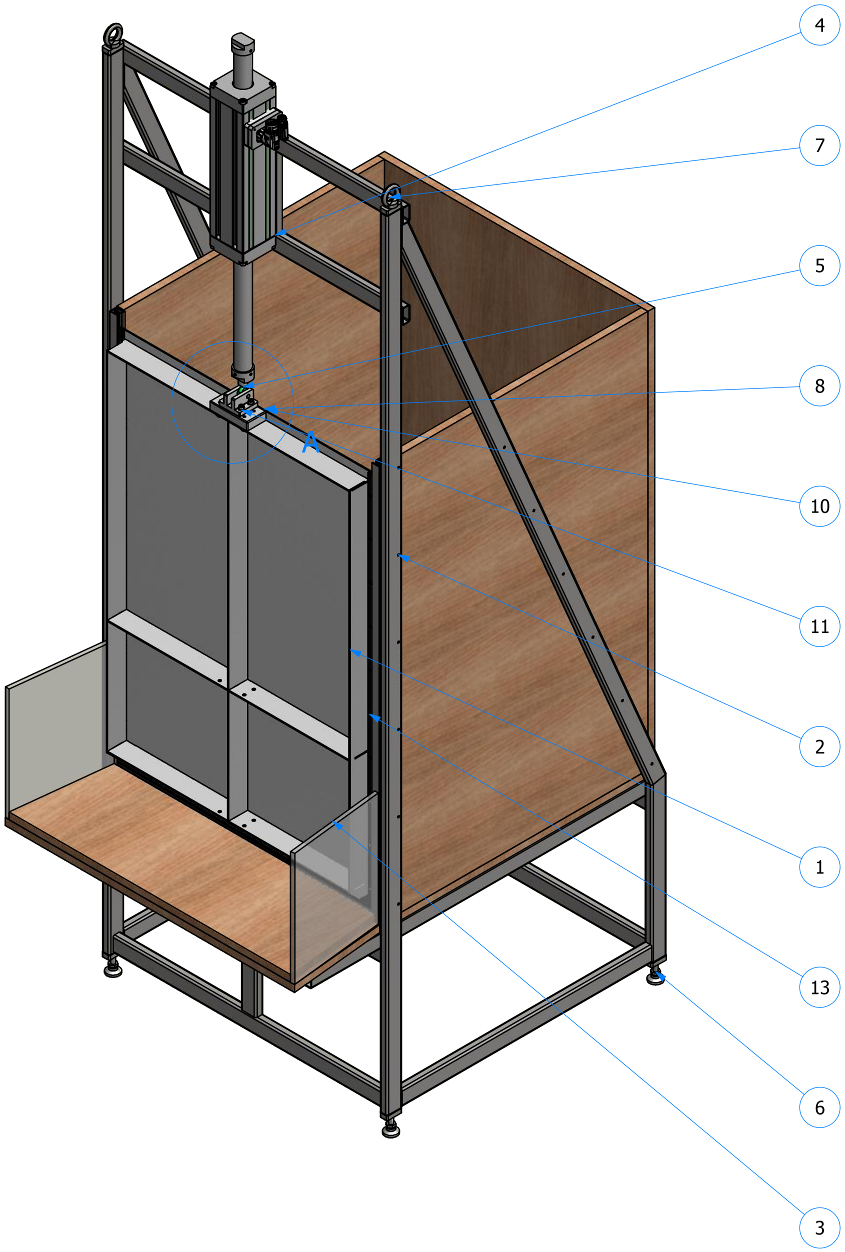

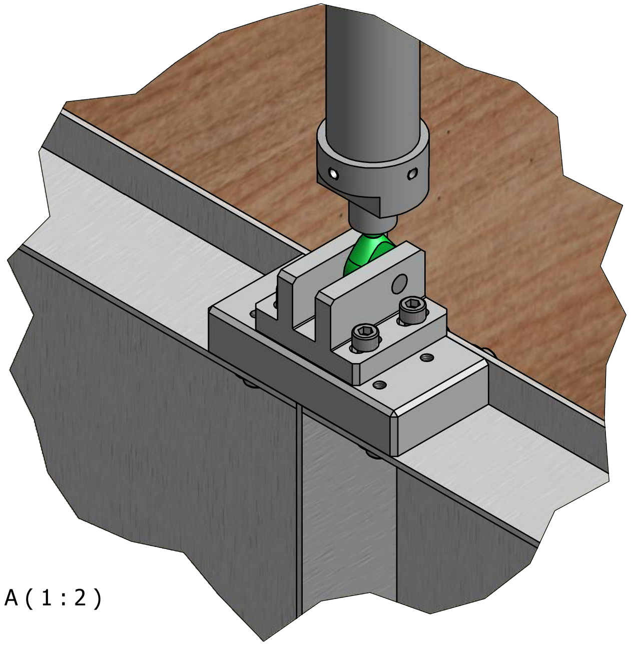

A (1 : 2)

St.nr.	Aant.	Benaming	Nummer	Materiaal	Opmerkingen
14	1	Bzk. Stelschroef ISO4026 - M3 x 8		RVS A2-70	Fabory nummer: 51240.030.008
13	10	Laagcillinder Binnenzeskant DIN7984 - M3 x 10		RVS A2-70	Fabory nummer: 51040.030.010
12	17	Laagcillinder Binnenzeskant DIN7984 - M3 x 8		RVS A2-70	Fabory nummer: 51040.030.008
11	4	Binnenzeskant DIN912 - M6 x 20		RVS A2-70	Fabory nummer: 51050.060.020
10	8	Binnenzeskant DIN912 - M6 x 16		RVS A2-70	Fabory nummer: 51050.060.016
9	4	Binnenzeskant DIN912 - M6 x 12		RVS A2-70	Fabory nummer: 51050.060.012
8	8	Sluitring 3xd ISO7093 - M6		RVS A2-70	Fabory nummer: 51530.060.001
7	2	Oogbout_gesmeed_DIN580_A2_M10		RVS A2-70	Fabory nummer: 51941.100.001
6	4	Levelling_Pads_2259_NH_M10		Stainless Steel	Maedler nummer: 65521091
5	1	Rod_ends_GT-R_DIN_12240-4_ K_M10		Stainless Steel	Maedler nummer: 63299808
4	1	Linear actuator			Nitek: GD350XS-350-S
3	1	Overtopping_Hout	GEL709-S004		
2	1	Overtopping_Frame	GEL709-S003		
1	1	Overtopping_Deur	GEL709-S002		

Getekend	Tom Phillips	Benaming Overtopping_Simulator_Assembly			
Controle					
Datum	26-10-2016	Project Overtopping simulator			
Status	Concept				
Materiaal		Eenheid mm	Schaal 1:10	Tekening nummer GEL709-S001	Blad nr. 1 / 1
Aantal	1				
TUDelft DEMO www.demo.tudelft.nl			Ra Alle vlakken tenzij anders vermeld	Toleranties volgens NEN-EN-ISO 1101:2013 en NEN-ISO 2768-mH Ruwheden volgens NEN-EN-ISO 1302:2002 Auteursrecht voorbehouden volgens de Wet	Formaat A3

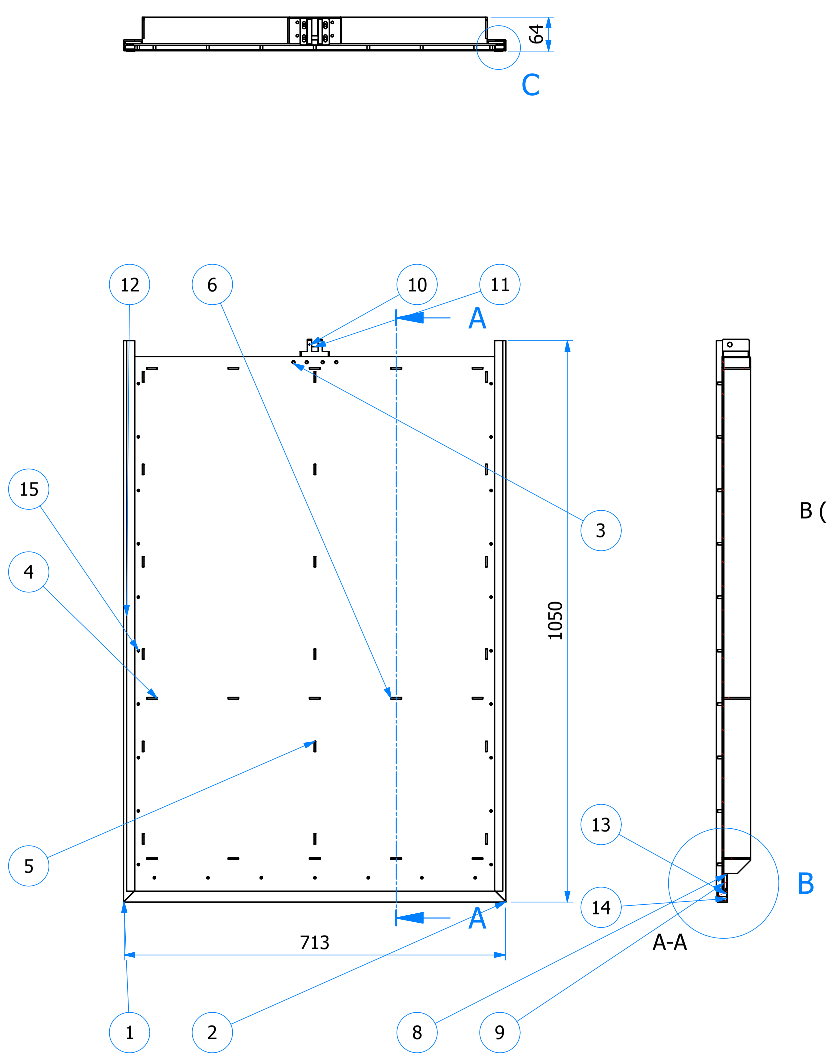

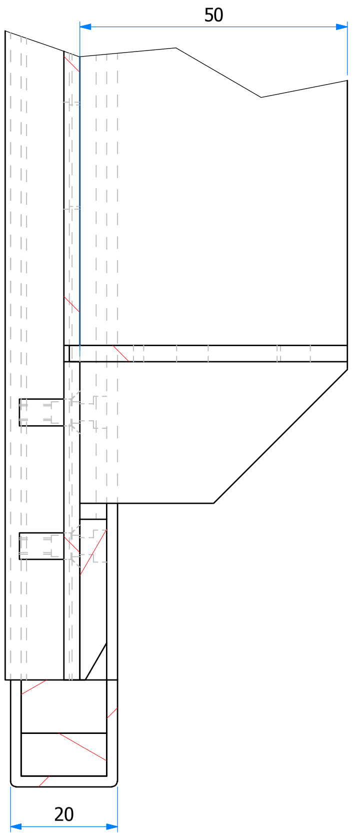

B (1 : 1)

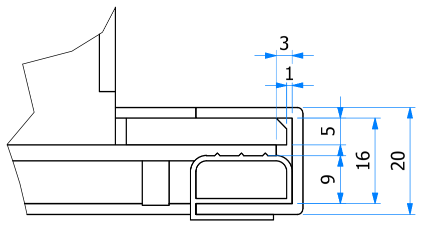

C (1 : 1)

St.nr.	Aant.	Benaming	Nummer	Materiaal	Opmerkingen
15	27	Blindklinkmoer verzonken kop		Aluminium	
14	1	Rechthoekprofiel_CR_sponsrubber_zwart_16x8	10000083	Rubber	ERIKS
13	1	Rechthoekprofiel_CR_sponsrubber_zwart_16x10	10000081	Rubber	ERIKS
12	2	E-profiel_NR_volrubber_65_wit_3383	10000325	Rubber	ERIKS
11	1	Pen	GEL709-M020	RVS 316L (1.4404)	
10	1	ActuatorKoppelPlaat	GEL709-M016	Alu 7075-T6 (AlZnMgCu1,5)	
9	1	POMStripOnder	GEL709-M014	POM	
8	1	POMStripL	GEL709-M013	POM	
7	1	POMStripR	GEL709-M012	POM	
6	3	PlaatStripKort	GEL709-M011	Alu 5754 (AlMg3, H111)	Lasersnijden
5	3	PlaatStripLang	GEL709-M010	Alu 5754 (AlMg3, H111)	Lasersnijden
4	1	PlaatDeur	GEL709-M009	Alu 5754 (AlMg3, H111)	Lasersnijden
3	1	DeurKoppelStuk	GEL709-M008	Alu 7075-T6 (AlZnMgCu1,5)	
2	1	UOnder	GEL709-M007	RVS 304 (1.4301)	
1	2	UZij	GEL709-M006	RVS 304 (1.4301)	

Getekend	Tom Phillips	Benaming Overtopping_Deur			
Controle					
Datum	26-10-2016	Project Overtopping simulator			
Status	Concept				
Materiaal	Aluminum 6061, Welded	Eenheid mm	Schaal 1:10	Tekening nummer GEL709-S002	Blad nr. 1 / 1
Aantal	1				
TUDelft DEMO www.demo.tudelft.nl			Ra Alle vlakken tenzij anders vermeld	Toleranties volgens NEN-EN-ISO 1101:2013 en NEN-ISO 2768-mH Ruwheden volgens NEN-EN-ISO 1302:2002 Auteursrecht voorbehouden volgens de Wet	Formaat A3

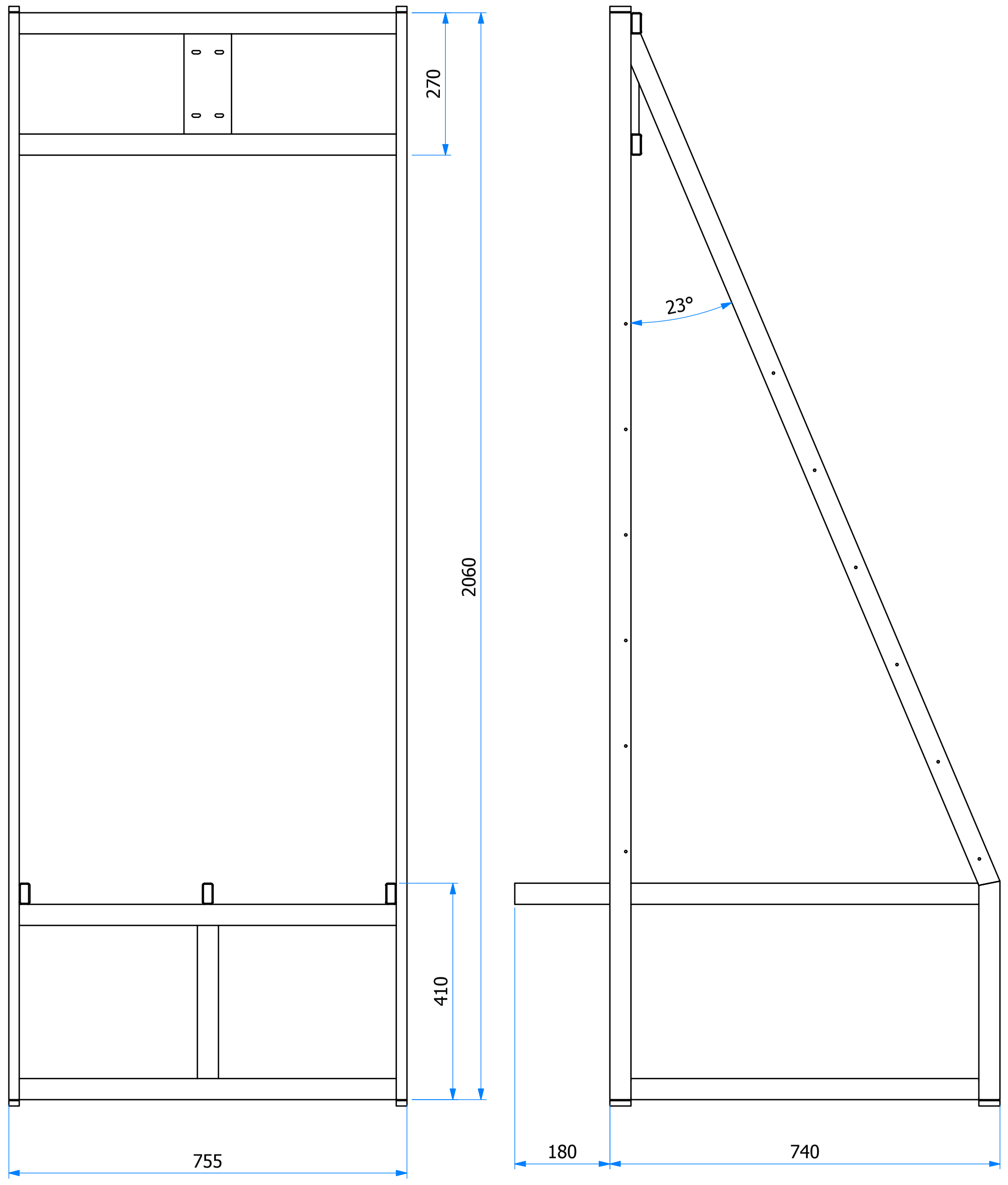

St.nr.	Aant.	Benaming	Nummer	Materiaal	Opmerkingen
10	1	ActuatorPlaat	GEL709-M015	RVS 304 (1.4301)	
9	6	HijsPlaat	GEL709-M017	RVS 304 (1.4301)	
8	2	Structural steels - Cold-formed, welded, structural hollow sections	ISO 4019 - 40x20x2 - 290	RVS 304 (1.4301)	
7	2	Structural steels - Cold-formed, welded, structural hollow sections	ISO 4019 - 40x20x2 - 1761,446	RVS 304 (1.4301)	
6	3	Structural steels - Cold-formed, welded, structural hollow sections	ISO 4019 - 40x20x2 - 920	RVS 304 (1.4301)	
5	2	Structural steels - Cold-formed, welded, structural hollow sections	ISO 4019 - 40x20x2 - 755	RVS 304 (1.4301)	
4	4	Structural steels - Cold-formed, welded, structural hollow sections	ISO 4019 - 40x20x2 - 715	RVS 304 (1.4301)	
3	2	Structural steels - Cold-formed, welded, structural hollow sections	ISO 4019 - 40x20x2 - 414,067	RVS 304 (1.4301)	
2	2	Structural steels - Cold-formed, welded, structural hollow sections	ISO 4019 - 40x20x2 - 660	RVS 304 (1.4301)	
1	2	Structural steels - Cold-formed, welded, structural hollow sections	ISO 4019 - 40x20x2 - 2060	RVS 304 (1.4301)	

Getekend	Tom Phillips	Benaming Overtopping_Frame			
Controle					
Datum	26-10-2016	Project Overtopping Simulator			
Status	Concept				
Materiaal		Eenheid mm	Schaal 1:4	Tekening nummer GEL709-S003	Blad nr. 1 / 1
Aantal	1				
TUDelft DEMO www.demo.tudelft.nl			Ra Alle vlakken tenzij anders vermeld	Toleranties volgens NEN-EN-ISO 1101:2013 en NEN-ISO 2768-mH Ruwheden volgens NEN-EN-ISO 1302:2002 Auteursrecht voorbehouden volgens de Wet	Formaat A3

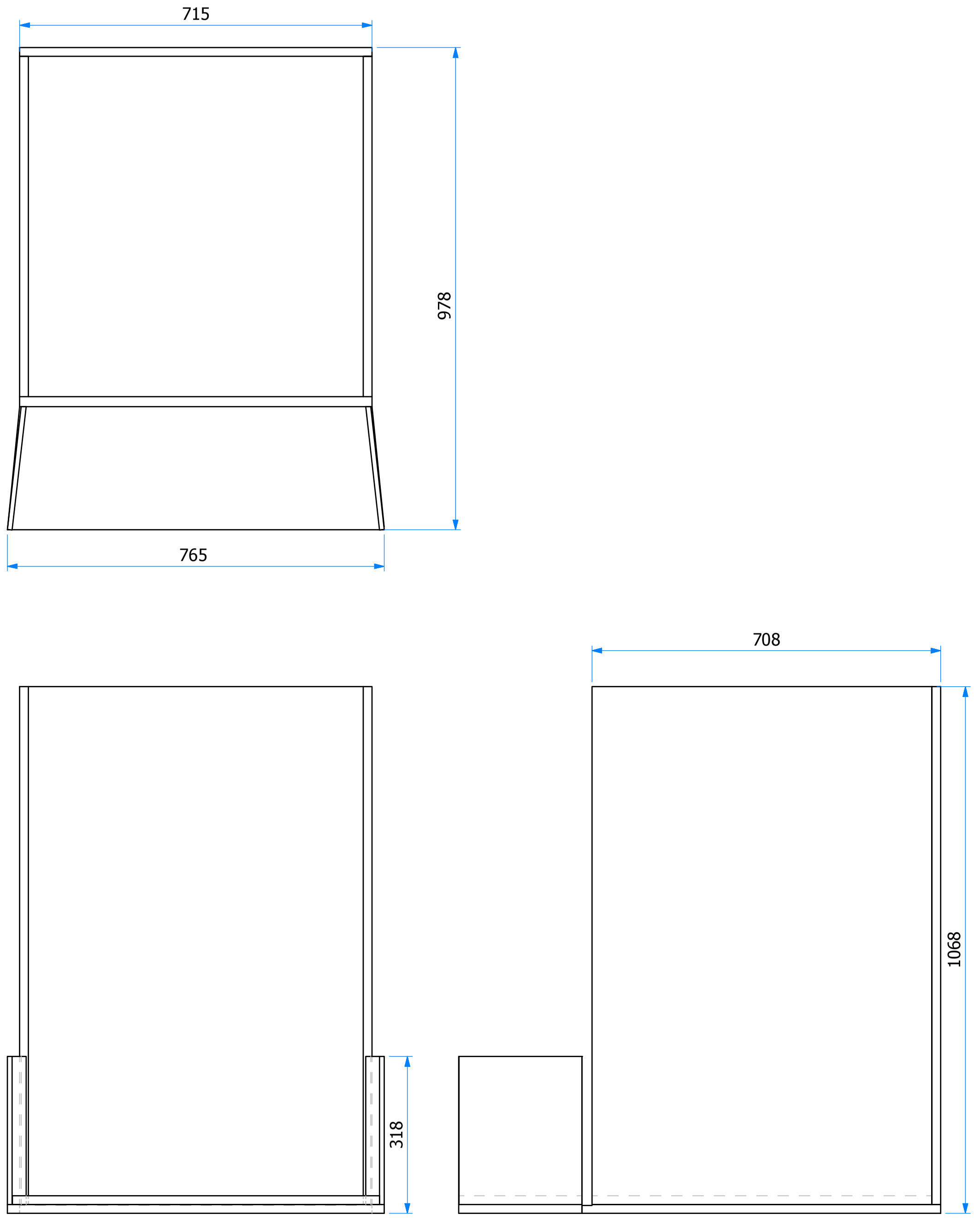

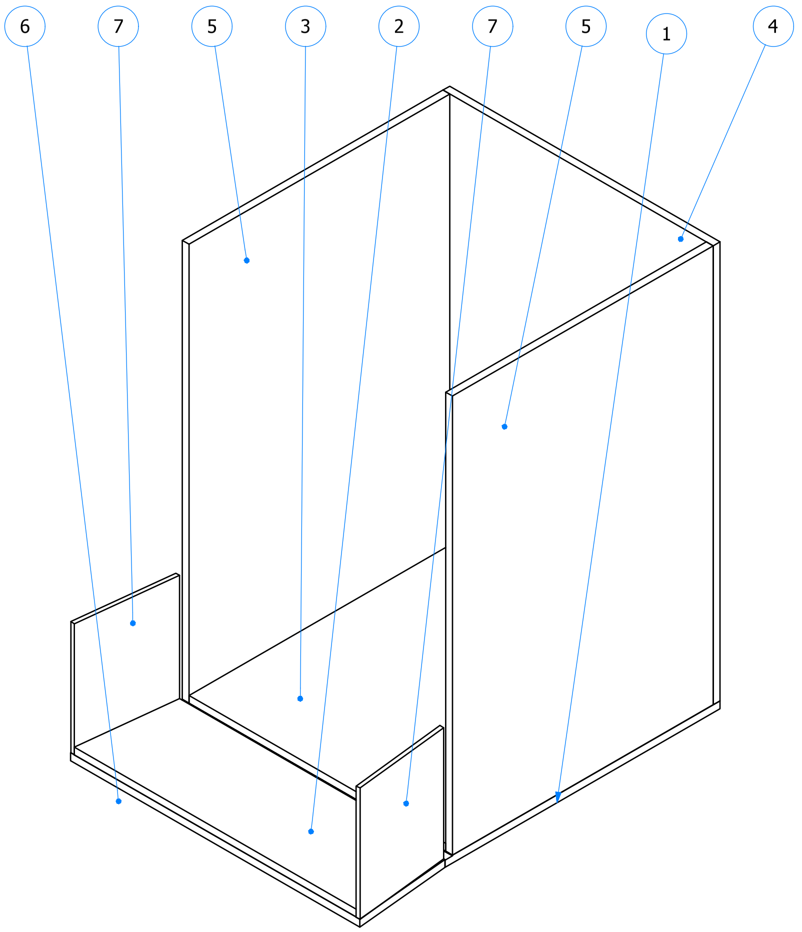

St.nr.	Aant.	Benaming	Nummer	Materiaal	Opmerkingen
7	2	Zij	GEL709-M019	PMMA (Plexiglas)	10mm
6	1	HoutOnderKort2	GEL709-M018	Multiplex	18mm
5	2	HoutZij	GEL709-M004	Multiplex	18mm
4	1	HoutAchter	GEL709-M005	Multiplex	18mm
3	1	HoutOnder	GEL709-M001	Multiplex	18mm
2	1	HoutOnderKort	GEL709-M003	Multiplex	18mm
1	1	HoutOnderLang	GEL709-M002	Multiplex	18mm

Getekend	Tom Phillips	Benaming	Overtopping_Hout
Controle			
Datum	26-10-2016	Project	Overtopping simulator
Status	Concept		
Materiaal		Eenheid: mm	Schaal: 1:10
Aantal	1	Tekening nummer: GEL709-S004	Blad nr.: 1 / 2

TUDelft DEMO
www.demo.tudelft.nl

Ra
Alle vlakken tenzij anders vermeld

Toleranties volgens NEN-EN-ISO 1101:2013 en NEN-ISO 2768-mH
Ruwheden volgens NEN-EN-ISO 1302:2002

Auteursrecht voorbehouden volgens de Wet

Formaat
A3

Appendix D

Tuning of the PID controller

Figure D.1 shows the block diagram of a PID controller. In this diagram, the 'plant' is in this case the linear actuator of the valve. The function of Digital-Analogue Converter (DAC) and Analogue-Digital Converter (ADC) are fulfilled by the actuator itself.

The actuator is tuned step-by-step, where the starting point was a set-up with solely the actuator with its shaft. Where after tuning of the fully build simulator could commence. Finally, the tuning of the filled overtopping simulator, including varying stick-slip of the door, was done. Starting with the derivative gain, then the proportional gain and ending with the integrator gain. The effects shown in Table D.1 were taken into account. The final values for the controller shown in Table D.2, are solely applicable for a well lubricated valve.

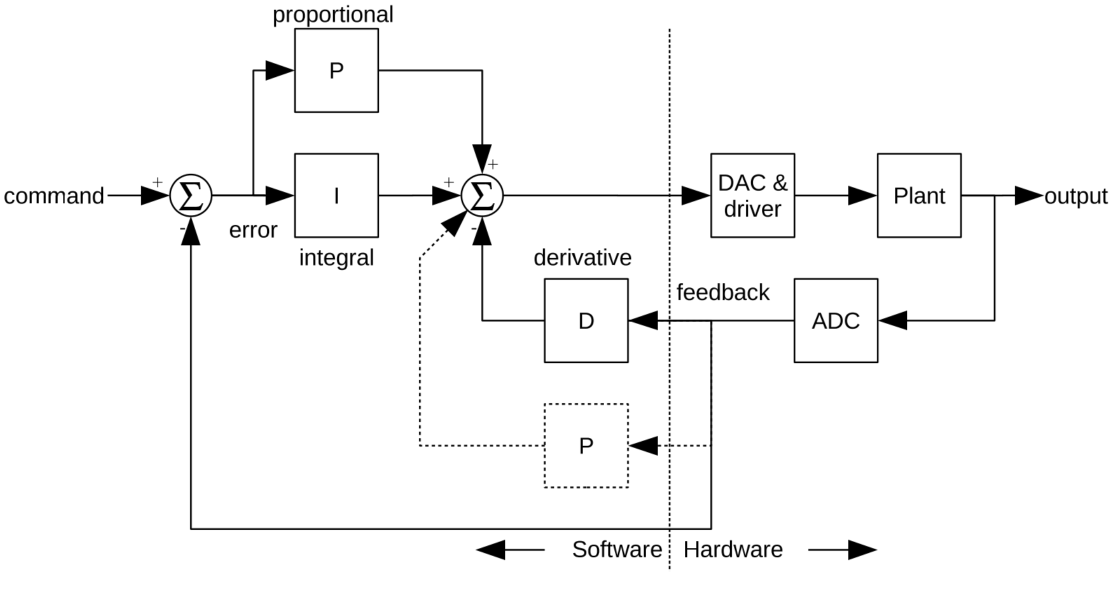

Figure D.1: Block diagram of PID controller (Wescott, 2016)

Table D.1: Effects of increasing a parameter independently (Ang et al., 2005)

Parameter	Rise time	Overshoot	Settling time	Steady-state error	Stability
K_p	Decrease	Increase	Small change	Decrease	Degrade
K_i	Decrease	Increase	Increase	Eliminate	Degrade
K_d	Minor change	Decrease	Decrease	No effect in theory	Improve if K_d small

Table D.2: Final values at used in the WOS

Position controller P gain	33.01	1/s
Velocity controller P gain	0.0550	A/(1/min)
Velocity controller integral action time	25.00	ms
Velocity feed-forward control	1.6	%
Filter time constant of the reference velocity value filter	6.50	ms
filter time constant of the reference current value filter	2.00	ms

Appendix E

Data Processing

E.1 Float Data Analysis

First the data per emptying cycle is extracted:

```
clear all; close all; clc;
filenaam = '.\Conf1\Conf1_036.ASC';
[pathstr,name,ext]  = fileparts(filenaam);

%% Inlezen Dasylab ascii-file:
data     = textread(filenaam,'','delimiter',';','headerlines',7);
nrows    = size(data,1);
ncolumns = size(data,2);
data     = data(:,1:ncolumns-1);
lengte   = length(data);

%% Boxgegevens
bd=0.676;
bl=0.705;
mu=0.50;

start    = 1;
t   =     data(start:lengte,1);
d1  =     0.0085+0.002+(-2.4913*data(start:lengte, 2) +23.849)/100; % deur opening in cm
wl  =     (5.1838*data(start:lengte, 3) + 56.093)/100; % waterlevel in cm

dt=t(2)-t(1);  % Bemonsteringsinterval [sec]

%% Filter hsim
y=doFilter(wl)/0.944;
idelay=110;
wlf=y(idelay+1:lengte); wlf(lengte-idelay:lengte)=0.0;

% Startpunt deur open
d2=d1(93000:end);
```

```
xd1= find(d2>0.003,1)+93000;

td1=xd1*dt;
wlo=wl(xd1); % waterlevel op dat tijdstip

% Inhoud
q = bd*bl*gradient(wlf(1:1:lengte),dt)/0.765; % Outflow per meter


% Save parameter

c1q20=q(xd1-500:end);
name= 'c1q20.mat';
save(name,'c1q20');
```

Next, the data is averaged over multiple cycles, and plotted.

E.2 Video Analysis

The detection of the water level is done using the following method. First, the stills of the videos are saved in separated JPG-files. These files are analysed using the following MATLAB script:

```

%%% Analyisis of Images

clc; clear all; close all;
map = num2str(0);
frontsp=zeros(16,1);

 for x=1 %wave configuration

xn=num2str(x,'%02d')
FolderName= ['.\Test_Videos\Conf0a\Conf' map '_0' xn '\side'];

D = dir([FolderName]);
num = length(D(not([D.isdir])));
dt=1/24;
loc=zeros(num,1);

%% Process images
for a=1:5%num-3 %3 for Skip isdir

     filename= [FolderName '\' D(a+3).name];
     A = imread(filename);

%% Distortion etc
[J,newOrigin] = undistortImage(A,cameraParamsside);

```

```
A=rgb2gray(A);

%Losse druppels weg
BW = im2bw(A,0.500);
BW = bwareaopen(BW,500);

BW(680:end,:)=0;
imshow(BW)

%% Prepare to find line

T=transpose(BW);
coli=zeros(size(A,2),1);
l =[1:size(A,2)]';
coli=[l coli];

%% Find upper waterline
for i=1:size(A,2);
    b =find(T(i,250:end),1); % Starting from 250 hence the border is not included
    if isempty(b)==1;
        coli(i,2)=0;
    else
        coli(i,2)=b;
    end
 end

%% Find front

loc(a,1) =find(coli(:,2)>1,1,'last');


end

coli(coli==0)=nan;

%% Final Figure of Single Image
coli(coli==0)=nan;
figure
imshow(A)
hold on;
plot(coli(:,1),coli(:,2)+250,'g','LineWidth',3);


%% Determine average front velocity
Uf=(loc(be+4)-loc(be+0))/(4*dt)
```

Appendix F

Simulated Waves

During the tests 36 different waves are tested. Table F.1 shows the settings of the WOS for every simulation.

Table F.1: Simulated waves

Wave nr.	Width[1](m)	Water column (m)	Valve opening (m)	Volume (m^3)
W1	0.70	0.2	0.05	0.14
W2	0.70	0.2	0.10	0.14
W3	0.70	0.2	0.15	0.14
W4	0.70	0.2	0.20	0.14
W5	0.70	0.4	0.05	0.28
W6	0.70	0.4	0.10	0.28
W7	0.70	0.4	0.15	0.28
W8	0.70	0.4	0.20	0.28
W9	0.70	0.6	0.05	0.42
W10	0.70	0.6	0.10	0.42
W11	0.70	0.6	0.15	0.42
W12	0.70	0.6	0.20	0.42
W13	0.55	0.2	0.05	0.11
W14	0.55	0.2	0.10	0.11
W15	0.55	0.2	0.15	0.11
W16	0.55	0.2	0.20	0.11
W17	0.55	0.4	0.05	0.22
W18	0.55	0.4	0.10	0.22
W19	0.55	0.4	0.15	0.22
W20	0.55	0.4	0.20	0.22
W21	0.55	0.6	0.05	0.33
W22	0.55	0.6	0.10	0.33
W23	0.55	0.6	0.15	0.33
W24	0.55	0.6	0.20	0.33
W25	0.40	0.2	0.05	0.08
W26	0.40	0.2	0.10	0.08
W27	0.40	0.2	0.15	0.08
W28	0.40	0.2	0.20	0.08
W29	0.40	0.4	0.05	0.16
W30	0.40	0.4	0.10	0.16
W31	0.40	0.4	0.15	0.16
W32	0.40	0.4	0.20	0.16
W33	0.40	0.6	0.05	0.24
W34	0.40	0.6	0.10	0.24
W35	0.40	0.6	0.15	0.24
W36	0.40	0.6	0.20	0.24

[1] In flume-axial direction

The discharges calculated using the measurements from the float in the reservoir of the WOS are shown in the next figures.

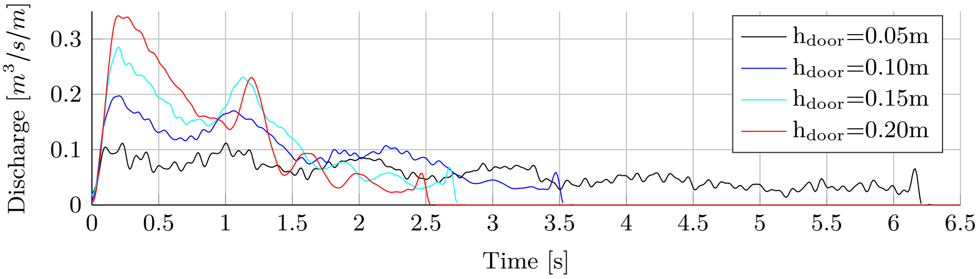

(a) Width=0.70 m

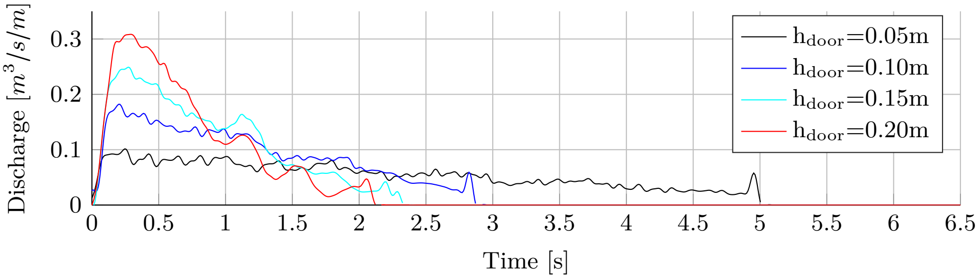

(b) Width=0.55 m

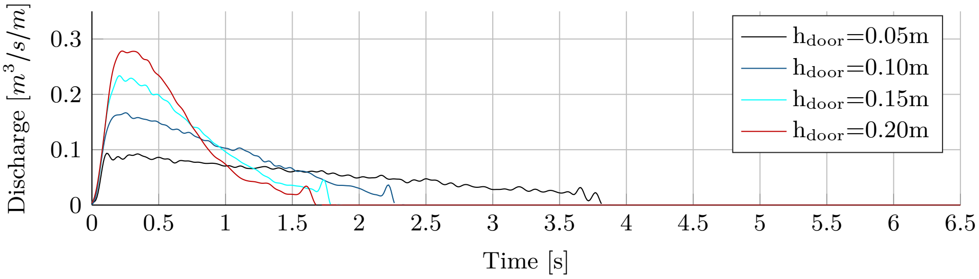

(c) Width=0.40 m

Figure F.1: Discharge in time with h_{res}(0)=0.60 m for different flume axial widths

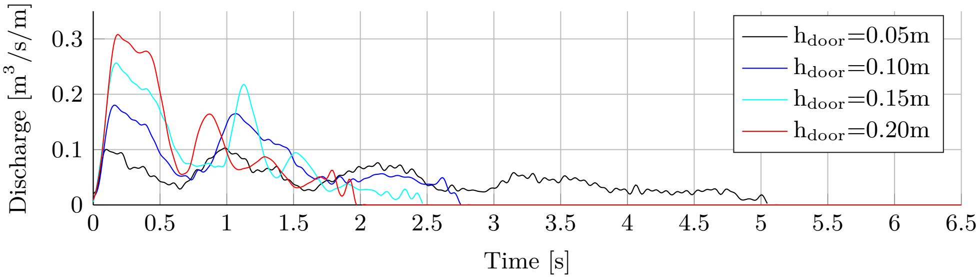

(a) Width=0.70 m

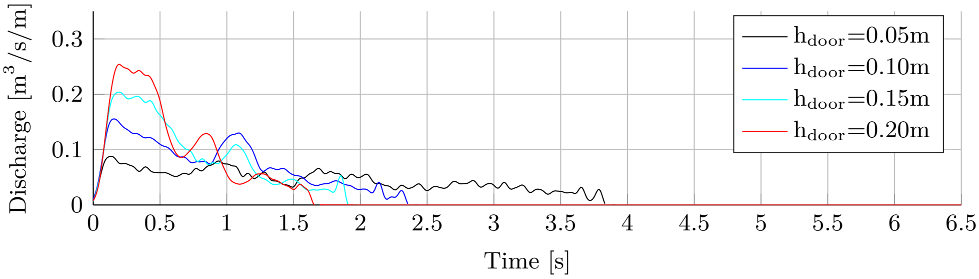

(b) Width=0.55 m

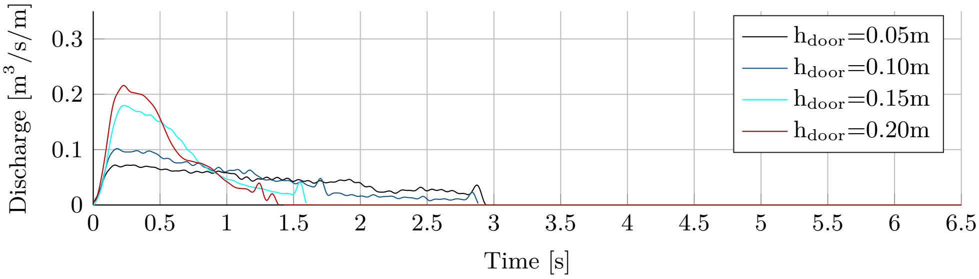

(c) Width=0.40 m

Figure F.2: Discharge in time with $h_{res}(0)$=0.40 m for different flume axial widths

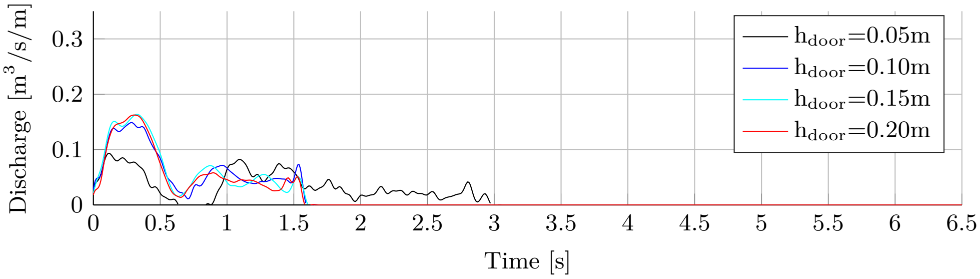

(a) Width=0.70 m

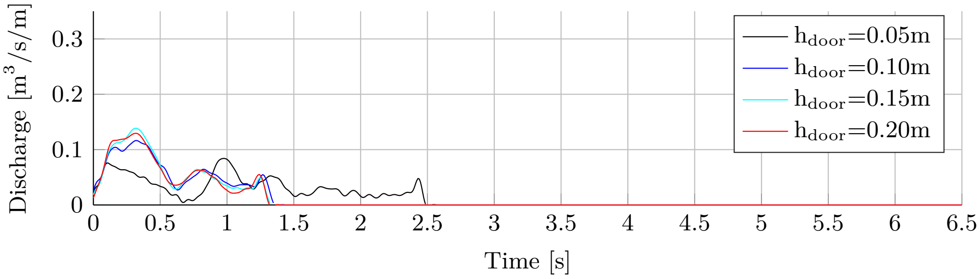

(b) Width=0.55 m

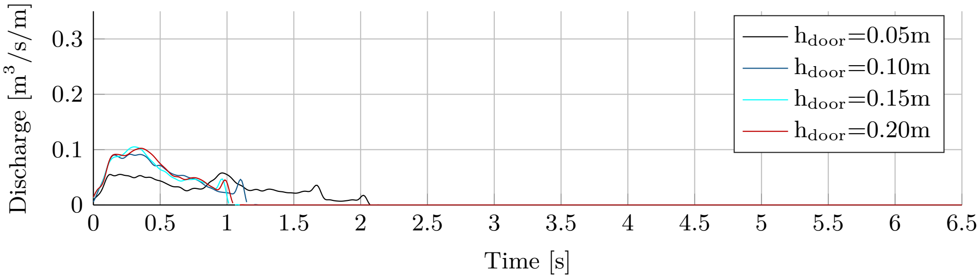

(c) Width=0.40 m

Figure F.3: Discharge in time with $h_{res}(0)$=0.20 m for different flume axial widths

Appendix G

Storm Simulation Example

As an example, a theoretical storm is elaborated in this Appendix. The simulated waves ordered in magnitude are shown in the figures below. As discussed in Chapter 3, presumably not all waves have to simulated to generate the normative loads. How this division is exactly made, could be incorporated in further research.

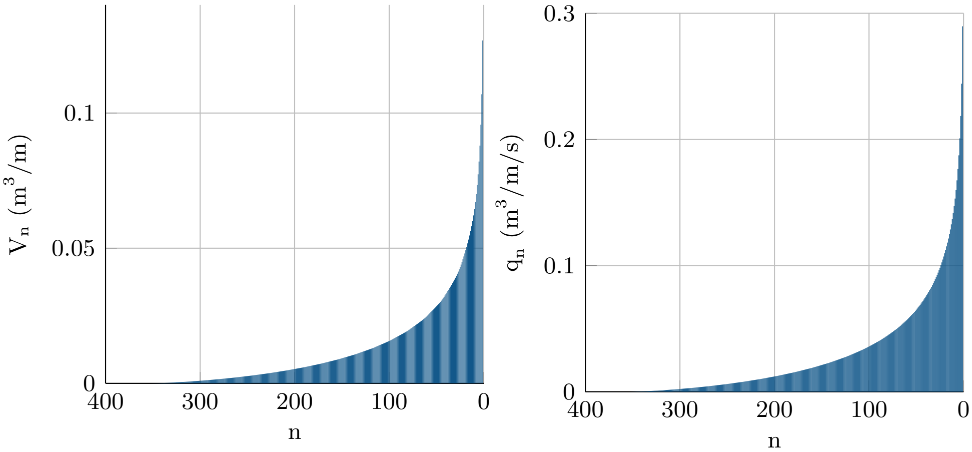

(a) Volume

(b) Discharge

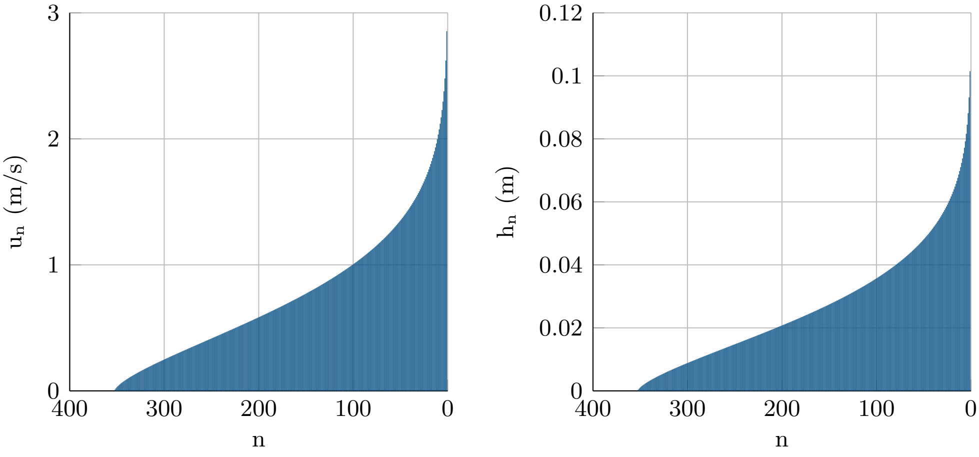

(c) Velocithy

(d) Layer thickness

Figure G.1: Theoretical waves in a storm. With $H_s = 0.24$ *m,* $s = 0.4$, $R_c = 0.35$ *m,* $t = 3$ *hours,* $\tan\alpha = 0.5$.

Appendix H

WOS Behaviour

To describe the behaviour of the simulator expressed in the water level height inside the reservoir (h_{res}), the door opening height (d_{valve}) and the resulting peak discharge (q_{peak}) as shown in Figure 3.28, a polynomial equation is opposed with 1 (h_{res}) and 3 (d_{valve}) degrees. See Equation H.1, with a rMSE of q_{peak} is 10.59 L/s/m.

$$q_{peak} = c_1 + c_2 \cdot h_{res} + c_3 \cdot d_{valve} + c_4 \cdot h_{res} \cdot d_{valve} + c_5 \cdot d_{valve}^2 + c_6 \cdot h_{res} \cdot d_{valve}^2 + c_7 \cdot d_{valve}^3 \quad \text{(H.1)}$$

Table H.1: Values of coefficients

$c_1=$	145.9
$c_2=$	-83.75
$c_3=$	-4269
$c_4=$	4985
$c_5=$	35050
$c_6=$	-15500
$c_7=$	-75330

This equation is solely valid for tests with w_{res} = 0.4. For different widths, tests with extra measurement points have to be executed.

Appendix I

Lessons Learned: Tips for Testing in the Fluid Mechanics Laboratory

In this chapter my experiences with testing in the Fluid Mechanics Laboratory are elaborated and it can be used as a warning for some pitfalls.

Breakwater tests en Measurements:

Colour rubble Make sure the colour of the different rubble layers and core is different. This makes it way more easy and quick to remove the filter layer from the core when changing a configuration.

Filter Use as many analogue filters for the measurement devices as possible, this makes measurements more accurate and saves a lot of time processing the measurement data.

Over dimension boundaries The toe stability was not in the scope of the project. In initial tests, the toe failed resulting from a to weak constructed toe. Tip: over dimension everything so you are 100% sure it will not fail.

General remarks:

Discuss By discussing your project with other people, new insights can be acquired. This may be very useful for your project.

Uncertainties When making your planning, always take into account things will go wrong.

Check Deliveries Check whether the delivered goods are actual the goods ordered. In my case the eventual delivered split gradation was different.